ENG 323-(EQC 1999/423)

Design of foundations to resist shear during earthquakes

Nigel Burdon, Hsueh-Lynn Kueh, Kevin J McManus, Department of Civil Engineering, University of Canterbury

ENG 323

DESIGN OF FOUNDATIONS TO RESIST SHEAR DURING EARTHQUAKES

EQC 99/423

Final Report, May 2004

Prepared by

UNIVERSITY OF CANTERBURY

Department of Civil Engineering

Christchurch

New Zealand

Authors

Nigel Burdon

Hsueh-Lynn Kueh

Kevin J McManus

Principal Investigator

Kevin J McManus

Prepared for

EQC Research Foundation

Box 311

Wellington, New Zealand

Summary

At present, there is no uniform approach to designing structures to resist base shear. Designers usually assume that most of the base shear will be resisted by passive resistance of soil acting against vertical surfaces such as beam sides and basement walls. This is a convenient assumption because such passive pressures calculated using traditional Rankine earth pressure theory are generally very large. The actual mechanisms of resisting base shear are not well understood.

This study has investigated the behaviour of three typical foundation systems under lateral loading: simple slab-on-grade, slab-on-grade with two parallel foundation beams, and a slab and beam foundation interacting with a pile. Details typical of New Zealand construction practice were followed as closely as possible.

The base sliding characteristics for simple slab-on-grade construction were determined by building large (2 m wide x 3 m long) slabs and pushing them back and forth with a hydraulic actuator. One and two layers of dampcourse were used and some slabs were weighted with ballast. Peak friction angles ranged from 28 degrees for a single layer of dampcourse with 6.6 KN/m2 contact pressure to 12 degrees for a double layer of dampcourse with 3.1 KN/m2. Mean friction angles were all 2 degrees less than for the peak friction angles.

Three shallow foundations each 4.25 m wide x 4.6 m long consisting of a 100 mm thick slab "on-grade" with two foundation beams 600 mm wide embedded 450 mm were constructed in coarse granular material. Each was tested by shoving back-and-forth by a powerful hydraulic actuator with several cycles of quasi-static lateral loading.

Lateral loading of the slab and beam foundations caused a wedge type of failure mechanism with significant passive soil pressures acting against the vertical faces of the foundation beams. The passive soil wedge developing against the trailing beam lifted one side of the structure vertically leaving hollow space beneath the floor slab. For the somewhat narrow structures tested, significant rotations of the structure occurred.

A simple method of analysis was developed and found to give good predictions for the experimental results while accounting for all of the main parameters. The analysis predicts that lateral load capacity is highly sensitive to the eccentricity (height above ground) of the applied lateral load.

Pile interaction with a slab and beam foundation was investigated by casting a single steel pipe pile (168 mm x 4.05 m long) into a slab and beam foundation and then subjecting the composite foundation to various cycles of lateral loading. The presence of the pile was found to increase the lateral load resistance of the foundation in two ways: by direct contribution from the lateral resistance of the pile reacting against the soil, and from uplift resistance of the pile adding to the "weight" of the foundation during the tilting and uplift associated with generation of the soil passive wedges.

A general approach for design and analysis of combined beam-slab-pile foundations using standard methodologies is given.

Acknowledgements

This project was funded principally by the Earthquake Commission under research grant EQC 99/423. The University of Canterbury contributed overhead costs and much of the capital equipment used in the testing.

This report contains substantial material extracted from the Masters reports of Nigel Burdon and Hsueh-Lynn Kueh by the Principal Researcher.

Special thanks is due to John van Dyk for performing most of the field construction and for his continual enthusiasm. Rosemary McManus re-typed the student theses.

CONTENTS

1 INTRODUCTION

During the Kobe earthquake, many buildings in the Kobe area were founded on piles and many piles were damaged by shear acting at the base of the structure. The exact mechanisms resisting base shear are not well understood but include base friction (which may disappear because of relative settlement of the soil), passive resistance of foundation beams and walls, and passive resistance of any piles.

At present, there is no uniform approach to designing structures to resist base shear. Designers usually assume that most of the base shear will be resisted by passive resistance of soil acting against vertical surfaces such as beam sides and basement walls. This is a convenient assumption because such passive pressures calculated using traditional Rankine earth pressure theory are generally very large. However, in reality it may be difficult to achieve these high theoretical values because the boundary conditions will generally be different and because very large displacements may be required. For these reasons, it is important that passive and frictional resistance to sliding be verified experimentally. Over-estimation of passive resistance from beams and walls in a foundation system may cause overloading of piles in shear and subsequent damage and the danger of pile failure. For foundation systems without piles, over-estimation of passive resistance may allow excessive sliding displacements of the structure and consequent damage to building lifeline systems.

Very little research has been conducted to date on the exact lateral load-resisting mechanisms of shallow foundations with regard to seismic excitation, even though much research has been carried out on the lateral load resistance of pile foundations, the lateral load capacity of retaining structures and the dynamic bearing capacity of shallow foundations.

1.1 Offshore gravity structure analysis using the upper bound method

Some of the work most closely linked to this topic to date has been done with regards to offshore structures (Murff and Miller, 1977). Offshore structures often involve complex foundation issues that include inclined eccentric loads, non-homogeneous anisotropic soil strengths and complex base geometries. The work by Murff and

Miller (1977) focuses on the effectiveness of the upper bound method for gaining reliable solutions for foundations for offshore gravity structures. This method is approximate as it utilises the upper bound theorem of plasticity. The major advantage of the upper bound method is the fact that one may postulate several failure mechanisms that give directly comparable results. This may eliminate many of the subjective decisions that are required in methods like the limit equilibrium method. Another advantage is the fact that one may easily optimise the variables that define the selected failure mechanism. However, care needs to be taken, as the answers given will, if incorrect, be too high (which is unconservative for design purposes).

The upper bound method requires the following steps:

1. The selection of collapse mechanisms.

2. Equating of internal energy dissipation to the rate at which the external forces do work.

3. Solving for the unknown external force that will cause failure.

The method is applied directly to foundations utilising shear keys and relates the maximum lateral resistance to the depth, spacing, and loading of the shear keys (see Figure 1.1).

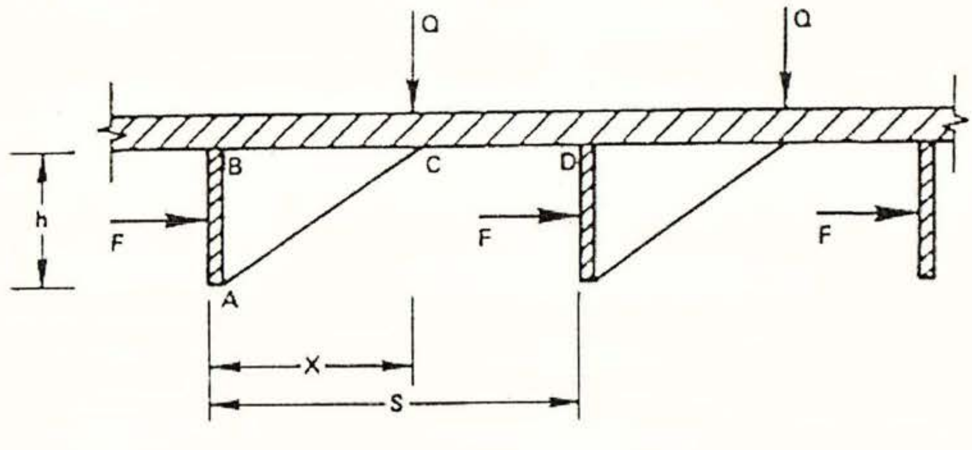

Figure 1.1 Diagram showing dimensions and loads used in the shear key analysis(Murff and Miller, 1977).

Major assumptions were that: Edge and end effects are ignored, the soil is assumed to behave as a purely cohesive material in the undrained condition, and that the surface along section CD is smooth, meaning that all the dissipation occurs along AC. By equating internal and external work done, and solving for the critical force F per shear key to cause failure, the relationship can be shown to be:

$$F = 2k_a\sqrt{\frac{Qh}{k_a + h^2}} \tag{1.1}$$

in which k_a = weighted average shear strength

Q = vertical load per unit width

h = the depth of the shear keys

and from Figure 1.1:

X = horizontal extent of the failure wedge

S = shear key spacing

This result allows evaluation of the vertical load required in each bay in order to achieve a desired level of horizontal force to induce failure. It should be noted that this relationship is very sensitive to shear strength variations.

Although this solution looks at a wedge failure, there are two further modes of failure that need to be considered. As shown in Figure 1.2 both a flow-under failure, and a tip-to-tip failure need to be considered (failure modes are shown in order of least resistance to maximum resistance).

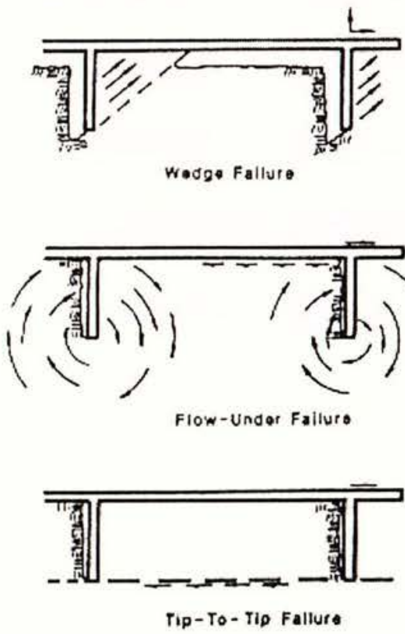

Figure 1.2 The three possible failure mechanisms of a shear key foundation (from Figure 4.20 of Fang, 1991)

The analysis was developed further to look at the relationship between vertical load and shear key spacing in order to create tip-to-tip shear failure. In practice, shallow foundations are generally spaced fairly wide apart. However, if the vertical load on the structure is great, the chance of tip-to-tip shear failure will be increased. With the vertical pressure per unit width, q being defined as Q/S, the following non-dimensional relationship can be derived.

$$\frac{q}{k_a} = \frac{1}{4}\left(\frac{k_h}{k_a}\right)^2 \frac{S}{h} - \frac{h}{S} \qquad (1.2)$$

in which:

k_h = horizontal shear strength

k_a = weighted average shear strength

q = vertical pressure per unit width

S = shear key spacing

If these results are plotted, as in Figure 1.3, a clear relationship can be seen between the non-dimensional critical pressure and the non-dimensional shear key spacing.

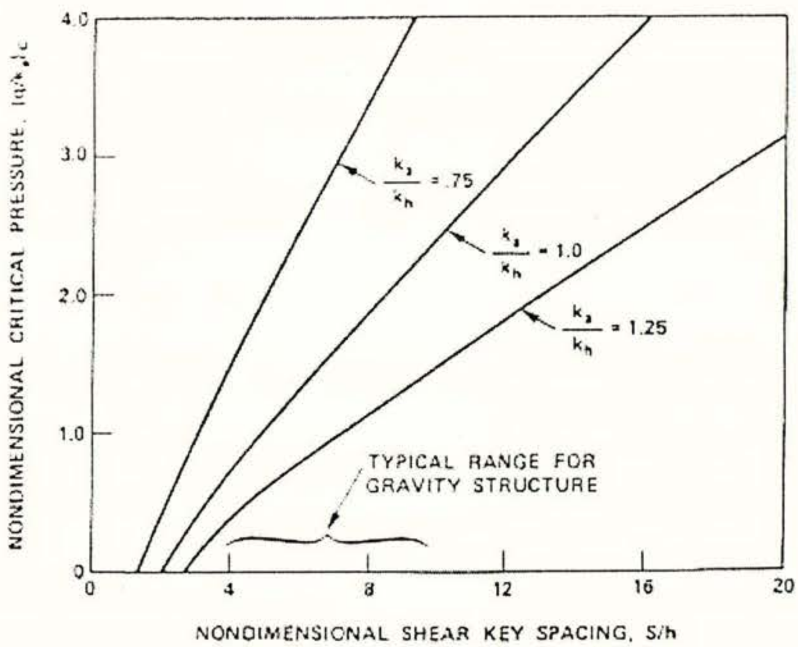

Figure 1.3. Graph showing the relationship between shear key spacing and critical pressure for a tip-to-tip shear failure (from Figure 10 of Murff and Miller, 1977)

As the horizontal shear strength becomes larger in relation to the average shear strength (that is, k_a/k_h decreases), the non-dimensional pressure load must either increase given a fixed shear key spacing, or the shear key spacing must decrease for a given vertical pressure, in order to obtain a tip-to-tip failure.

This work provides a basic understanding for potential behaviour of the foundation under lateral loading with the application of vertical loads.

1.2 Horizontal stiffness of arbitrarily-shaped foundations

Useful work was done by Gazetas and Tassoulas (1987) with regard to the horizontal stiffness of various different foundation shapes. It was noted that, although much work at that time had been carried out on circular embedded foundations, very little information was available for other foundation geometries. It was therefore common at that time to adapt the known circular foundation information to generate an equivalent circular shape for any given foundation geometry.

Both static and dynamic stiffnesses were evaluated in that work. In order to get around the problem of improper boundary conditions that results from radiation damping when using a finite element programme, a boundary-element formulation was used. The boundary-element formulation makes use of discretised boundaries, but applies analytical solutions within these boundaries. Gazetas and Tassoulas used this method to carry out a parametric study for many different rectangular foundation geometries and embedment depths.

The work isolated two effects that modify the behaviour of a foundation with increasing embedment. These are what are referred to as "sidewall contact" and the "trench effect" (see Figure 1.4). The method used to evaluate the effect of embedment applied multipliers for both of these effects to the horizontal static surface stiffness of a surface foundation. This is shown in the following equation and each component is shown in Figure 1.4.

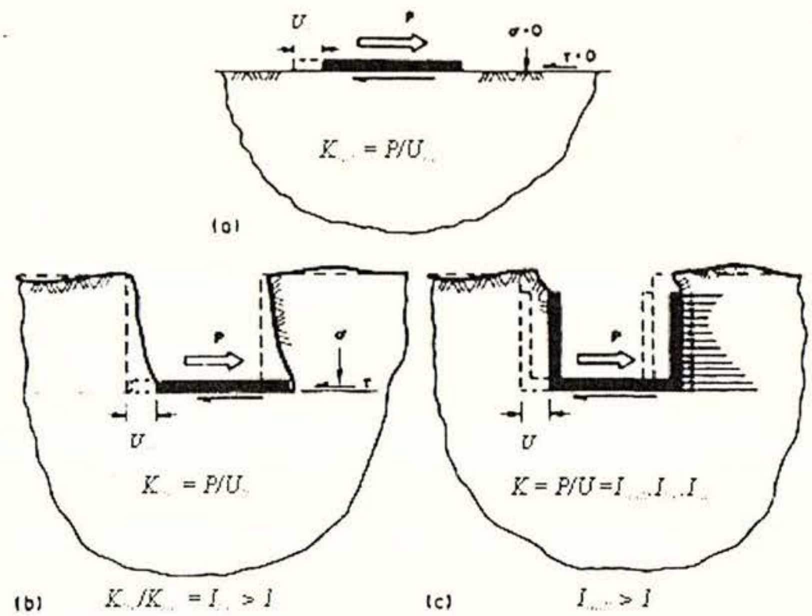

Figure 1.4. Diagram showing the components of resistance used by Gazetas and Tassoulas (1987): (a) Horizontally displaced surface foundation, (b) "trench" effect, (c) Combined "sidewall contact" and "trench" effects

$$K_{embedded} = {}_{wall}I_{trench}K_{sur} \tag{1.3}$$

in which:

$K_{embedded}$ =	the horizontal static stiffness of a rectangular embedded foundation
I_{wall} =	multiplier accounting for the contact of the sides of the foundation with soil due to the embedment
I_{trench} =	Multiplier accounting for the increase in stiffness of a flat surface when pushed along ground at some level of embedment as opposed to on a free surface
K_{sur} =	The horizontal static stiffness of a rectangular surface foundation

An equation resulting from the parametric study of the static stiffness is shown below:

$$\frac{k}{k_{x.sur}} \approx \frac{k}{k_{y.sur}} \approx I_{tre}I_{sur} \approx \left(1+0.15\sqrt{\frac{D}{B}}\right)\left[1+0.52\left(\frac{h}{B}\frac{A_w}{L}\right)^{0.4}\right] \tag{1.4}$$

in which:

D = depth of embedment to base of foundation

B = half the width of the foundation

h = depth to centre of foundation

L = half the length of the foundation

A_w = area of vertical sidewall in contact with soil

In order to evaluate dynamic effects, a variable dynamic multiplier was applied to the static stiffness. For embedded foundations testing was done for varying L/B for both K_y and K_x (K_y is stiffness parallel to the length of the foundation, and K_x is stiffness to orthogonal to length of foundation). It was shown that by increasing the ratio L/B the dynamic stiffness of the foundation decreased markedly. Interestingly, when the ratio D/B was increased, the stiffness of the foundation decreased under most frequencies of loading. This was attributed to the fact that although the horizontal stiffness was growing with increasing D/B, the effective inertia of the foundation was increasing more rapidly.

The result of that work is a series of simple design calculations that can be utilised to calculate the horizontal static and dynamic stiffness of arbitrarily-shaped foundations if certain material properties are known. These properties include: The shear wave velocity, Poisson ratio, density, and shear modulus of the soil.

1.3 Centrifuge testing of lateral loading on square embedded footings

Research into the behaviour of shallow foundations with respect to both lateral and vertical bearing capacity has been carried out using centrifuges. Centrifuge testing allows for the modelling of soil behaviour using scale models. Although there is much data available from real earthquakes, this data normally lacks information about how the foundation behaved during the earthquake and, therefore, about the mechanism of failure.

Gadre and Dobry (1998) carried out important work that isolated the contributions of base and side shearing and active and passive pressures. Seven tests were carried out, varying not only the components resisting the lateral movements, but also the vertical loading on the foundation. A centrifugal acceleration of 30 g was applied to the models as they were tested. This meant that all values were multiplied by 30 to get the prototype (or full-scale) values, and force values were correspondingly multiplied by 30 squared. The model dimensions were 38 mm x 38 mm x 28 mm to simulate a

1.14 m x 1.14 m x 0.84 m foundation footing. This was a static test as one second in model time corresponded to 30 seconds in prototype time; meaning that the loading was applied very slowly. Six load cycles were applied for each test, beginning a 3 mm of prototype displacement and increasing to an amplitude of as much as 110 mm in the final load cycle. It is interesting to note that this was approximately 0.1 times the width of the foundation.

When the testing was carried out it was noted that significant degradation of stiffness occurred at around 25 mm of prototype displacement, and that ultimate lateral capacity was reached at somewhere between 40 mm and 50 mm of prototype displacement. It could be seen that when base shear was isolated as the only component resisting lateral movement, that by doubling the vertical force the ultimate lateral capacity was doubled. When only the friction of the soil on the sides of the foundation was imposed the lateral load resistance of the foundation was relatively low, perhaps indicating that the influence of side friction in this project's experimental work is negligible (Figure 1.5).

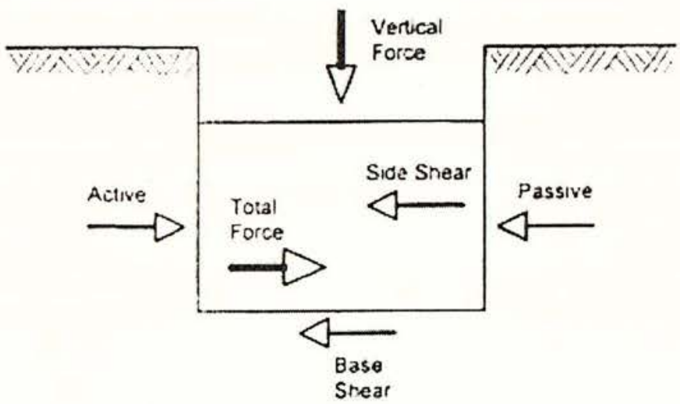

Figure 1.5. Diagram showing the components of resistance isolated in the testing (Gadre and Dobry, 1998).

Tests isolating each of the three components of resistance were carried out before combinations of each were then undertaken. The results are given in Table 1.1.

Table 1.1 Summary of Experimental Data (Gadre and Dobry, 1998)

Test No.	Base Shear	Sidewall Shear	Passive/Active Force	Vertical Load at the Base (kN)	Ultimate Lateral Capacity (kN)
1	Yes	No	No	53	44
2	Yes	No	No	108	88
3	No	Yes	No	53	38
4	No	No	Yes	53	124
5	No	Yes	Yes	53	165
6	Yes	Yes	Yes	53	214
7	Yes	Yes	Yes	108	245

It is significant to the results of the current project that the ultimate load capacity of a test containing various contributions appears to be accurately predicted through merely summing the isolated ultimate lateral capacities of each contributing factor.

Also investigated were both the secant stiffnesses of the various tests, and the material damping (as radiation damping was negligible owing to the slowness of the loading). It was found that these also closely observed the additive relationship displayed by the ultimate lateral load capacity.

1.4 Rocking stiffness of embedded foundations

Another paper involving the work of Tassoulas and Gazetas looks at the rocking stiffness of arbitrarily shaped embedded foundations (Hatzikonstantinou et al, 1989). The rocking static and dynamic stiffnesses were evaluated in very much the same manner as in Gazetas and Tassoulas (1987), as this was in fact a continuation of the earlier work on horizontal and vertical stiffnesses.

It was discovered that the trench effect (see the section on horizontal stiffness of arbitrarily-shaped foundations for an explanation of terminology), has very little effect on rocking stiffness and can be regarded as negligible. This is interesting to note as it proved to have a significant effect on the vertical and horizontal stiffnesses in previous work. However, as would be intuitively expected, the contribution of sidewall contact was significant and numerical relationships were established for different foundation geometries.

1.5 Effect of lateral loading on bearing capacity

Although not directly applicable to this project, the effect on bearing capacity as a result of lateral loading was considered to be potentially important. The following papers give an indication of the research in this field over the last 15 years.

In a paper that preceded Gazetas and Tassoulas (1987) "The Horizontal Stiffness of Arbitrarily Shaped Foundations", Gazetas and Dobry (1985) performed a very similar analysis on the vertical response of arbitrarily shaped embedded foundations. A method very similar to that used in the subsequent paper was used to determine both the vertical stiffness and damping coefficients of embedded foundations.

Work was carried out by Sarma and Iossifelis (1990) which established a pseudo-static method to adjust bearing capacity factors for seismic loading (an adjustment to the Terzagi-Buisman bearing capacity formula). The idea behind this research was to include the effect of the inertia of the soil mass under the footing.

Later, Richards et. al. (1993) proposed a simple design procedure by using Newmark's sliding-block method to determine bearing capacity factors. This research used Coulomb's failure mechanism for retaining walls and Newmark's sliding block to calculate displacements. The classic Prandtl failure surface used in the Terzaghi-Buisman bearing capacity formula was simplified to a triangular failure mechanism in order to determine new bearing capacity factors from the resulting two coulomb wedges. This research indicated that a threshold acceleration can be determined at which foundation settlement occurs due to what is referred to as "shear fluidisation". One can therefore approach the problem by considering two sliding blocks and where movement only occurs incrementally when a seismic pulse exceeds a critical value.

This idea is a progression from the paper published by Richards et al. (1990) that discussing a critical level of acceleration at which the properties of the soil change resulting in "seismic shear fluidisation". This is not the same as liquefaction as it is not reliant on excess pore pressures, but can result in excess pore pressures that will in turn trigger liquefaction. When liquefied, the soil behaves as a viscous fluid.

The work of Zeng and Steedman (1998) made use of centrifuge testing to show a high correlation between accumulated rotation of the foundation and failure. The results from the testing did not prove to be consistent with Newmark's sliding block method, although this could be attributed to lack of vertical acceleration. While the testing was done with saturated soil, the permeability was so high that excess pore pressures were not developed. The most interesting observation from the testing was that failure occurred when the level of shaking was still high, but past its peak, while the level of accumulated rotation was highest (see Figure 1.6). This result differs from the ideas of Richards et. al. (1993) where the greatest movement was thought to coincide with the peak acceleration of the earthquake.

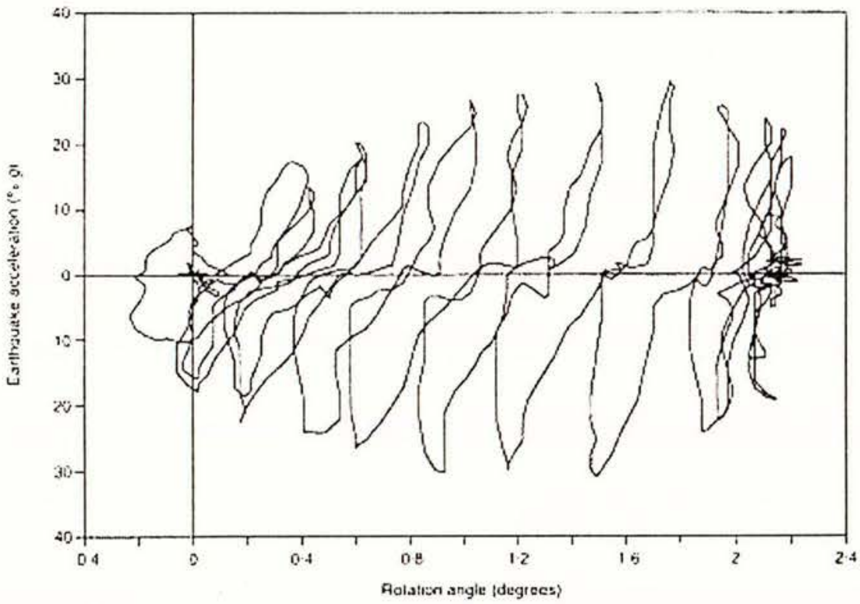

Figure 1.6. Graph showing the relationship between earthquake acceleration androtation for an embedded foundation beam (from Figure 12 of Zeng and Steedman, 1998).

1.6 Lateral resistance of piles

Estimating the lateral resistance of piles is one of the more difficult challenges of geotechnical engineering. Resistance depends not only on properties of the soil but significantly on structural properties of the pile. Pile head deflections may be large so that some soil will be highly strained and yielding and gaps may form between the pile and soil near the surface, while at depth the soil is only lightly stressed (Figure 1.7). The pile itself may yield at relatively low load levels and so good knowledge of the un-cracked, cracked, and strain hardening characteristics of the pile need to be well understood and accounted for.

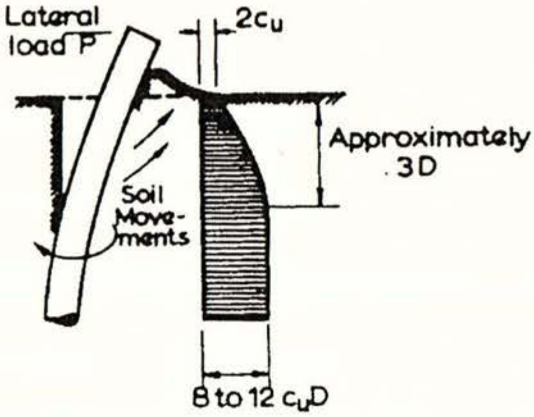

Figure 1.7. Distribution of lateral resistance(after Poulos and Davis, 1980)

Methods of estimating lateral capacities of pile foundations fall generally into one of three categories: (a) methods for estimating ultimate capacity based on limiting equilibrium; (b) methods for estimating displacements at modest load levels based on elastic theory and pseudo-elastic approaches using Winkler springs; and (c) methods for estimating the complete load-displacement response using elasto-plastic Winkler springs.

1.6.1 Ultimate Capacity by Limiting Equilibrium

1.6.1.1 Broms's Theory

The most familiar method for estimating ultimate lateral capacity of piles is that proposed by Broms (1964a and1964b). This method assumes that the full passive resistance of the soil is mobilised. Soils are idealised as being either cohesive or non-cohesive, pile heads are either fully restrained or free, and piles hinge at known yield moments. The following summary has been extracted from Poulos (1980).

Assumed failure mechanisms for free-head piles in cohesive soils are shown in Figure 1.8. The soil to a depth of 1.5 diameters is assumed not to contribute to lateral resistance and below that depth the ultimate lateral resistance is assumed to be constant at 9 C_u , these values being based on empirical evidence. From Figure 1.8 and consideration of statics the following equations may be derived:

$$f = \frac{H_u}{9c_u d} \tag{1.5}$$

in which f is the location of zero shear in the pile and thus gives location of the maximum bending moment,

$$M_{max} = H_u(e + 1.5d + 0.5f) \tag{1.6}$$

also,

$$M_{max} = 2.25dg^2c_u \tag{1.7}$$

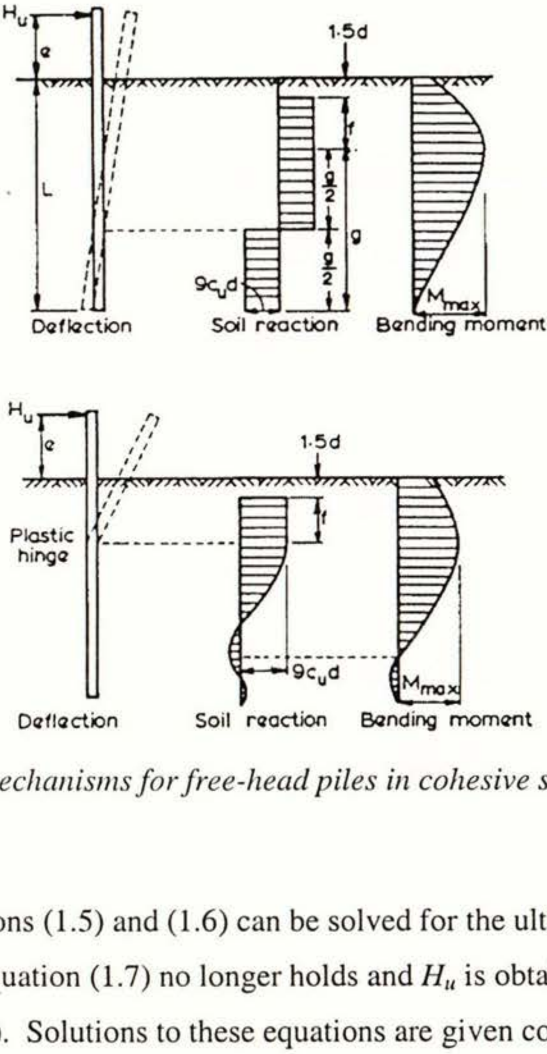

Figure1.8. Failure mechanisms for free-head piles in cohesive soil [Broms, 1964(a)]

For short piles Equations (1.5) and (1.6) can be solved for the ultimate lateral load, H_u. For long piles, Equation (1.7) no longer holds and H_u is obtained by setting M_{max} = M_y in Equation (1.6). Solutions to these equations are given conveniently in Figure 1.9.

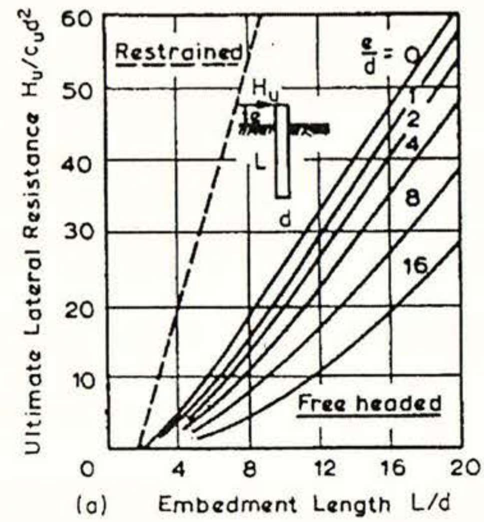

(a) Short Piles

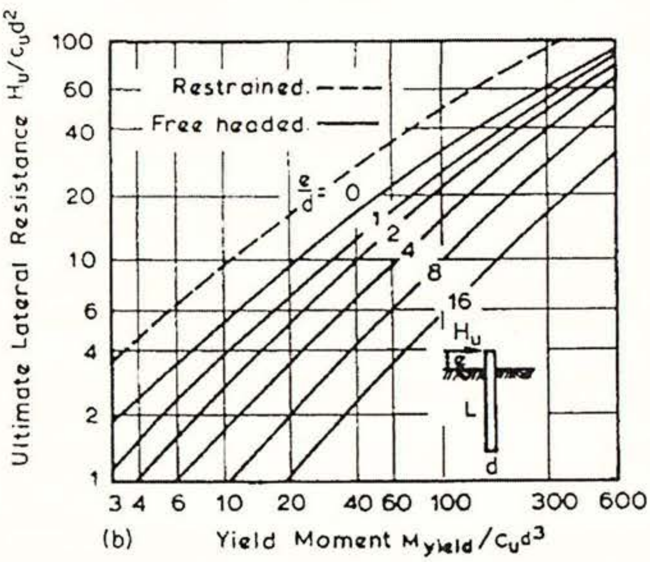

(b) Long Piles

Figure 1.9. Ultimate lateral resistance in cohesive soils:(after Broms, 1964)

Assumed failure mechanisms for fixed-head piles in cohesive soils are shown in Figure 1.10. For fixed-head piles either one, two, or no hinges may form in the pile depending on the relative length of the pile.

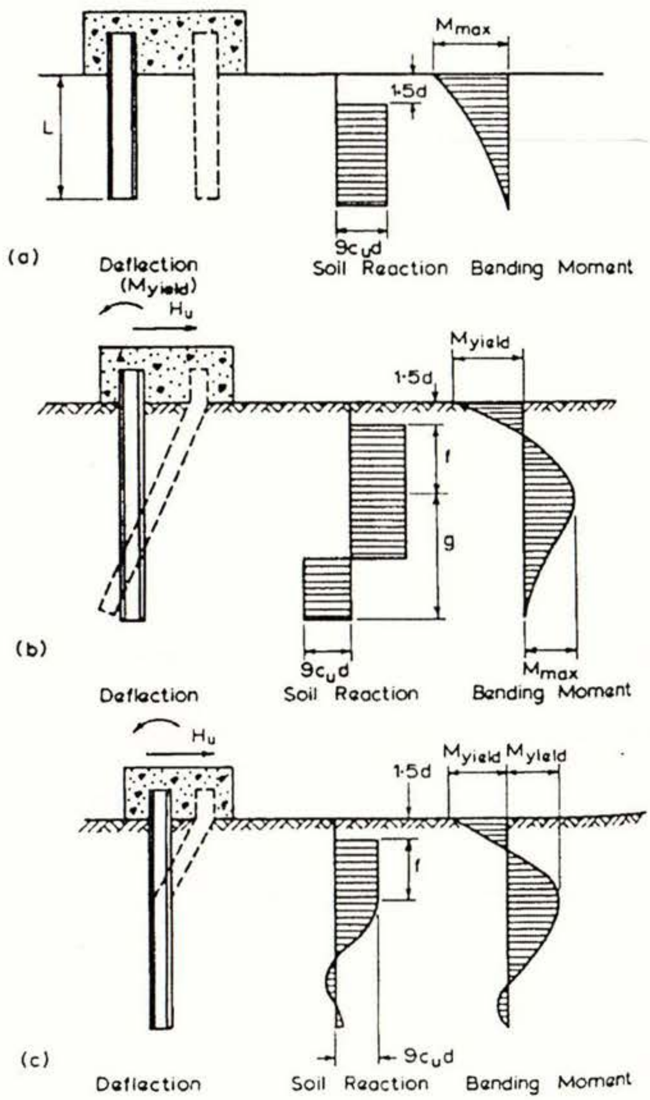

Figure 1.10. Restrained piles, in cohesive soil: (a) short,(b) intermediate, (c) long (after Broms, 1964a)

Again, from considerations of statics, the following equations may be derived. For short, strong piles:

$$H_u = 9c_u D(L - 1.5D) \tag{1.8}$$

$$M_{\max} = H_u(0.5L + 0.75d) \tag{1.9}$$

For "intermediate" piles, hinging occurs at the pile head and the following equation may be derived:

$$M_y = 2.25c_u dg^2 - 9c_u df(1.5d + 0.5f) \qquad (1.10)$$

This equation, together with the relationship $L = 1.5d + f + g$, may be solved for H_u. It is necessary to check that the maximum positive moment is less than M_y otherwise two hinges will form and the mechanism of Figure 1.10 (b) applies with the following relationship:

$$H_u = \frac{2M_y}{(1.5d + 0.5f)} \qquad (1.11)$$

Solutions for fixed-head piles in cohesive soils are given conveniently in Figure 1.9.

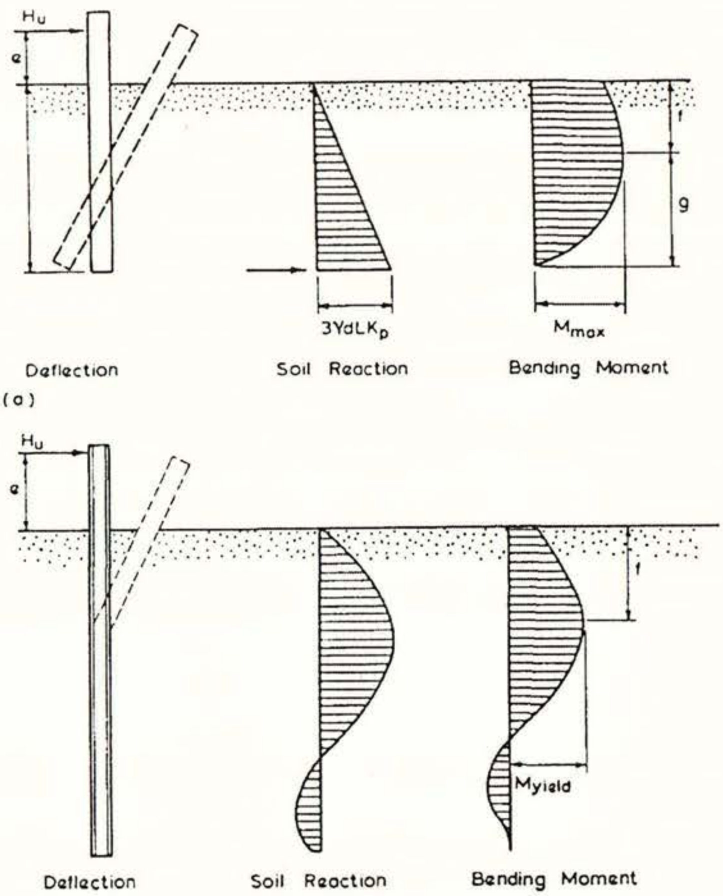

Figure 1.11. Free-head piles in a cohesionless soil

For piles in cohesionless soils, the following assumptions are made in the analysis by Broms(1964b) based on limited empirical evidence:

1. The active earth pressure acting on the back of the pile is neglected.

2. The distribution of passive pressure acting on the front face of the pile is equa to three times the Rankine passive pressure.

3. The shape of the pile section does not matter.

4. The full passive resistance is mobilised at the movement considered.

Assumed failure mechanisms for free-head piles in non-cohesive soils are shown in Figure 1.11. For short, strong piles that do not yield, the pile is assumed to rotate about a point close to the tip, and the high pressures acting near this point are replaced by a single concentrated force at the tip. Again, statics are used to derive the following equation:

$$H_u = \frac{0.5\gamma DL^3 K_p}{(e+L)} \tag{1.12}$$

The maximum bending moment in the pile must be checked to ensure that hinging does not occur. The maximum moment occurs at depth f, the location of zero shear in the pile, where:

$$H_u = \frac{3}{2}\gamma dK_p f^2 \tag{1.13}$$

and the maximum moment is:

$$M_{max} = H_u\left(e + \frac{2}{3}f\right) \tag{1.14}$$

For cases where hinging occurs, H_u may be calculated by setting and solving equations 1.13 and 1.14 simultaneously. Solutions to these equations are conveniently provided in Figure 1.12.

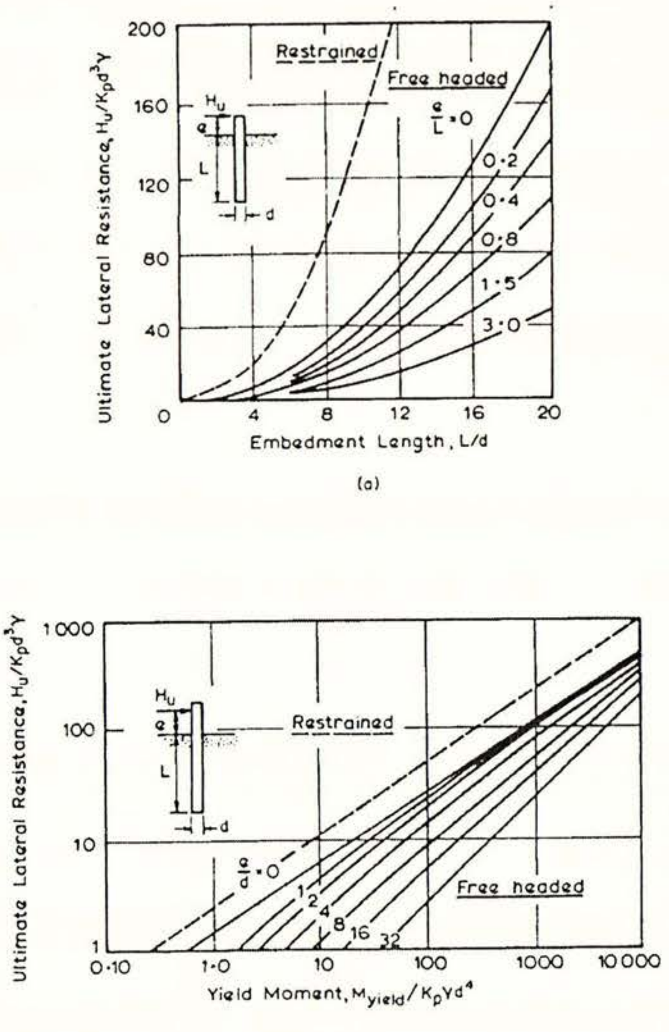

Figure 1.12. Ultimate lateral resistance of piles in non-cohesive soils (a) short; (b) long (after Broms, 1964b)

Assumed failure mechanisms for free-head piles in non-cohesive soils are shown in Figure 1.13. Again, piles may have one, two, or no hinges, depending on the relative length of the pile. For a short, strong pile that does not hinge, the following equation may be derived from statics:

$$H_u = 1.5\gamma L^2 d K_p \tag{1.15}$$

The bending moment under the pile cap must be checked to ensure that hinging does not occur. The maximum moment under the cap is given by:

$$M_{\max} = \frac{2}{3} H_u L \tag{1.16}$$

If a hinge forms under the pile cap then the failure mode of Figure 1.13 (b) is assumed. For horizontal equilibrium:

$$F = \frac{3}{2} \gamma d L^2 K_p - H_u \tag{1.17}$$

Thus:

$$M_y = 0.5 \gamma d L^3 K_p - H_u L \tag{1.18}$$

which yields a solution for H_u. The maximum moment in the pile at depth f, given by Equation 1.13, should also now be checked to see if a second hinge forms. More simply, the assumption of two hinges can be made with the resulting value of H_u given by:

$$2M_y = H_u \left(e + \frac{2}{3} f \right) \tag{1.19}$$

The lesser value of H_u given by Equations 1.18 and 1.19 will be correct. Solutions to these equations are conveniently given in Figure 1.12.

1.6.1.2 Brinch Hansen's Theory

The work of Brinch Hansen (1961) pre-dates the work of Broms (1964a and 1964b) but is less familiar, probably because it was difficult to implement prior to the widespread use of personal computers. The ultimate soil resistance to pile movement is given for the general case of a c - ϕ soil as a function of depth according to the expression:

$$p_u = \overline{q} K_q + c K_c \tag{1.20}$$

in which:

$\overline{q}$ = effective vertical overburden pressure

c = cohesion

K_c , K_q = earth pressure coefficients.

K_c and K_q are plotted in Figure 1.14, while the limiting values for the ground surface and for infinite depth are plotted in Figure 1.15.

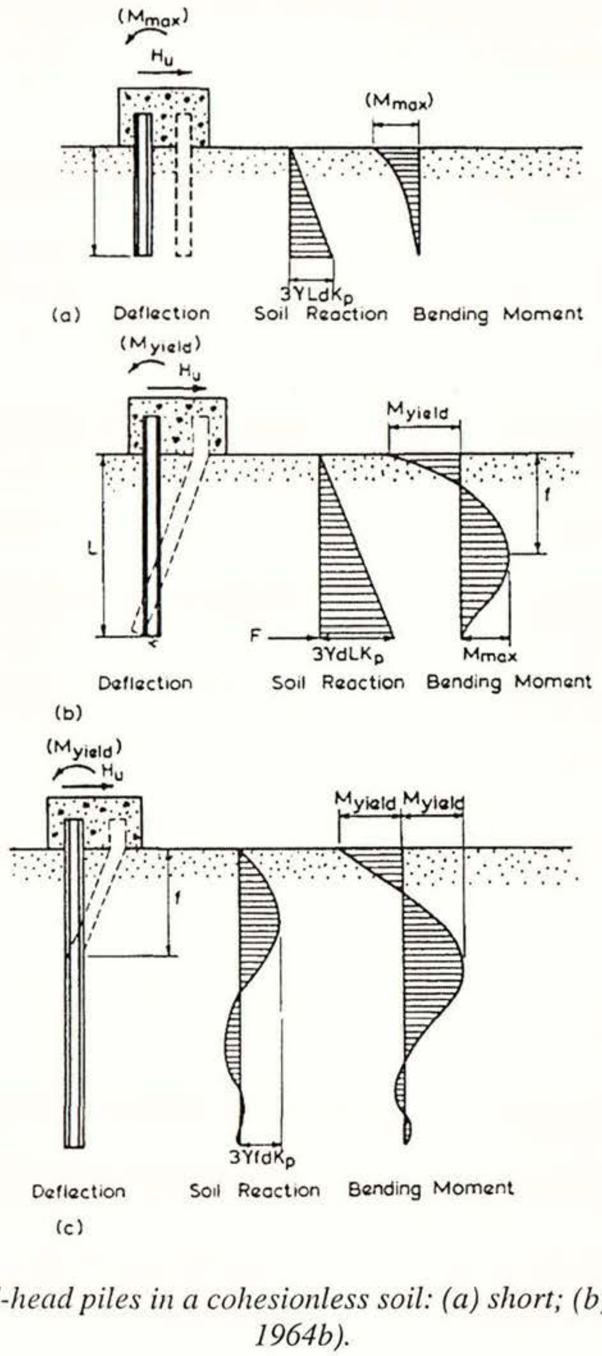

Figure 1.13. Fixed-head piles in a cohesionless soil: (a) short; (b) long (after Broms, 1964b).

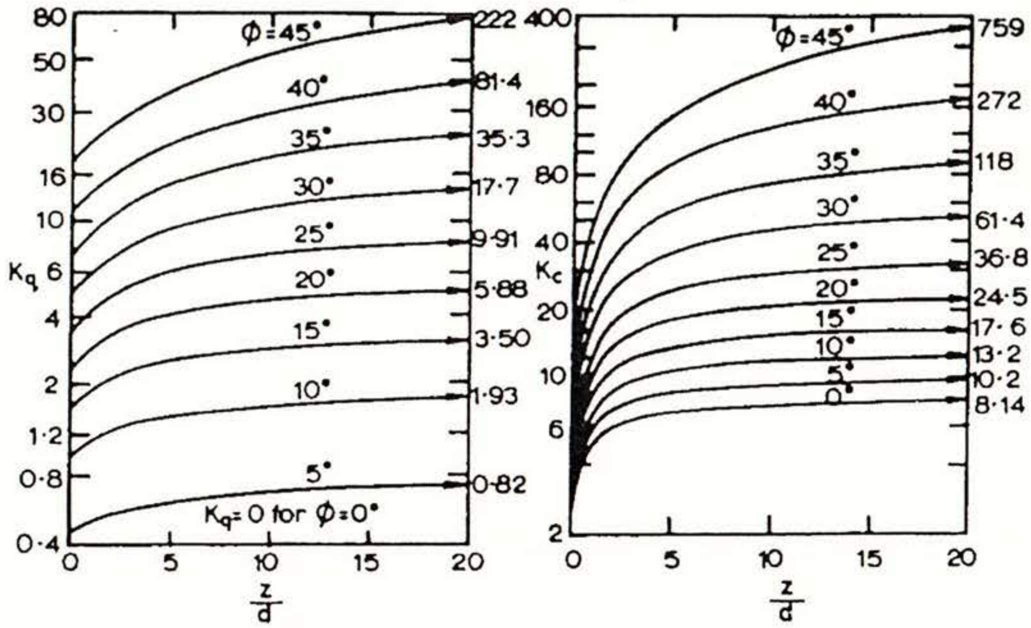

Figure 1.14. Lateral resistance factors K_q and K_c (after Brinch Hansen, 1961)

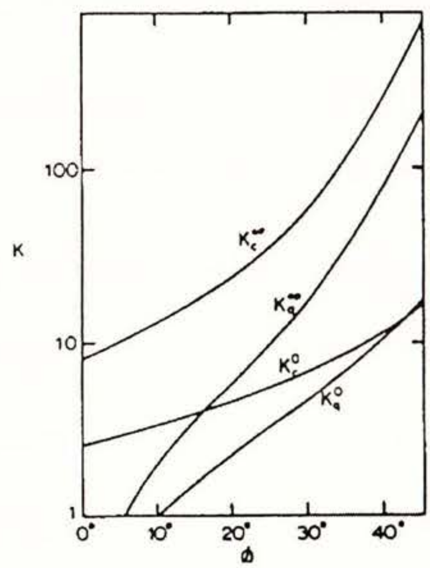

Figure 1.15 Lateral resistance factors at ground surface and at great depth (after Brinch Hansen, 1961)

The analysis was based on a combination of solutions: At shallow depth, earth pressure theory for a rough retaining wall was used, for intermediate depths solutions for a smooth wall were used, and at greater depths a plasticity solution for a deep strip footing was used. The final profile for lateral soil resistance with depth is developed from an empirical curve fit to all three conditions. Values of K_c and K_q may be calculated from the following equations:

$$K_q = \frac{K_q^0 + K_q^\infty a_q \dfrac{D}{B}}{1 + a_q \dfrac{D}{B}} \tag{1.21}$$

$$K_c = \frac{K_c^0 + K_c^\infty a_c \dfrac{D}{B}}{1 + a_c \dfrac{D}{B}} \tag{1.22}$$

in which D = depth, B = foundation width, and :

$$K_q^0 = e^{(\frac{\pi}{2}+\phi)\tan\phi} \cos\phi \tan\left(\frac{\pi}{4}+\frac{\phi}{2}\right) - e^{-(\frac{\pi}{2}-\phi)\tan\phi} \cos\phi \tan\left(\frac{\pi}{4}-\frac{\phi}{2}\right) \tag{1.23}$$

$$K_c^0 = \left[e^{(\frac{\pi}{2}+\phi)\tan\phi} \cos\phi \tan\left(\frac{\pi}{4}+\frac{\phi}{2}\right) - 1 \right] \cot\phi \tag{1.24}$$

$$K_c^\infty = N_c d_c^\infty \tag{1.25}$$

$$K_q^\infty = K_c^\infty \cdot K_0 \tan\phi \tag{1.26}$$

$$N_c = \left[e^{\pi\tan\phi} \tan^2\left(\frac{\pi}{4}+\frac{\phi}{2}\right) - 1 \right] \cot\phi \tag{1.27}$$

$$K_0 = 1 - \sin\phi \tag{1.28}$$

$$d_c^\infty = 1.58 + 4.09 \tan^4\phi \tag{1.29}$$

A rigorous limiting equilibrium analysis is possible using the resulting values of p_u by using the approach indicated in Figure 1.16. However, since p_u varies continuously with depth, the analysis is complex and is best obtained by using a computer based numerical integration algorithm. The centre of rotation may be determined by trial and error, invoking rotational equilibrium about the point of load application.

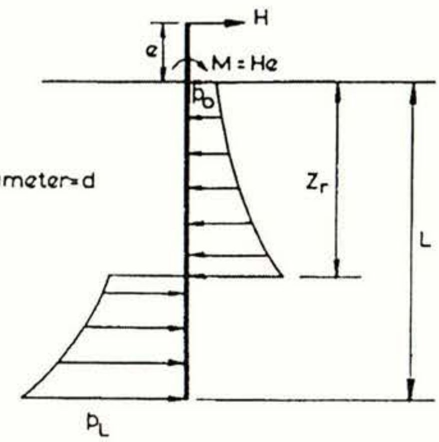

Figure 1.16. Unrestrained laterally loaded pile (after Poulos, 1980).

Variations in soil properties with depth may readily be incorporated into the analysis, which is a significant advantage over the more simple analysis of Broms. The major limitation is the necessary assumption that the pile is rigid and does not yield.

1.6.2 Load-Displacement by Elastic Analysis

1.6.2.1 Subgrade-reaction analysis

Subgrade-reaction analysis, commonly called "Winkler" analysis after the original proponent of the technique, characterises the soil as a series of linear-elastic springs

$$p = k_h \rho \qquad (1\text{-}30)$$

in which p = pressure, ρ = displacement, and k_h = the modulus of subgrade reaction with units of force/length^3.

$$E_p I_p \frac{d^4 \rho}{dz^4} = -pd \qquad (1.31)$$

in which E_p = modulus of elasticity of the pile, I_p = moment of inertia of the pile, z = depth in soil, and d = width of the pile.

$$E_p I_p \frac{d^4 \rho}{dz^4} + k_h d\rho = 0 \qquad (1.32)$$

$$\frac{d^2 M}{dz} + (P_z)\frac{d^2 \rho}{dz^2} - p = 0 \qquad (1.33)$$

in which M = moment at depth z, P_z = axial load on pile at depth z, and p = soil reaction per unit length.

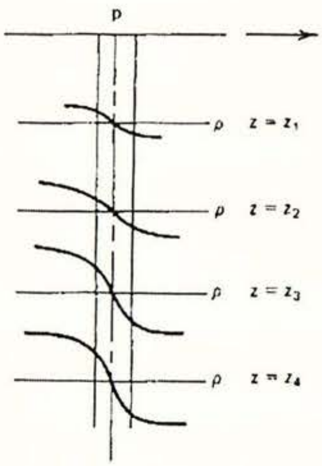

Figure 1.17. Concept of p-y or p-ρ curves (Poulos, 1980).

Elastic solutions in which the soil has been considered as an elastic continuum have been developed by various authors and are summarised by Poulos (1980). The pile is assumed to be a thin rectangular vertical strip with constant flexibility. Solutions for the ground line displacement, ρ, and rotation, θ, for single free-head piles in soil with constant soil modulus are given by:

$$\rho = \frac{H}{E_s L}\left(I_{\rho H} + \frac{e}{L}.I_{\rho M}\right)\frac{1}{F_\rho} \tag{1.34}$$

in which $I_{\rho H}, I_{\rho M}$ =elastic influence factors for constant soil modulus, E_s, and F_ρ= yield displacement factor (ratio of pile displacement in elastic soil to pile displacement in yielding soil.)

$$\theta = \frac{H}{E_s L^2}\left(I_{\theta H} + \frac{e}{L}.I_{\theta M}\right)\frac{1}{F_\theta} \tag{1.35}$$

in which $I_{\theta H}, I_{\theta M}$ =elastic influence factors for constant soil modulus, E_s , and F_ρ= yield displacement factor (ratio of pile displacement in elastic soil to pile displacement in yielding soil.)

Values for influence factors are given as a series of graphs by Poulos (1980).

Solutions for the ground line displacement, ρ, for single fixed-head piles in soil with constant soil modulus are given by:

$$\rho = \frac{H}{E_s L}\left(I_{\rho F}\right)\frac{1}{F_{\rho F}} \tag{1.36}$$

in which, $I_{\rho F}$ =elastic influence factor and $F_{\rho F}$ =yield displacement factor to account for soil non-linearity.

Solutions for the ground line displacement, ρ, and rotation, θ, for single free-head piles in soil with linearly increasing soil modulus are given by:

$$\rho = \frac{H}{N_h L^2}\left(I'_{\rho H} + \frac{e}{L}.I'_{\rho M}\right)\frac{1}{F'_\rho} \tag{1.37}$$

in which $I'_{\rho H}, I'_{\rho M}$ =elastic influence factors for linearly varying soil modulus, E_s, and N_h = rate of increase of soil modulus E_s with depth.

$$\theta = \frac{H}{N_h L^3}\left(I'_{\theta H} + \frac{e}{L}.I'_{\theta M}\right)\frac{1}{F'_\theta} \tag{1.38}$$

in which $I'_{\theta H}, I'_{\theta M}$ =elastic influence factors for linearly varying soil modulus, E_s, and N_h = rate of increase of soil modulus E_s with depth. Solutions for the ground line displacement, ρ, for single free-head piles in soil with linearly increasing soil modulus are given by:

$$\rho = \frac{H}{N_h L^2}\left(I'_{\rho F}\right)\frac{1}{F'_{\rho F}} \tag{1.39}$$

in which, $I'_{\rho F}$ =elastic influence factor and $F'_{\rho F}$ =yield displacement factor to account for soil non-linearity.

2 SLIDING OF SLAB ON GRADE

The simplest shallow foundation is a concrete slab poured on grade, usually with either one or two layers of polymer damp course (DPC). Also, more complex foundations with foundation beams and other elements often incorporate slabs poured on grade. It is important, therefore, to understand the sliding characteristics of such systems as a first step in characterising the lateral resistance of shallow foundations. In this study, large-size tests were undertaken to determine the sliding characteristics of slab on grade foundations using construction details common to New Zealand practice.

2.1 Construction Details

Concrete slabs 2 m wide x 3 m long x 135 mm thick were constructed without edge beams but otherwise using standard construction details and materials. One and two layers of DPC were used and some slabs were weighted with ballast. Each test slab was forced to slide back and forth parallel to its long axis while measurements of force and displacement were taken. A diagram of the test set-up is given in Figure 2.1.

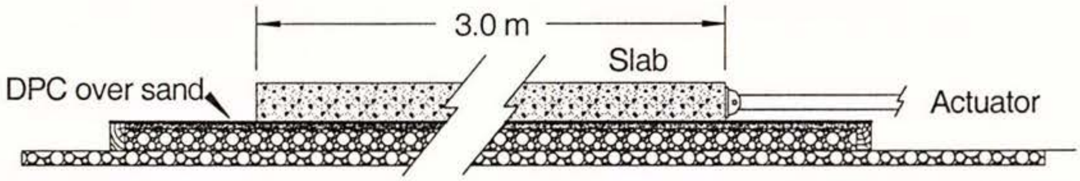

Figure 2.1. Section showing details of base sliding tests.

A wooden frame 3 m wide by 4 m long by 100 mm deep was constructed first. This was filled with pit-run granular material topped with a 25 mm thick sand blinding. The sand surface was levelled by screeding and then the DPC was rolled out and stapled to the wooden frame. The concrete slab then was constructed by pouring concrete into a steel form lying on top of the DPC. The concrete was cured for several days and then a hydraulic actuator was bolted to the slab and anchored to an adjacent large-size pile head. A 100 KN load cell was used to measure the force required to cause sliding while slab movement was monitored by a displacement transducer. Data was recorded electronically. A view of a completed slab ready for testing is shown in Figure 2.2.

Figure 2.2. View of a completed slab ready for testing.

A simple test procedure was used as follows: each slab was pushed slowly, driven by a hand operated hydraulic pump, for 25 mm in one direction. Then the pump direction was reversed and the slab was dragged back to its starting position. Three or four cycles of load were applied in similar fashion until a steady load-displacement response was achieved. The results are summarised in Table 2.1.

Table 2.1. Base sliding friction for "slab-on-grade" foundations.

Foundation Type	Contact Pressure (KPa)	Peak Friction Angle (degrees)	Mean Friction Angle (degrees)
Single Layer DPC	3.0	23	21
	6.6	28	26
Two Layers DPC	3.1	12	10
	6.2	24	22

For some tests, the slab was ballasted by laying a previously tested slab on top supported on timbers laid at quarter points, effectively doubling the interface contact pressure. All tests were conducted on freshly made slabs.

2.2 Sliding Test Results

For a single layer of DPC, there was a slight increase in friction with increased surcharge, probably caused by indentation of the sand grains into the soft material of the membrane. Some scuffing of the DPC was evident after testing.

Placing two layers of DPC resulted in halving of the interface friction angle for the single slab without ballasting. However, ballasting of the slab to 6.2 KPa caused the interface friction to increase significantly and to be nearly the same as for a single layer of DPC. This result is surprising and no explanation is immediately obvious. A small amount of "bulldozing" of sand occurred in front of each slab (as shown in Figure 2.3) as it was pushed back and forth, more for the ballasted slabs than the non-ballasted slabs. However, the effect of such "bulldozing" should be the same whether one or two layers of DPC were used. Further testing of interface friction using increased weights of ballast are recommended to investigate this phenomenon.

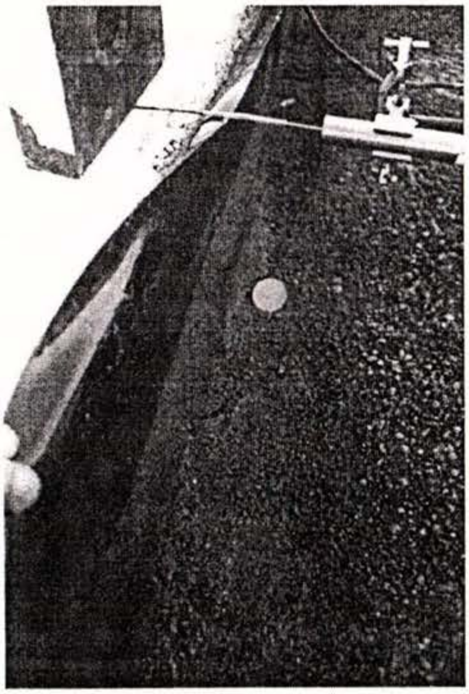

Figure 2.3. Typical view of "bulldozing" of sand adjacent to slab after testing.

A view of the sand substrate after completion of testing and removal of a test slab is shown in Figure 2.4.

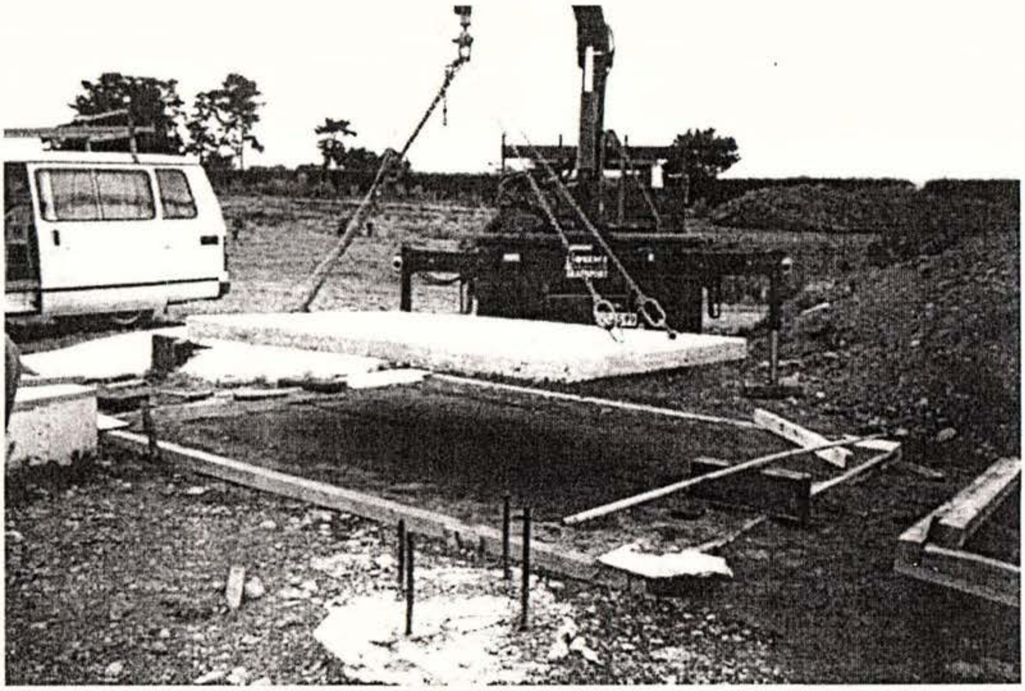

Figure 2.4. View of sand substrate after completion of a test and removal of test slab.

3 SLAB AND BEAM EXPERIMENTS

Few foundations are ever made that consist only of "slab-on-grade" with no down turned foundation beams of some type. Most shallow foundations have foundation beams of some description together with floor slabs that are either suspended or built "on-grade". Even when slabs are built "on-grade" they usually are structurally connected to the foundation beams, or should be. Isolated pad foundations supporting individual columns may also be part of a foundation design and sometimes these will not be inter-connected using beams. However, most foundations will have perimeter beams at least and it is beams that offer most potential for generating passive resistance to lateral movements.

A main objective of this study was to investigate the interaction between the passive resistance to lateral movement generated against vertical embedded surfaces such as beams and attached horizontal surfaces such as floor slabs. Therefore, a simplified structure consisting of two parallel foundation beams connected by a floor slab constructed "on-grade" was designed to incorporate the essential features of interest. The structures were built as large as practicable given the limitations of available hydraulic actuators and field reaction points, the intention being to simulate behaviour at full-scale. This section describes in detail the three tests that were carried out in this study.

3.1 The test site

The test site was a little used gravel pit immediately west of the city of Christchurch. The test site material is the Halkett member of the Springston Formation, of recent geologic age. The soil comprises fluvial gravel, sand, and a small fraction of silt, all largely derived from the degradation of older gravels (Waimakariri River sourced). Inspection of the exposed faces of the gravel pit indicated that the material was superficially uniform, with minimal layering. The depth to water table at the gravel pit was found to be in excess of eight metres, below the intended depth of the piles.

Preliminary investigations at the test site revealed the gravels to be very dense. It was intended to initially use the site for cyclic axial load tests of bored piles and pullout load tests, and, if the bored piles were constructed in such dense material then the pullout loads would be excessive. Therefore, it was decided to loosen the site material by excavating and re-depositing it using heavy earthmoving equipment. A large open pit was excavated to a depth of six metres using an excavator. Then the pit was refilled by carefully replacing the soil with the excavator placing one bucketful at a time with minimum drop. This re-deposition of the material had benefits additional to reduction in density: The soil was mixed and replaced as a more uniform deposit, the soil gradation was better known, the soil in-situ stress state was better known, and any undesirable cementing was removed.

3.2 Soil Properties

During the re-working of the site materials, field density tests were performed by having the excavator deposit soil into large buckets simulating the re-deposition process. These buckets were then weighed and the soil moisture content determined by usual means. The friction angle, ϕ, for the material was determined by testing remoulded soil in a large (355 x 285 x 195 mm) shear box. All of the known soil properties are summarised in Table 3.1. Particle gradation curves are given in Figure 3.1.

Table 3.1. Soil properties at the test site.

Property	Symbol	Value
Bulk unit weight	γ	17.2 KN/m^3
Dry unit weight	γ_d	16.4 KN/m^3
Moisture content	w	4.6 %
Mean particle size	D_{50}	15 mm
Friction angle	ϕ	43°

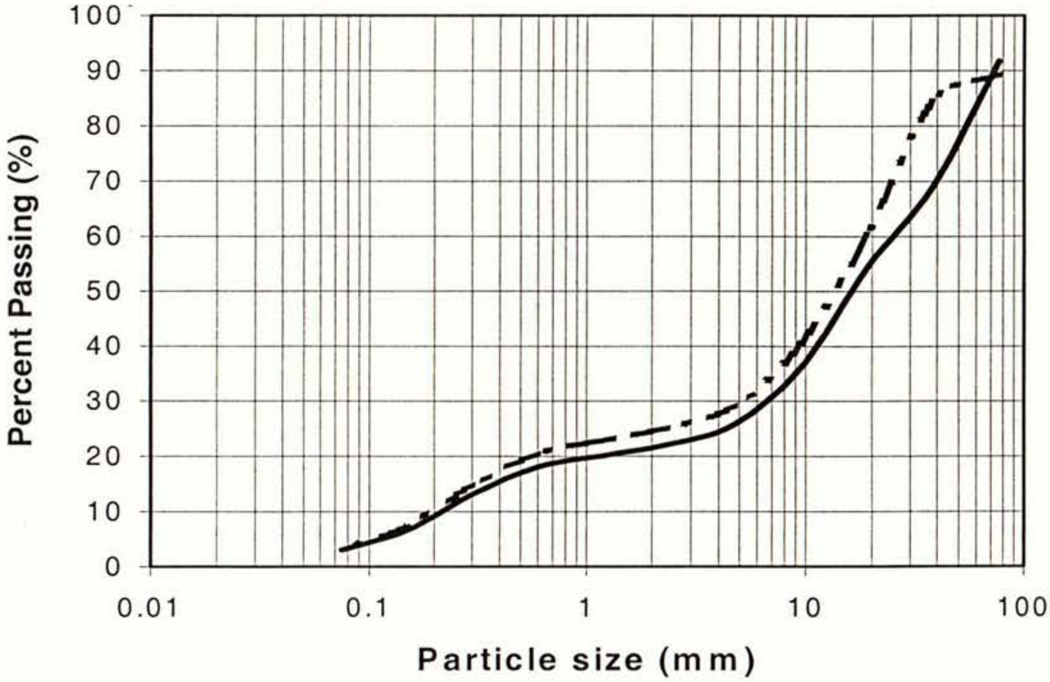

Figure 3.1. Particle gradation curves for the soil of the test site.

For the earlier bored pile testing, nine piles, each of nominal size 750 mm diameter by 5.5 m deep, were constructed on a three-by-three grid at 3.5 m spacing. These were subjected to various axial load regimes but were left undamaged and in place (McManus, 1997). Subsequently, these piles were connected by a rigid pile cap and subjected to lateral shaking tests (McManus and Alabaster, 2004). Again, the piles and pile cap were left undamaged and in place and were used in this study as a convenient reaction block for the lateral loads to be applied to the shallow foundations. Accordingly, the test specimens for this study were constructed adjacent to the existing pile cap, as shown in Figure 3.2.

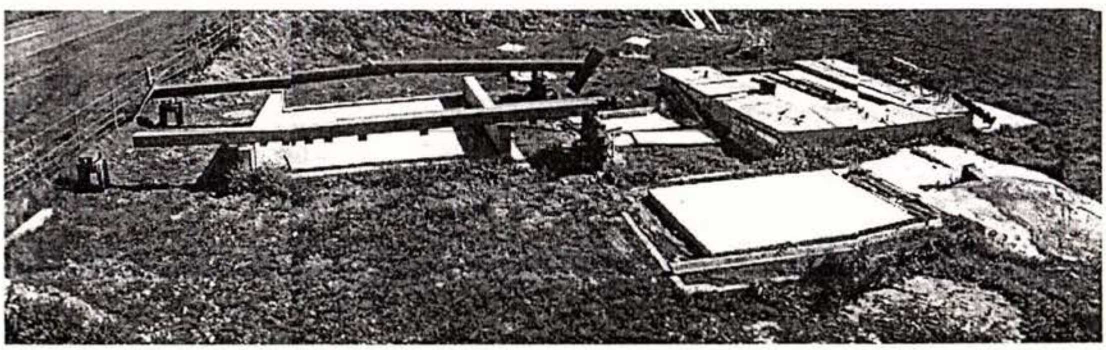

Figure 3.2. A view of the test site showing the fence line (left), test structure 1(centre left) and the reaction pile cap (right rear)

3.3 Construction procedure

Three similar structures were built with typical details given in Figure 3.3. A summary of structural details is given in Table 3.2. The first test was abandoned after unexpected rotations of the structure caused difficulties with the loading system. The second test was successful but a flexural failure occurred in the slab at the connection between the slab and beam and so additional ties were placed between the beam and slab for Test 3.

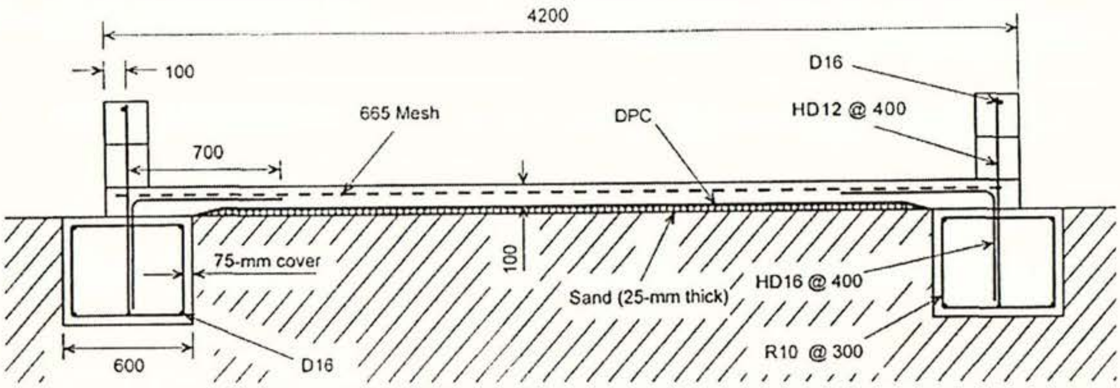

Figure 3.3. Section showing construction details of Test 3.

Table 3.2. Construction details for the slab and beam experiments.

	Test 1 (Preliminary Trial)	**Test 2**	**Test 3**
Additional loading	None	None	63 KN per foundation beam
Loading rig	Designed and built by technician and unsuitable due to tendency to uplift the structure when loaded	Designed with two universal joints and applied load with approximately 150 mm eccentricity to slab centre line	Improved design from Test 2 by ensuring load was essentially applied directly through the centreline of the slab
Concrete strength	17.5 MPa	17.5 MPa	25 MPa for foundation beams (non-critical) and 30 MPa for the slab and masonry wall grout

Slab mesh	668	668	665
Starter bars	HD 12 at 400 mm centres	R 10 at varied spacings	HD 12 at 400 mm centres
Slab ties	None	None	HD 16 at 400 mm centres bent into slab
Polyethylene placement	Continued between slab and foundation beam	Continued between slab and foundation beam	Terminated such that slab concrete could bond with the foundation beams
Soil preparation	Compacted by excavator	Compacted by excavator	Compacted in part by excavator, and in part by hand-operated soil compactor

The soil was first excavated to a depth that corresponded to the bottom of the foundation beams. An area exceeding the dimensions of the structure by at least 1.5 metres was dug out prior to each test, to ensure that the soil was consistently prepared. Once the hole was completely excavated, the excavating machinery was used to carry out compaction of the soil. This was done by a 5.5 tonne Hyundai 553 Excavator "track rolling" the exposed soil in a systematic fashion. The compaction of the underlying soil was not treated as critical, owing to the low level of loading on the test specimens, and the fact that the zone of influence of the foundation movement was at or above this excavation depth.

Next, the formwork for the foundation beams was erected on the prepared ground. Each foundation beam was 600 mm in width, 500 mm in depth and 42100 mm in length. This was a convenient size for construction as commercially available formwork of these dimensions was available. It was considered that 4 metres was a sufficient length of foundation beam to ensure that end effects did not unduly affect the soil structure interaction being investigated.

The reinforcing cage in each beam consisted of four longitudinal D16 bars with R10 stirrups at 300 mm centres. This reinforcing detail contains slightly less steel than a typical commercial foundation detail, but is representative of a foundation beam layout where the loads from the overlying structure are not great. Cover to the reinforcing was 75 mm. A view showing beam formwork in place is given in Figure 3.4.

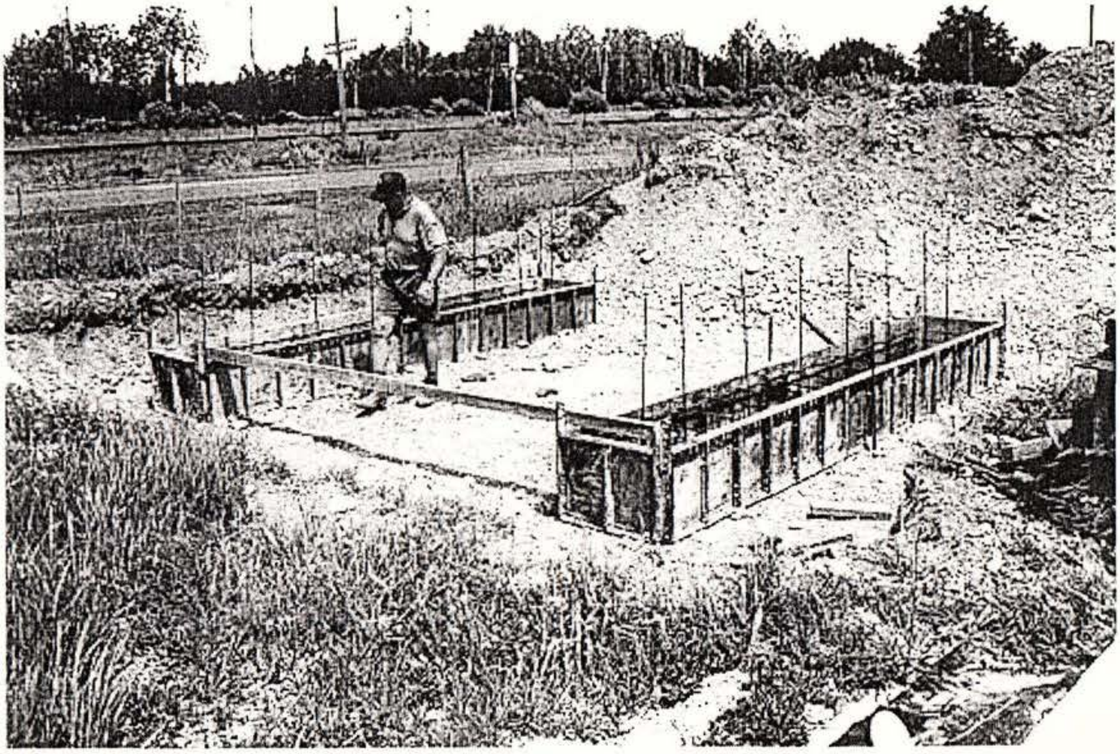

Figure 3.4. Formwork and reinforcing in place for the foundation beams.

Starter bars were designed to begin in the foundation beam and run up through the slab into the masonry wall. For Tests 1 and 3 these bars consisted of HD12 bars at 400 mm centres. Again, this detail was intended to be representative of the typical quantity and type of reinforcing bar used in a foundation detail of this type. A gap of 600 mm was allowed between the two bars at the centre of the foundation beam, in order to allow for the loading beam to pass through, and to create a symmetrical configuration of bars to fit the length of wall being constructed.

At each end of the starter bars the reinforcing was bent to a 90 degree hook with a 150 mm leg. A D16 bar was then run across the top of the wall to stiffen it, in order to minimise any effects that might arise from the artificially premature termination of the wall.

Unfortunately, there was an error as to the type and spacing of reinforcing bars used for the starter bars supplied on site for the construction of Test 2. Test 2 contained R10 starter bars at greater spacing than the other two leading to a reduction of steel area from 1131 mm2 (as used in Tests 1 and 3), to 628 mm2 per foundation beam. Also, the R10 bars had a yield strength of 300 MPa instead of 430 MPa specified and were undeformed. However, the 90o hooks at both ends of each bar provided sufficient anchorage to develop their full strength.

For Test 3, additional slab ties were added to prevent the flexural failure of the slab that occurred in Test 2. In addition to the HD12 starter bars at 400 mm centres, HD16 slab ties were turned into the slab at 400 mm centres and terminated 700 mm from the bend, as shown in Figure 3.3.

Once the concrete beams had cured, the formwork was stripped and the beams were backfilled to a level flush with the top of the foundation beams and compacted, as shown in Figure 3.5.

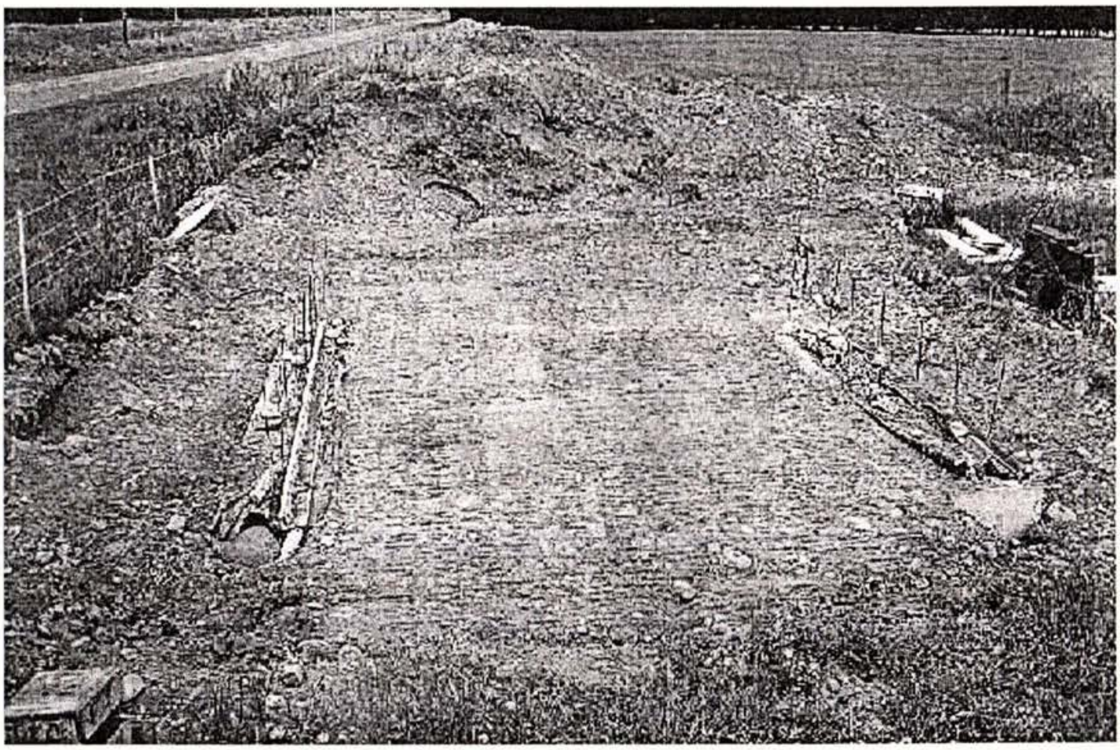

Figure 3.5. View showing the centre of the specimen filled in and compacted by the excavator.

In each of the first two tests the soil was completely filled in and then the soil between the two beams was "track rolled" by the excavator. The soil immediately outside each of the beams was more difficult to compact because of a lack of room between the beams and either the fence line or the nearby piles. So a 2.5 tonne Bobcat 753 Excavator with narrower tracks was used to compact the soil outside of the two beams. However, there was only room for the machine to drive across in one path with its tracks immediately adjacent to the concrete foundation beams. This procedure was repeated similarly for each of Test 1 and 2.

The same procedure could not be used for Test 3 because the HD16 slab ties were required to be pre-bent and they prevented the excavator from "track rolling" the backfill. Therefore, a hand-operated Wacker BS 500 Soil Compactor was used to compact these areas. In all three tests the compaction was carried out all in one operation, after all of the backfill had been placed.

Next, sand blinding of 25 mm thick was placed, the DPC was laid out, formwork prepared, and reinforcing mesh placed in readiness for pouring the slab, as shown in Figure 3.6.

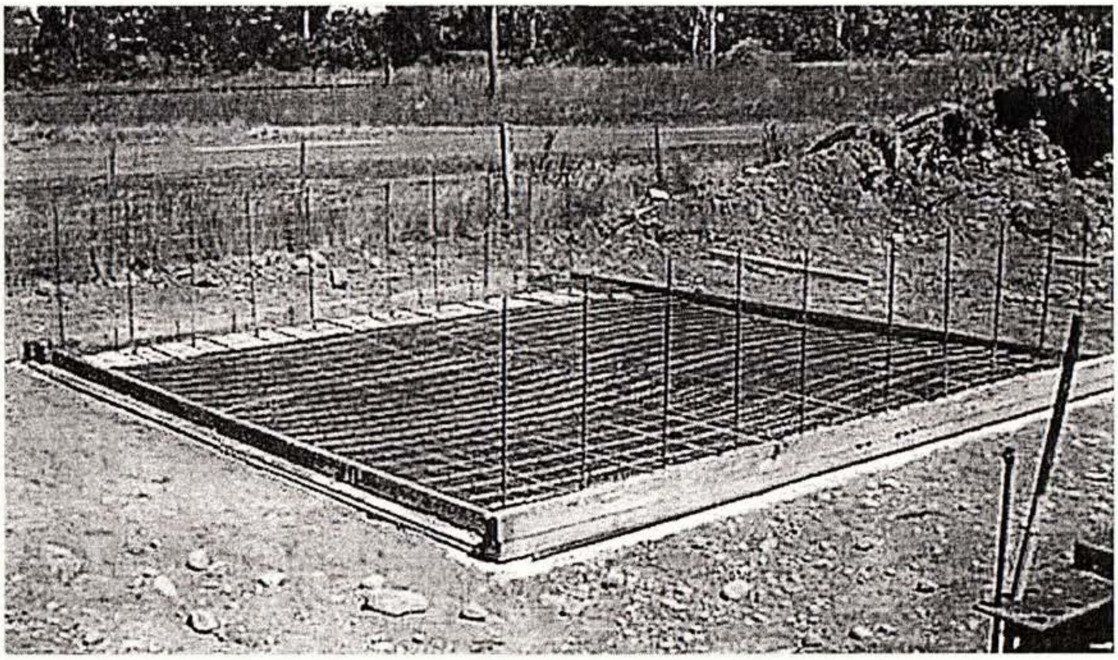

Figure 3.6. Slab ready for pouring, Test 3.

The slabs varied in thickness from 125 mm at each foundation beam to 100 mm in depth for most of the area of the slab spanning between the foundation beams. The transition in thickness occurred in a tapering that began at the inside of each foundation beam and extended approximately 500 mm towards the centre of the structure on both sides. It was intended that 665 mesh was to be used in all three tests as this is the standard mesh size used in slabs of this type. However, the mesh used in the earlier two tests did vary from the prescribed design. The mesh was laid with 50 mm from the top of the slab.

The DPC for the first two tests was carried right over the foundation beams such that the slab concrete could not bond with the foundation beams. This is common for residential foundation details, but may or may not be used for commercial details. Accordingly, the DPC was terminated at the inside edge of the foundation beams for Test 3, to see if there was any observable increase in performance of the structure if bonding was allowed between the slab and foundation beams, as shown in Figure 3.7.

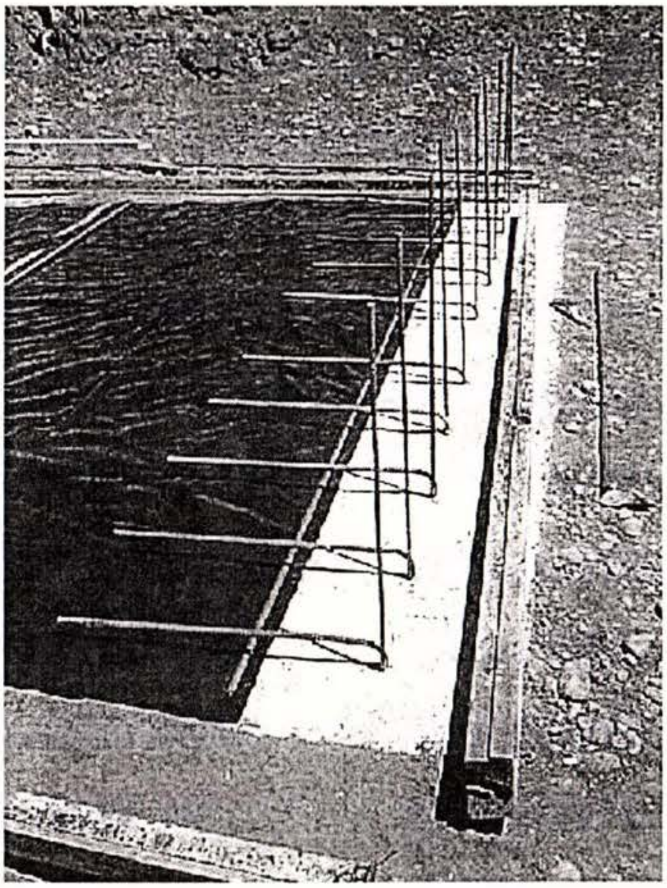

Figure 3.7. View showing the termination of the DPC for Test 3.

To provide anchorage to the slab starter bars, the beginning of a masonry wall was built on top of the slab and beam foundations, as shown in Figure 3.8. The walls were all laid two blocks in height and were fully grouted.

Figure 3.8. View of masonry wall built on top of slab and beam.

3.4 Loading Rig

The loading rig was intended to impose horizontal loading to the structures through the plane of the floor slab, by pushing against the reaction structure consisting of heavy bored piles and pile cap. Displacement controlled, quasi-static loading was applied, consisting of a number of cycles of load applied slowly. The design of the loading rig evolved over the three tests because of unexpected rotations of the test structures during loading. Detailed drawings of each loading rig used are given in Appendix A. The general layout of the loading rig is shown in Figure 3.9 for Test 3.

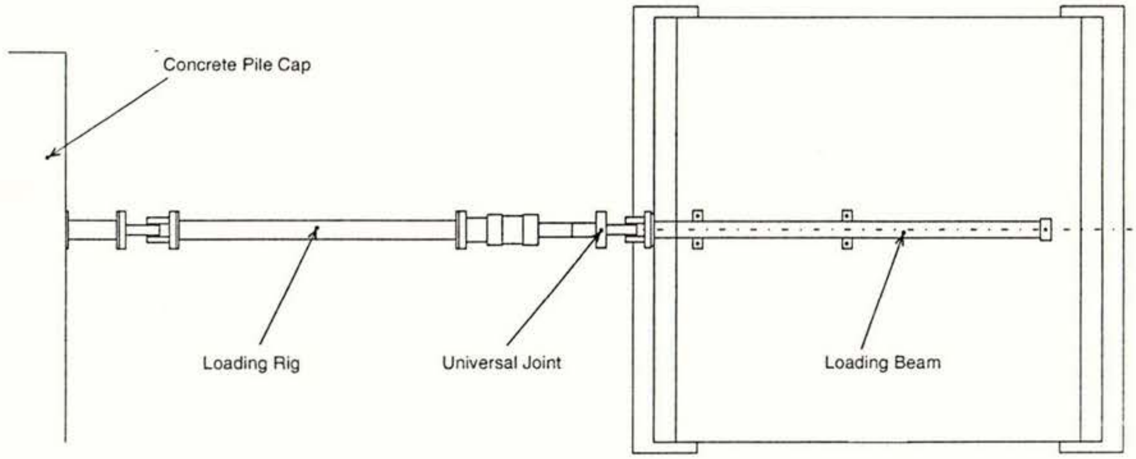

Figure 3.9. Layout of the loading rig for Test 3.

For Test 1, the load was applied via a 200UC46 steel column bolted to the slab, with the hydraulic actuator mounted close to the reaction pile cap, as shown in Figures 3.10. Unfortunately, unexpected rotations of the structure were amplified by this arrangement causing the actuator to apply significant out of plane loads.

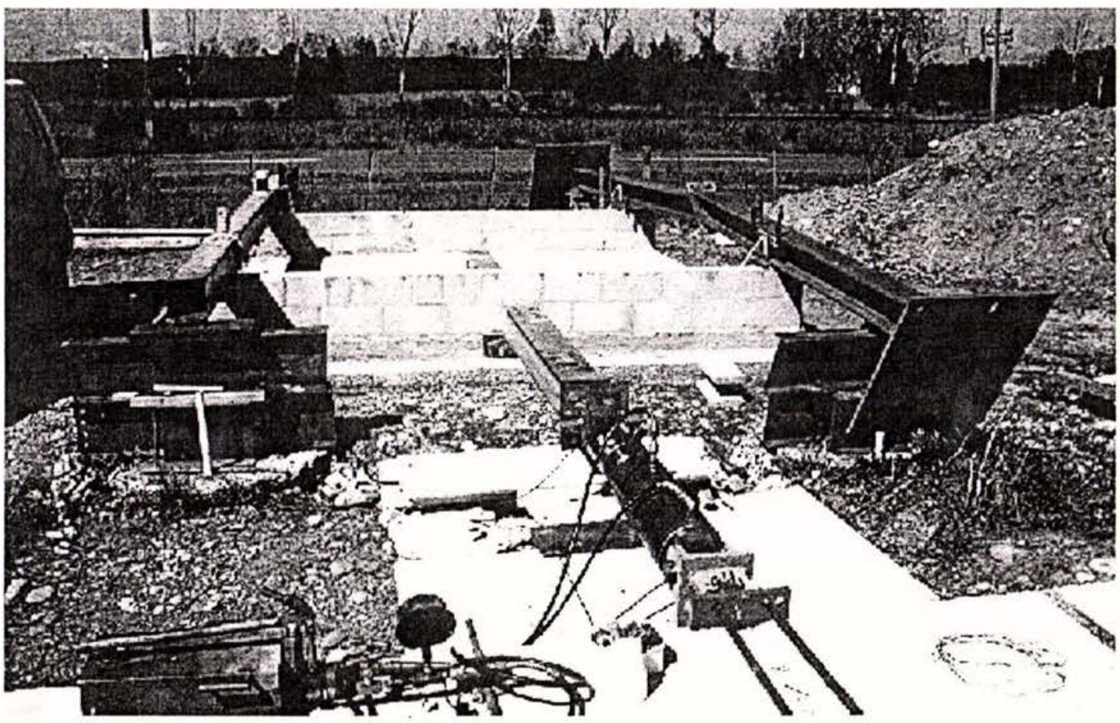

Figure 3.10. View of loading rig for Test 1.

The rig was re-designed for Test 2 by placing universal joints at each end of the rig where it was connected to the reaction pile cap and the test structure, as shown in Figures 3.11 and 3.12. This design allowed significant rotation and vertical movement of the test structure to take place without causing any significant out of plane loading by the actuator.

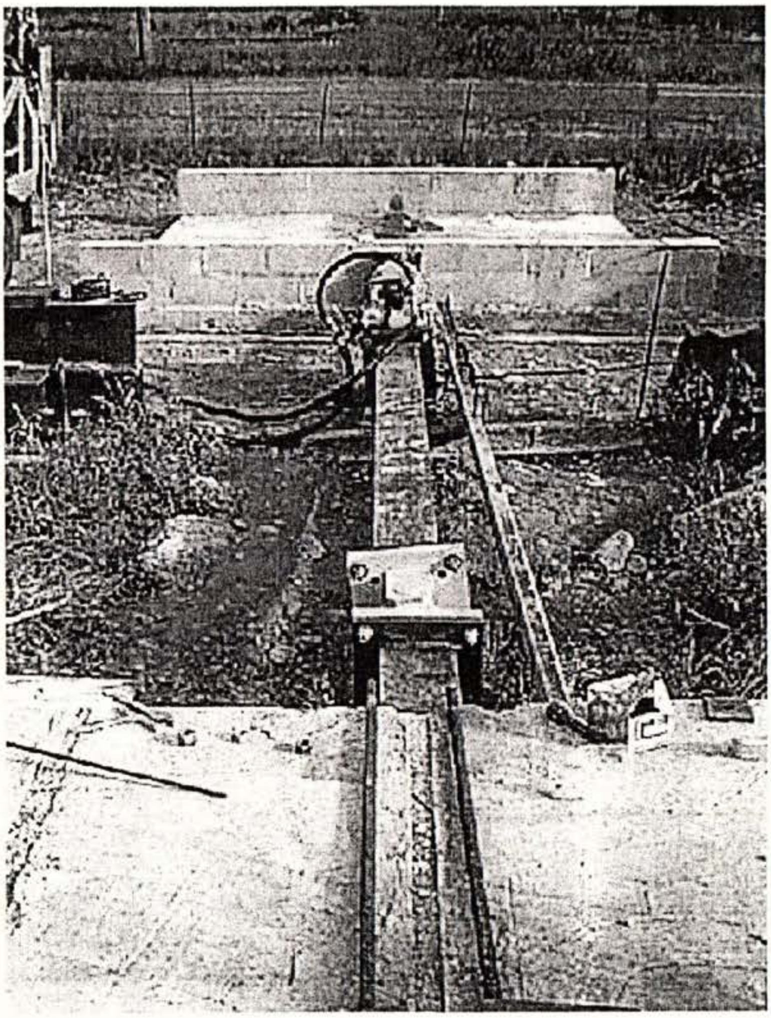

Figure 3.11. View of loading rig for Test 2.

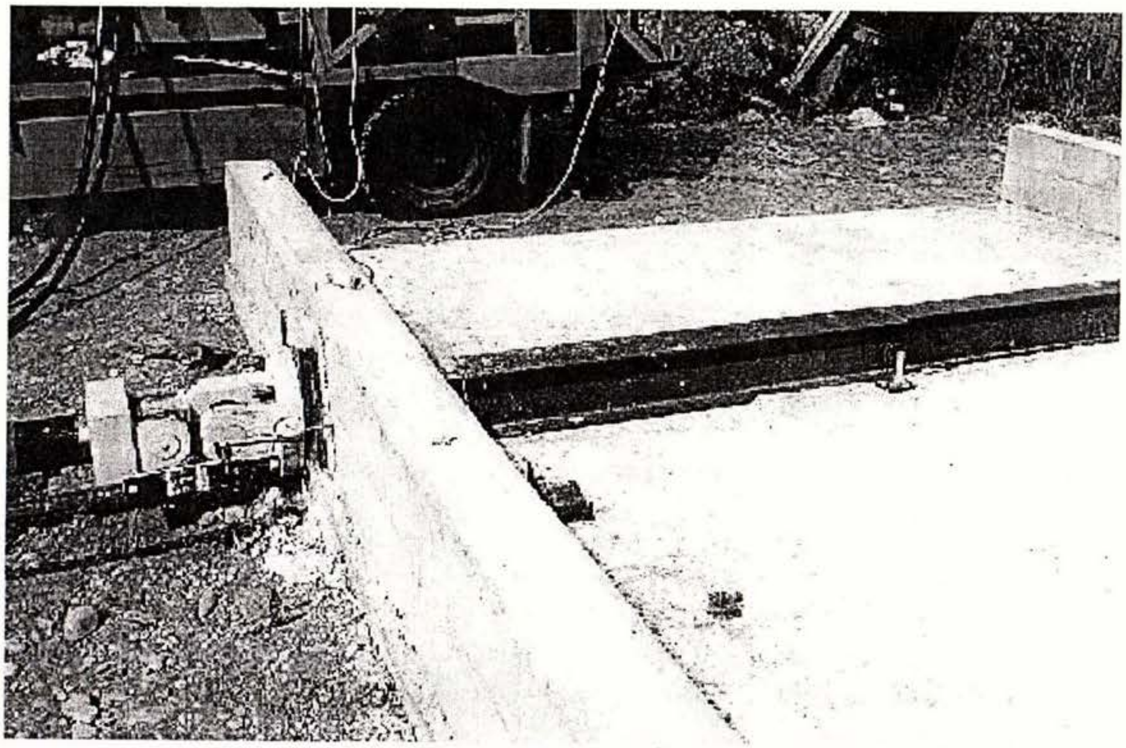

Figure 3.12. View showing connection of loading rig to Test structure for Test 2.

For both Test 1 and Test 2, the loads were not applied exactly in the plane of the floor slab, but through a plane 150 mm above the floor level, as shown in Figure 3.13. For Test 3, this eccentricity was removed by altering the connection detail, as shown in Figure 3.14.

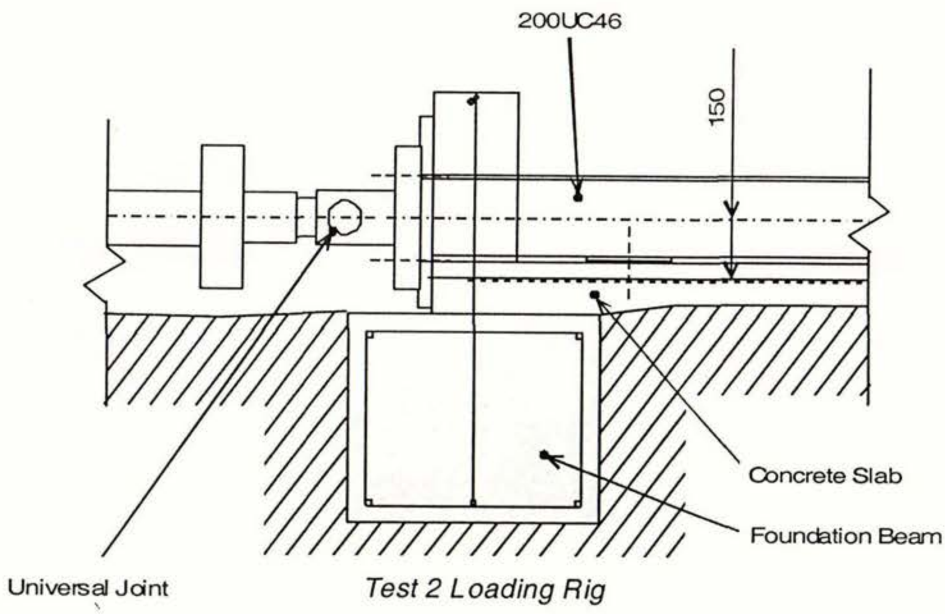

Figure 3.13. Loading rig connection detail for Test 2.

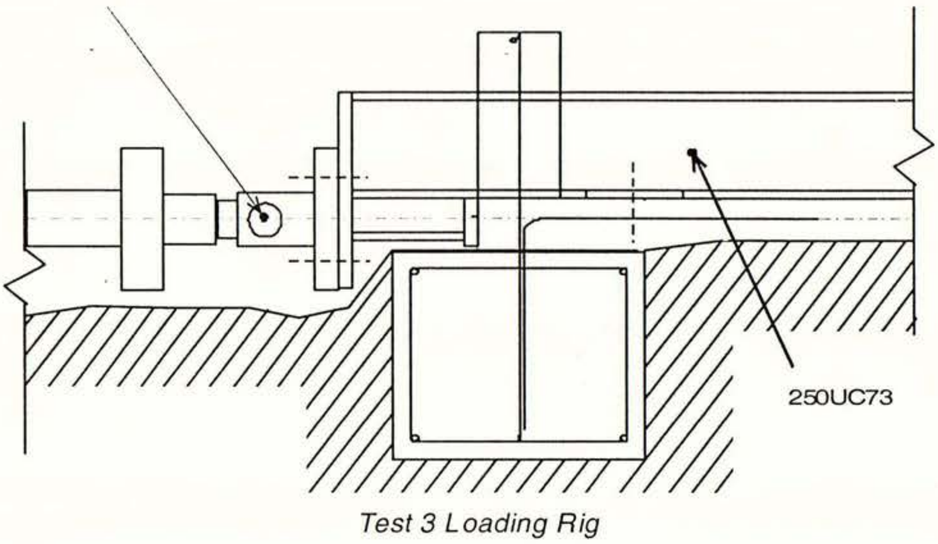

Figure 3.14. Loading rig connection detail for Test 3.

Loads were applied by a MTS model 204.81 servo-hydraulic actuator of 500 KN capacity and 152 mm stroke. Loading was displacement controlled using an active closed-loop feedback system according to the schematic shown in Figure 3.15. A constant rate of displacement of XX mm/min was used for the testing.

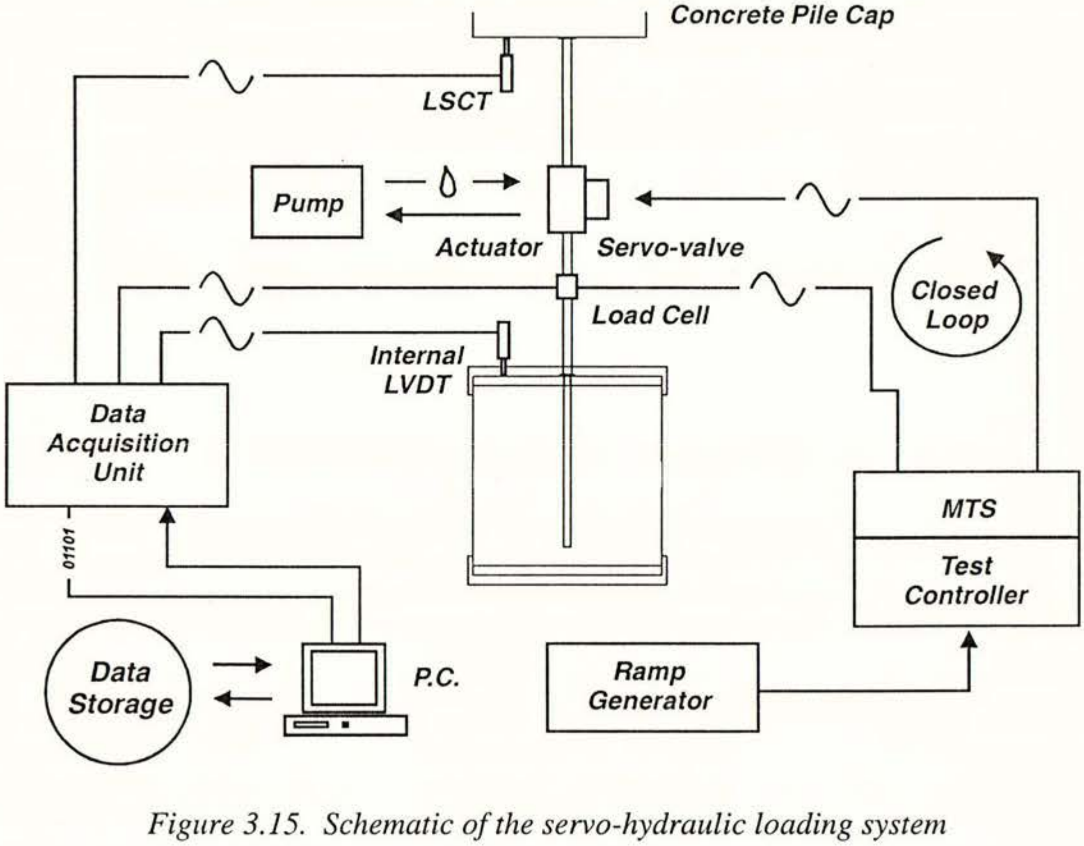

Figure 3.15. Schematic of the servo-hydraulic loading system

Measurements of horizontal load and displacement were recorded digitally during each test from an electric load cell connected directly to the hydraulic actuator and an internal LVDT.

For Test 3, the dead weight of the structure was increased by placing the exhumed structure of Test 1 directly on top of the test structure for Test 3, as shown in Figure 3.16.

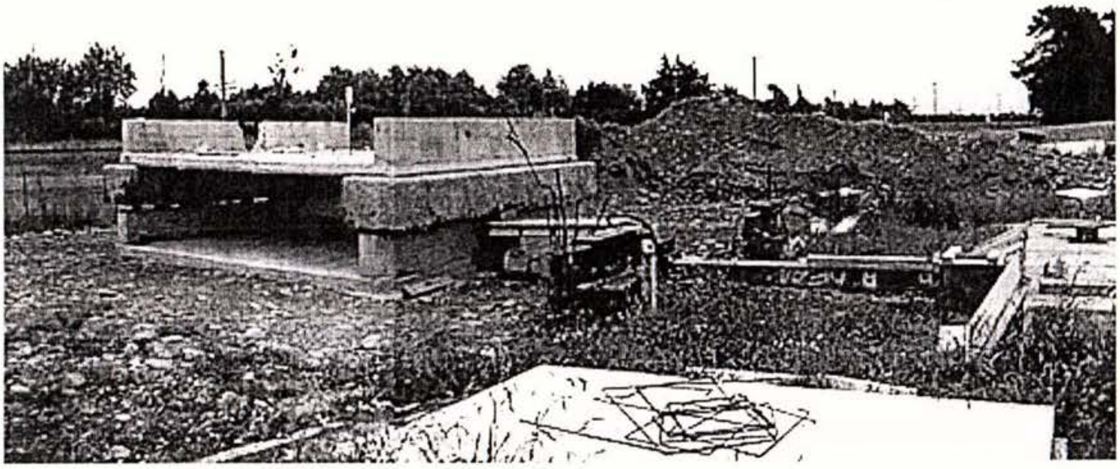

Figure 3.16. View of Test 3 with carcass of Test 1 placed on top.

Other than the load and displacement measurements, careful observations of soil and structural movements and cracking were made and photographed, as described in the following section.

4 SLAB AND BEAM RESULTS

This section describes the results of the three slab and beam tests in detail. Each Test is treated separately, including the loading regime, the measurements of load and displacement, together with detailed observations of soil and structural movements and cracking.

4.1 Test 1

Test 1 must be considered as a "shake down" of the experimental system because of unacceptable difficulties that were encountered, specifically rotations and uplift of the test structure during loading. Nevertheless, the general observations and qualitative behaviour of the test structure are informative and are recoded below, even though the quantitative measurements may be unreliable because of significant out of plane loading caused by rotations of the hydraulic actuator.

The complete load history of Test 1 is shown as a load-displacement graph in Figure 4.1, with key points summarised in Table 4.1. Positive loads and displacements are for loading away from the reaction pile cap.

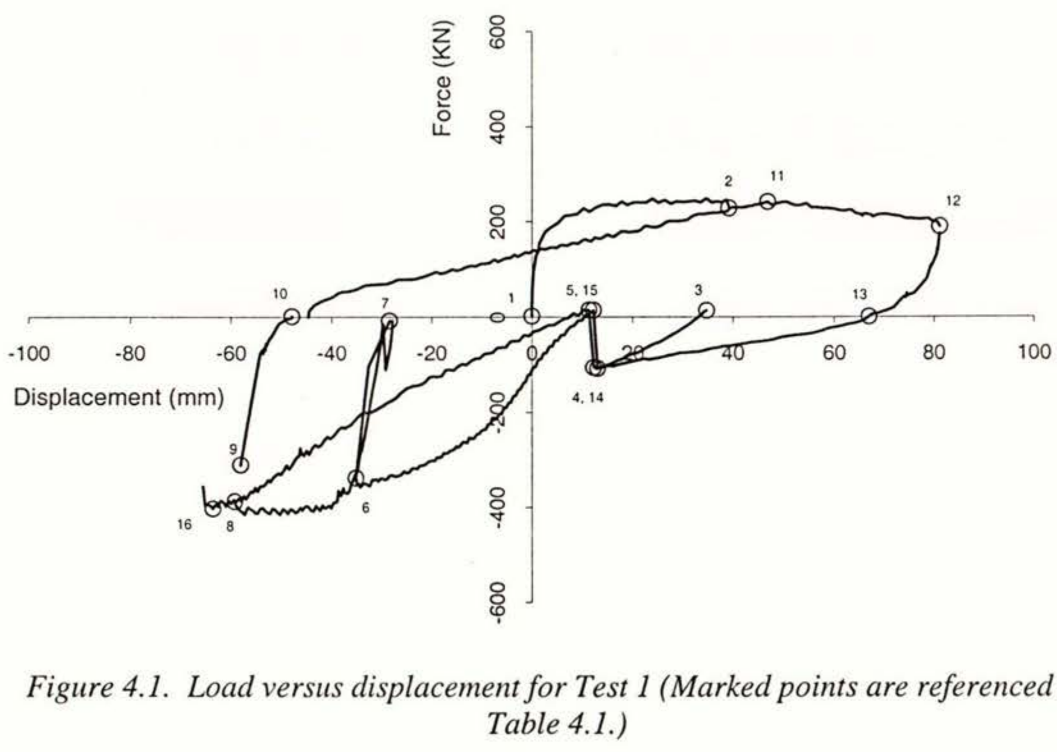

Figure 4.1. Load versus displacement for Test 1 (Marked points are referenced in Table 4.1.)

Table 4.1. Summary of significant load steps for Test 1

Point Number	Displacement (mm)	Load (kN)	Load Step No.
1	0	1.5	1
2	39.2	228.0	1,2
3	34.8	13.3	2
4	13.0	-107.8	2
5	12.2	14.1	2
6	-35.1	-339.0	2
7	-28.4	-8.3	2,3
8	-59.2	-388.9	3,4
9	-58.1	-311.4	4
10	-48.1	1.1	4
11	46.9	240.9	4
12	81.2	189.2	4,5
13	66.9	0.2	5
14	12.2	-106.4	5
15	11.3	13.9	5
16	-65.6	-357.1	5

4.1.1 **Load step 1** (Points 1-2 on Figure 4.1)

The first step of the testing was to push the test structure away from the reaction pile cap. The test structure was pushed until the load had reached a plateau that corresponded to the maximum load of 248 KN in this direction, and then was stopped at a displacement of 39.2 mm. It should be noted that the maximum load in this direction was developed very quickly as shown in Figure 4.1.

Even at this early stage of the testing, rotation of the structure was observed with 27 mm uplift being measured at the foundation beam nearest to the reaction pile cap, as shown in Figure 4.2.

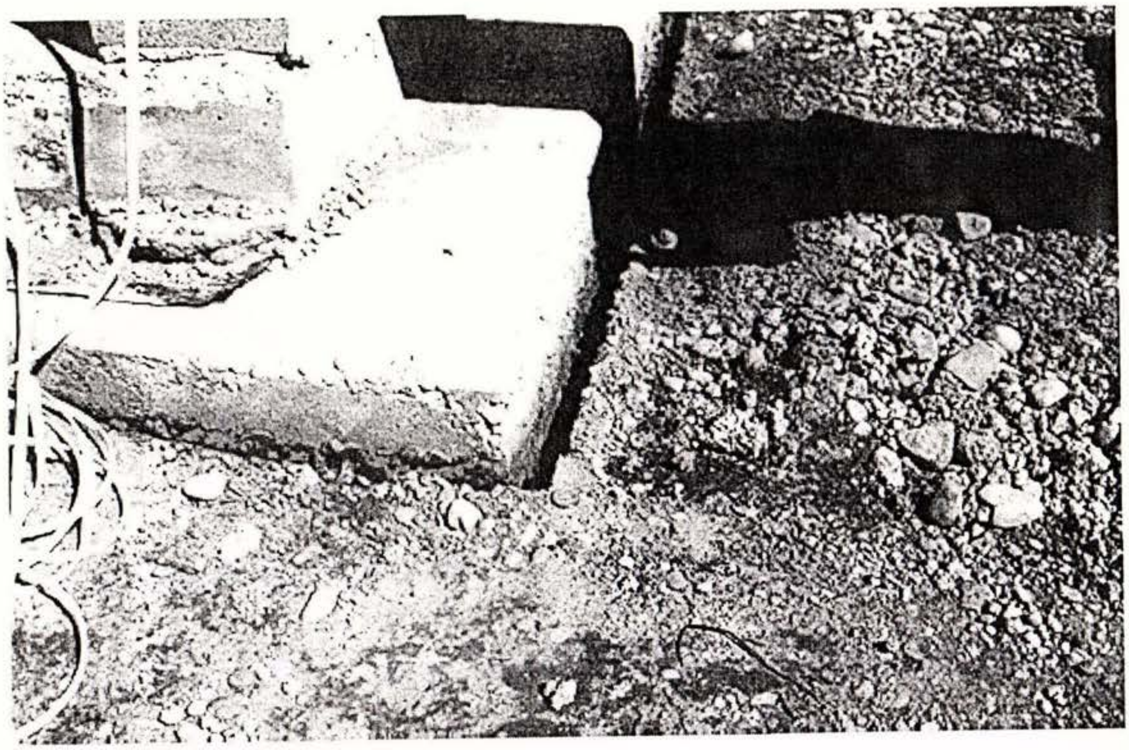

Figure 4.2. Uplift of foundation beam, load step 1.

For both foundation beams, cracking in the soil could be clearly observed around the corners of the concrete on the side that was being pushed through the soil. The soil adjacent to the foundation beam had sufficient cohesion to form a trench where the foundation beam had moved away, creating significant gaps between the soil and the foundation beams for the larger load cycles.

4.1.2 **Load step 2** (Points 2-7 on Figure 4.1)

Direction of loading was now reversed, with loads initially dropping to zero (points 2-3) then increasing in "tension" as the test structure was pulled towards the reaction pile cap. Data was lost between points 2 and 3, but the load was seen to drop rapidly to zero over 6 mm.

At point 4, the load was seen to drop suddenly to zero before increasing steadily again, apparently caused by rotation of the test structure and slack in the loading rig.

At point 6 (-339 KN), the test structure was unloaded to point 7.

4.1.3 **Load step 3** (Points 7-8 on Figure 4.1)

From points 7 to 8 the test structure was re-loaded in "tension" until a steady maximum load of -416 KN was reached, much greater than the +248 KN achieved in the opposite direction of loading.

This highly unsymmetrical response of the test structure was evidently caused by the rotation of the structure interacting with the loading rig to cause an upwards leverage in the outwards or "compression" direction tending to lift the structure out of the soil. In the inwards or "tension" direction of loading the opposite was occurring with the loading rig pulling the structure down into the soil.

When the loading reached point 8, heave in the soil became apparent through cracks running parallel approximately 500 mm from the foundation beam nearest the reaction pile cap.

4.1.4 **Load step 4** (Points 8-12 on Figure 4.1)

The direction of loading was again reversed to push the test structure away from the reaction pile cap with a maximum value of load of +241 KN achieved at point 11 (+46.9 mm). Beyond point 11, the loading was continued to a maximum value of +81.2 mm with load dropping slowly to 189 KN.

At point 12, the uplift of the test structure was becoming severe, as shown in Figure 4.3. The drop off in load between points 11 and 12 is probably explained by the reduction in contact between the soil and the structure.

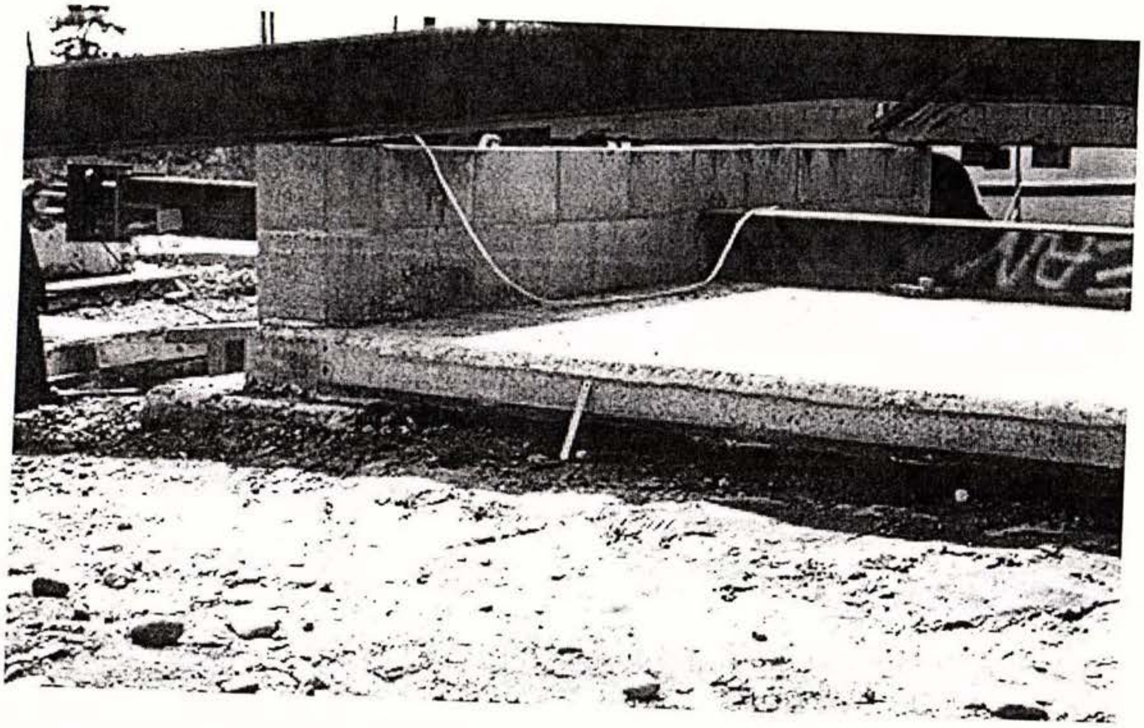

Figure 4.3. Test structure uplifting during load step 4.

Very slight hairline cracking in the top of the slab was observed approximately 400 mm off the masonry wall overlying the foundation beam furthest from the reaction pile cap and was the only sign of structural deformation noticed at this point.

4.1.5 Load step 5 (Points 12-16 on Figure 4.1)

The direction of loading was again reversed to pull the test structure towards the reaction pile cap with a maximum value of load of -403 KN achieved at a displacement of -63 mm. Again, a sudden drop in load was observed at point 14, presumably because of slack in the loading rig. Beyond point 15, the load stiffness was much less than for the first cycle of load (points 5 to 8) but a slightly higher maximum load was achieved (-403 KN at point 16 compared with -389 KN at point 8 for the first load cycle).

At point 16 significant gap opened up adjacent to the foundation beam furthest from the reaction pile cap and the soil, as shown in Figure 4.4.

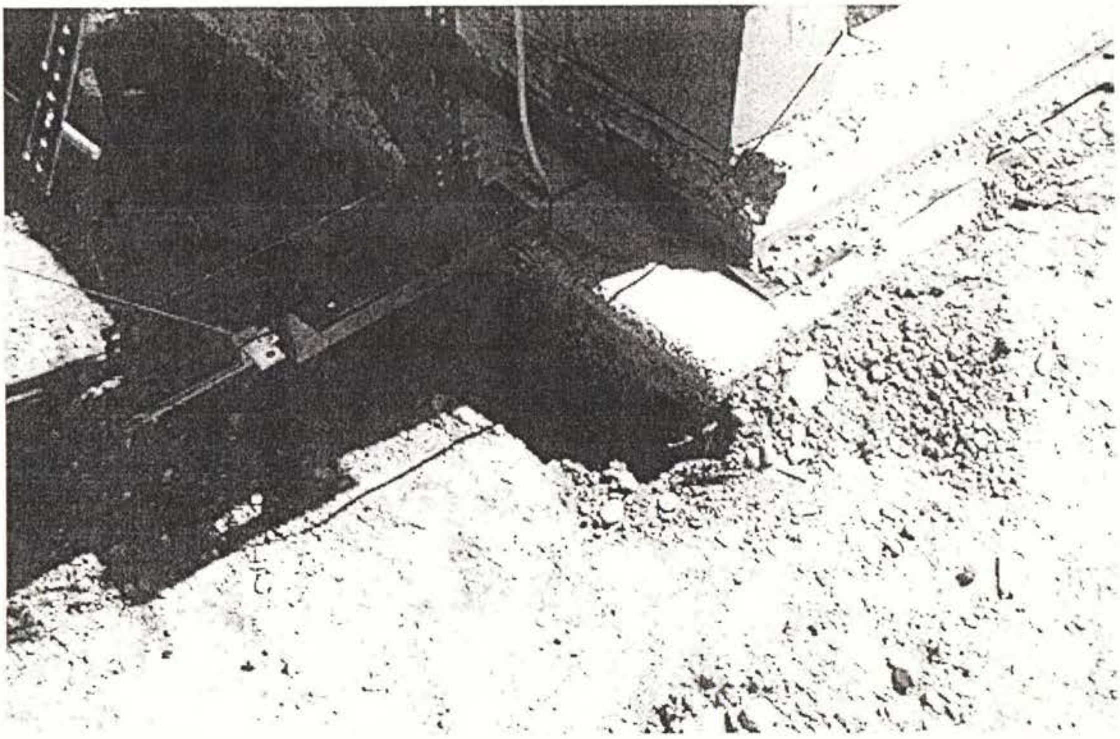

Figure 4.4. Gap between soil and foundation beam furthest from the reaction pile cap, load step 5.

Slight hairline cracking in the top of the slab was observed approximately 400 mm off the masonry wall overlying the foundation beam nearest to the reaction pile cap and was the only sign of structural deformation noticed at this point.

4.1.6 Test 1 summary

The maximum loads achieved for each load cycle are summarised in Table 4.2. Rotation of the test structure during loading combined with inadequacies of the loading rig caused the structure to be lifted out of the soil during load steps 1 and 4, and so the maximum load achieved was only 60% of that in the opposite direction. The higher forces observed for load steps 2, 3 and 5 can be attributed to the fact that the loading rig actually pulled the structure down into the soil and thus generated more resistance from the soil. As a result of this, neither direction of loading gave a realistic maximum lateral capacity: One was too high, and the other too low. Therefore, the true horizontal load capacity of the test structure might be taken as the average of the capacity in each direction (332 KN). The loading rig was re-designed for the remaining two tests to eliminate these difficulties.

Table 4.2. Maximum horizontal loads for each load cycle of Test 1.

	Load step 1	*Load steps 2&3*	*Load step 4*	*Load step 5*
Load (kN)	248	-416	241	-404

The observed behaviour of the soil gave an indication of what to look out for in the subsequent tests: Significant cracking in the soil was observed around the corners of the foundation beams, and heave was observed parallel to the outside of each of the foundation beams and around the edges of the junction of the slab and the foundation beams.

It was concluded from this test, that the mechanism of failure of the structure under horizontal loading was formation of passive failure wedges adjacent to the foundation beams and not a tip-to-tip failure. This conclusion was based on direct observation through the movement of the slab with respect to the blinding sand and the small amount of heave observed against the inside of the foundation beam immediately beside the concrete slab.

Some slight cracking was observed in the top of the concrete slab at full displacement in each direction. No other structural degradation was observed.

4.2 Test 2

Test 2 was essentially a repeat of Test 1 but with improvements to the loading rig to better accommodate rotations of the structure. Testing was again quasi-static, with loading being applied at a constant rate of displacement of xx mm/min. Loading was paused at each extreme displacement to allow visual observations of ground displacements and structural cracking etc. Testing was spread over two days because of overheating of the hydraulic loading system.

The load history of Test 2 is shown as two load-displacement graphs for each day of testing in Figures 4.5 and 4.6, with key points summarised in Table 4.3.

Table 4.3. Summary of significant load steps for Test 2.

Point Number	Displacement (mm)	Load (kN)	Load Step No.
1	-2.3	-6	**1**
2	-36.2	-281	**1,2**
3	-17.8	-3	**2**
4	-0.2	78	**2**
5	6.5	139	**2**
6	31.0	264	**2,3**
7	11.3	2	**3**
8	0.5	-29	**3**
9	-69.7	-304	**3,4**
10	-39.9	-1	**4**
11	-0.9	70	**4**
12	7.5	74	**4**
13	81.9	281	**4,5**
14	32.9	2	**5**
15	23.7	-6	**5**
16	26.3	5	**5**
17	0.2	-47	**5**
18	-34.3	-92	**5,6**
19	-19.7	-1	**6**
20	-0.4	41	**6**
21	34.7	98	**6,7**
22	14.8	0	**7**
23	0.4	-30	**7**
24	-35.6	-93	**7,8**
25	-21.0	-1	**8**
26	-0.7	40	**8**
27	35.9	104	**8,9**
28	14.5	0	**9**
29	0.1	-30	**9**
30	-35.6	-95	**9**
31	-55.0	-160	**9**

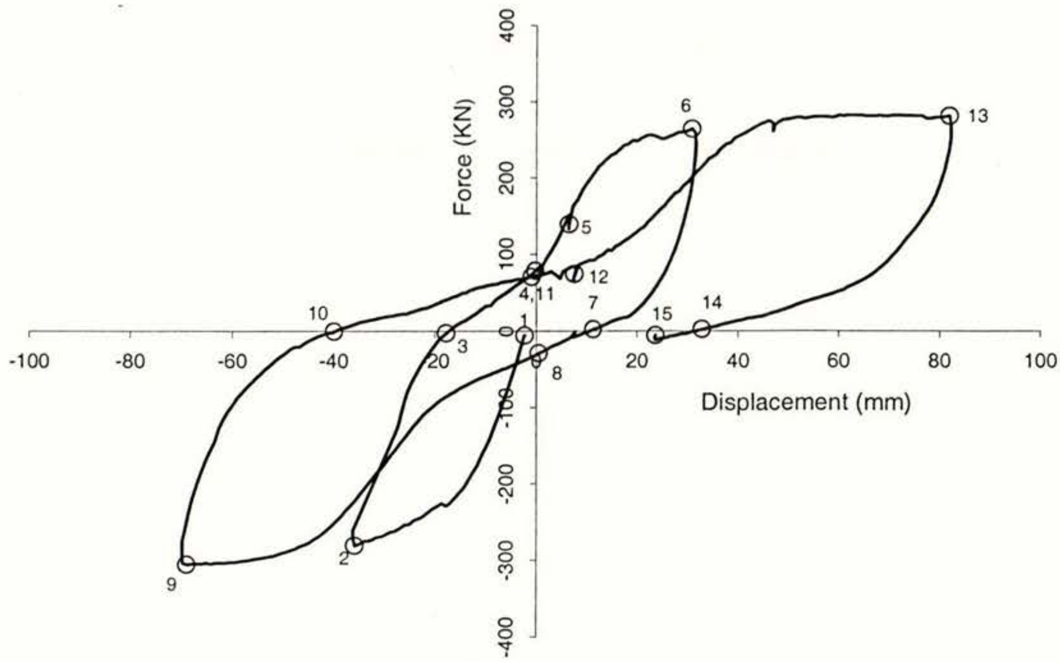

Figure 4.5. Load versus displacement for Test 2, day 1 (Marked points are referenced in Table 4.2)

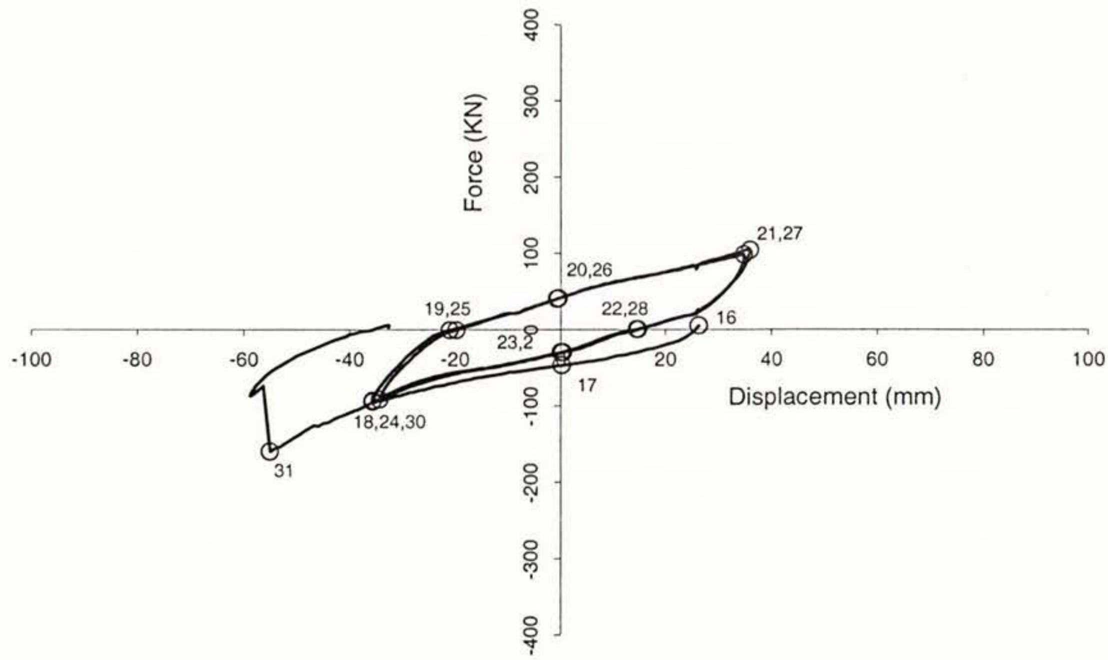

Figure 4.6. Load versus displacement for Test 2, day 2 (Marked points are referenced in Table 4.2)

4.2.1 **Load step 1** (Points 1-2 on Figure 4.5)

The first step of the testing was to pull the test structure towards the reaction pile cap until an initial "yield" load was reached (-281 KN at -37 mm displacement).

At this point there was little observable soil deformation. A small amount of cracking was observed in the soil around the foundation beams, and gaps opened up where the foundation beams were moving away from the surrounding soil.

Slight cracking in the top of the slab was observed near to the foundation beam nearest to the reaction pile cap. The cracking was observed from 600 mm off the masonry wall at the right hand side of the structure to 450 mm off the masonry wall at the left and is shown in Figure 4.7.

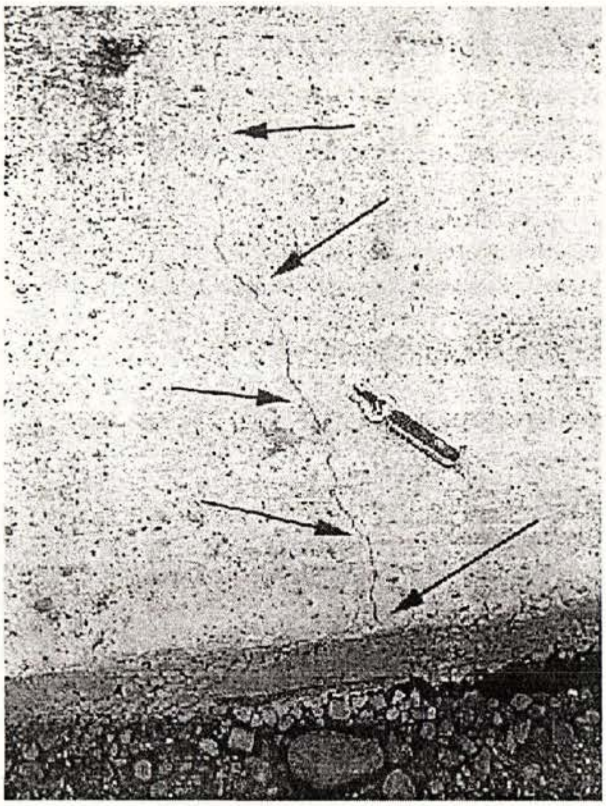

Figure 4.7. Cracking in slab after load step 1.

4.2.2 **Load step 2** (Points 2-6 on Figure 4.5)

The structure was unloaded and then pushed until initial "yield" was reached (264 KN at 31 mm displacement). From points 2 to 3 unloading was rapid, but then The development of positive load was relatively slow between points 3 and 4 (low stiffness) as the foundation beams were being pushed back to close the gaps created in load step 1. Load stiffness increased after the structure returned to the starting position (point 4) and the foundation beams came back into contact with soil on their leading faces.

Cracking was again observed in the soil around the corners of the foundation beams.

Cracking in the slab was noticed near to the foundation beam furthest from the reaction pile cap. The cracking was much more significant than for load step 1, presumably because the loading beam bolted to the top of the slab terminated at this location, as shown in Figure 4.8. Cracks extended across the width of the slab at approximately 300 mm off the masonry.

Figure 4.8. Cracking in slab after load step 2

4.2.3 **Load step 3** (Points 6-9 on Figure 4.5)

The structure was unloaded and then pulled until "yield" was again reached (-306 KN at 70 mm displacement). From points 6 to 7 unloading was rapid, but then The development of negative load was relatively slow between points 7 and beyond 8 (low stiffness) as the foundation beams were being pushed back to close the gaps created in load step 2. Load stiffness increased after the structure returned to the near the maximum displacement reached during load step 2 (but not quite) and the foundation beams came back into contact with soil on their leading faces.

The cracks observed in the top of the slab during load step 1 (near to the foundation beam closest to the reaction pile cap) again became evident. The cracks continued to widen as the load and displacement were increased. Also, there was slight rotation of the foundation.

The foundation beam furthest from the reaction pile cap was seen to undergo a small amount of uplift that appeared to be due to soil heave underneath the slab. Heave of the ground parallel to the nearest foundation beam became evident as the displacement exceeded –50 mm, extending 600 mm in front of the beam at each end and 800 mm in front of the centre of the beam. Also, cracking was observed around the compression corners of the foundation, as shown in Figure 4.9

Figure 4.9. Soil cracking and heave in front of the test structure after load step 3.

4.2.4 **Load step 4** (Points 9-13 on Figure 4.5)

The structure was unloaded and then pushed until "yield" was again reached (272 KN at 47 mm displacement), and then pushed further to investigate the post-yield response (281KN at 82 mm). From points 9 to 10 unloading was rapid, but then development of negative load was relatively slow between point 10 and beyond point 12 (low stiffness) as the foundation beams were being pushed back to close the gaps created in load step 3. Load stiffness increased after the structure returned to the near the maximum displacement reached during load step 3 (but not quite) and the foundation beams came back into contact with soil on their leading faces, but load stiffness remained significantly below that of load step 3.

Rotation and uplift were observed for the foundation beam nearest to the reaction pile cap, as shown in Figure 4.10. The opposite foundation beam also showed rotation together with the masonry wall and part of the slab, as shown in Figure 4.11, presumably because of lack of stiffening from the loading beam. Rotation was about the crack that had previously opened up across the width of the slab through the position of the end loading-beam bolt. The crack became much larger as the rotation increased and the outmost edge of the structure was turned into the ground.

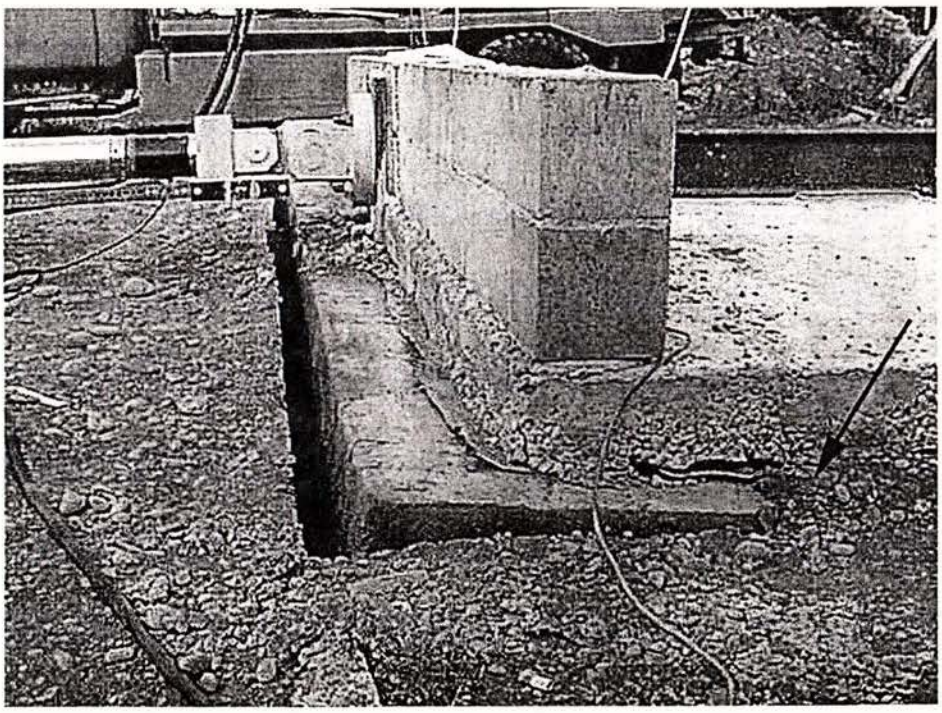

Figure 4.10. Rotation and uplift of the foundation beam nearest to the reaction pile cap, load step 4.

Figure 4.11. Rotation of the foundation beam, masonry wall, and part of slab furthest from the reaction pile cap.

Soil heave was observed parallel to the foundation beam (shown by arrows in Figure 4.11). Heave was accompanied by soil cracking at about 600 mm from the face of the foundation beam. Heave was also clearly evident under the slab adjacent to the foundation beam nearest to the reaction pile cap (shown by arrow in Figure 4.10). The uplift of this foundation beam appeared to be a result of this heave.

4.2.5 Load step 5 (Points 13-15 on Figure 4.5)

The structure was unloaded resulting in 26 mm permanent displacement.

4.2.6 Load step 6-10 (Points 16-31 on Figure 4.6)

Load steps 6 - 10 were performed after a break of 4 days. However, there was no weather that would have noticeably changed the condition of the soil in the interim.

The idea behind these additional load steps was to perform two additional hysteresis loops within the "trenches" (defined by gapping either side of the foundation beams) that the foundation beams had formed from the previous higher-displacement load steps eliminating, presumably, the contribution of passive soil resistance. There were no notable visual observations made during this phase of the testing because of the relatively low displacements.

The initial increase in load as the specimen was moved from Point 16 in Figure 4.6 towards Point 18 was quite rapid, but then flattened off slightly as the specimen moved through zero displacement, with the rate of load increase beginning to increase again as Point 18 was reached (-34 mm displacement).

Starting at Point 18 and ending at Point 30, two hysteresis loops were formed during load steps 6 to 9. The hysteresis loops showed very little degradation in load carrying capacity and were relatively symmetrical about the central displacement. However, there are several features worth noting

First, the force attained at zero displacement was approximately 40 KN in load steps 6 and 8 while it was only –30 KN in load steps 7 and 9. The earlier, more rapid, increase in load when the specimen was pushed away from the concrete pile cap anchor was also shown in the larger displacement cycles. Almost an identical difference in load was observed in the peak loads for the respective directions of loading despite the displacements being almost identical. Likewise, the movement required to attain zero load after the loading rig had been in compression was also greater than that in the opposite direction, as in the larger-displacement cycles. It appears that these differences in behaviour were related to the uplift and, to a lesser extent in the low-displacement cycles, the greater rotation of the foundation beams in the compression direction of loading for the loading rig.

In both directions, the manner in which the load increased with respect to displacement from total unloading was very similar, although the rate of increase in negative load was slightly slower. The effect of passive resistance contributing to the load resistance was most evident between –20 mm and –36 mm in load steps 7 and 8 where the load obviously began to increase instead of stabilising to a constant value (the lateral capacity of the frictional mechanism only). This observation also applied (to a lesser extent) in the opposite direction.

The final load step in this test was carried out with the intention of taking the test specimen out to the full retraction point of the actuator once more (that is, a displacement of –70 mm). However, when Point 31 was reached there was sudden pullout failure of firstly the end bolt of the loading beam, and subsequently the central two bolts as the load was redistributed resulting in the bolts pulling completely out of the concrete and the loading beam pulling up off the concrete slab, as shown in Figure 4.12.

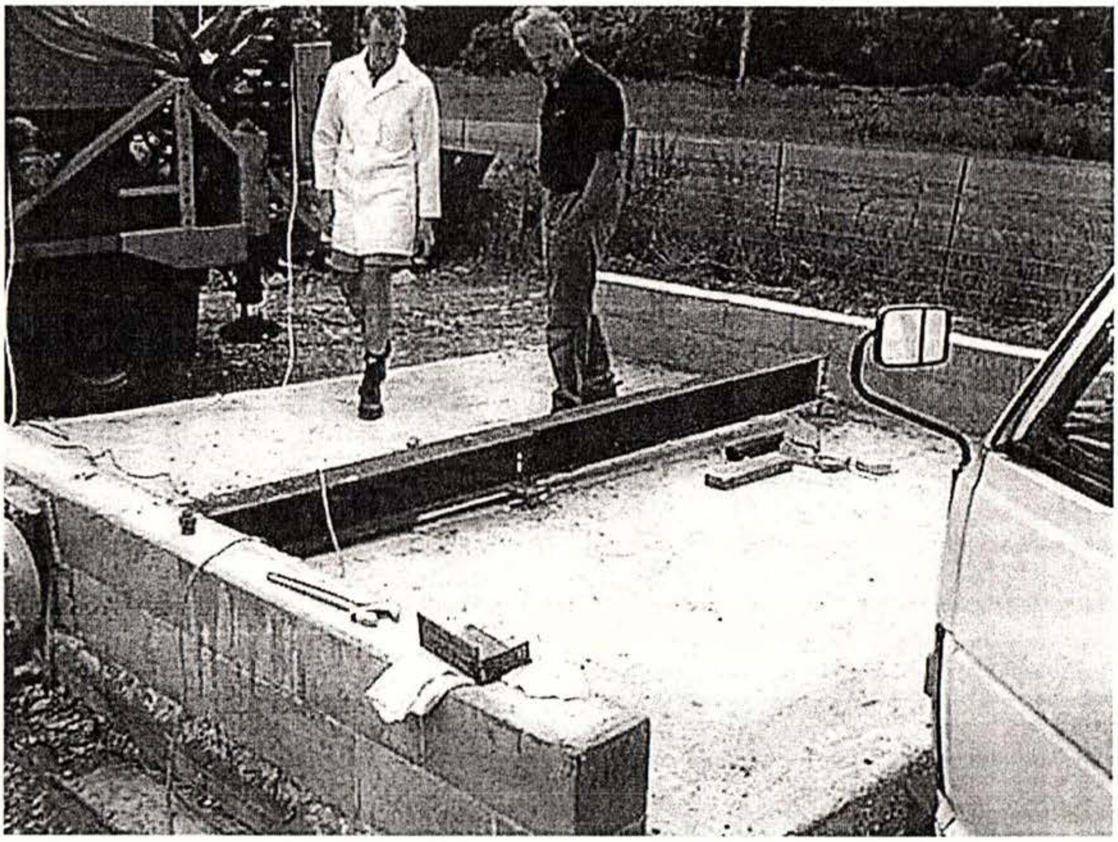

Figure 4.12. Loading beam with connection bolts pulled out of the slab, Test 2.

4.2.7 Test 2 summary

The loading rig for this test performed much better than that in Test 1. However, a crucial factor affecting the results was the poor performance of the structure, mainly caused by the reduced quantity of starter bars, the smaller than specified quantity of mesh used, and the use of 17.5 MPa concrete.

Despite the structural difficulties experienced with Test 2, the load versus displacement record of the specimen in the soil was relatively symmetrical for both directions of loading, and is expected to be largely unaffected. It is interesting to compare the average peak load in this test, 293 KN, with the value 332 KN that was obtained by averaging the two peaks in Test 1. The fact that the Test 2 value is lower probably may reflect the more flexible structure in Test 2, but may also reflect the inevitable small differences in preparing the two test structures. The peak values in each direction for this test are summarised in Table 4.4.

Table 4.4. Summary of maximum loads achieved in each direction of loading, Test 2.

Load Step No.	**3**	**4**
Load (KN)	-304	281

For the second day of loading, with the specimen being cycled back and forth within the trench formed by the large-displacement load cycles, the degradation of load over two hysteresis loops was almost nonexistent. The hysteresis loops were slightly skewed towards higher forces when the test specimen was pushed away from the concrete pile cap.

In the limited-displacement hysteresis loops, it could be seen that the load displacement plots did not allow for the maximum frictional resistance to be clearly determined. The displacement able to be achieved without passive resistance contributing was not great enough to clearly determine this value in either direction.

Uplift in the structure at the foundation beams was clearly seen to be a result of heave in the underlying soil bearing against the underside of the concrete slab.

4.3 Test 3

The objective for Test 3 was to investigate the effect of increased vertical loading on the lateral response of a combination beam and slab foundation so that an analytical model might be developed. Also, improved structural details were used to try and prevent the structural failure observed during Test 2, even under the increased lateral loads expected.

The loading rig, actuator and instrumentation used in this test were identical to that used in Test, and are described in Section 3. The only significant difference was in the design of the loading beam, which was altered to allow the line of action of the loading to pass directly through the centre of the slab.

The complete load history for Test 3 is shown in Figure 4.13, with measured values for key points summarised in Table 4.5.

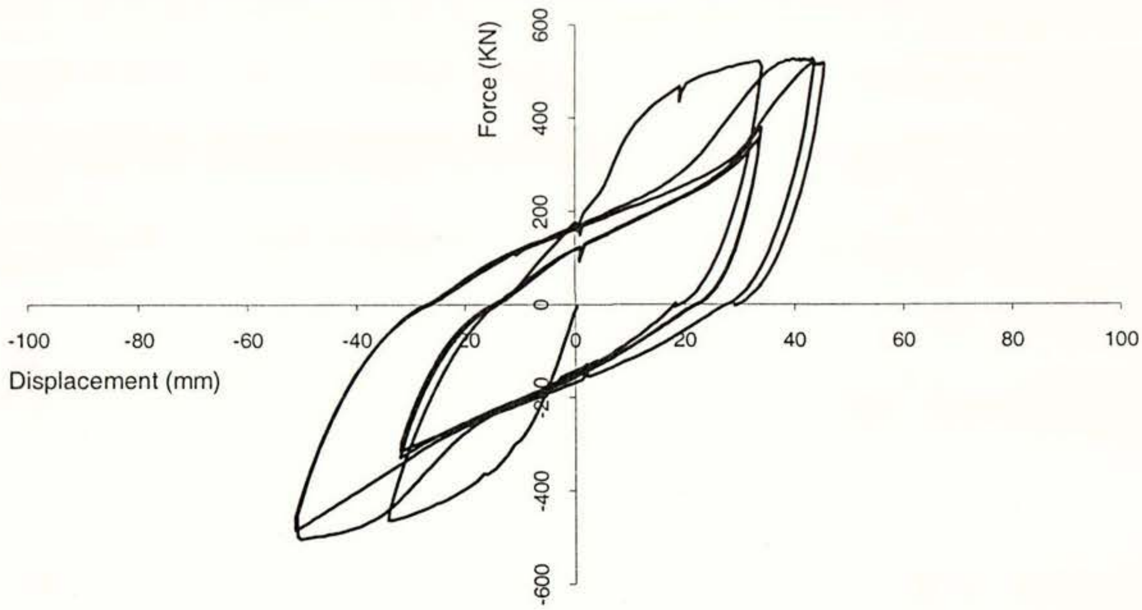

Figure 4.13. Load versus displacement for Test 3.

Table 4.5. Summary of significant load steps for Test 3.

Point Number	Displacement (mm)	Load (kN)	Load Step No.
1	0.3	-5	**1**
2	-34.3	-463	**1,2**
3	-14.6	-4	**2**
4	0.0	176	**2**
5	33.5	521	**2,3**
6	18.9	-1	**3**
7	-2.6	-156	**3**
8	-50.5	-504	**3,4**
9	-26.7	2	**4**
10	-0.4	166	**4**
11	43.3	527	**4,5**
12	27.1	-2	**5**
13	0.1	-168	**5**
14	-32.0	-316	**5,6**
15	17.0	-1	**6**
16	0.3	116	**6**
17	33.5	356	**6,7**
18	21.9	-2	**7**
19	-0.1	-150	**7**
20	-32.0	-329	**7,8**
21	-14.6	-2	**8**
22	-1.0	112	**8**
23	34.1	379	**8,9**
24	21.8	-1	**9**
25	0.5	-154	**9**
26	-51.4	-485	**9,10**
27	-26.3	0	**10**
28	0.1	162	**10**
29	43.6	518	**10,11**
30	29.1	0	**11**

4.3.1 **Load step 1** (Points 1-2 on Figure 4.13)

The direction of movement in this first load step, as with load step 1 in Test 2, was towards the reaction pile cap. The effect of the additional dead load was evident from the outset of this test as the load increased more quickly and up to much higher values for a given displacement than previously observed in Test 2. As with the behaviour observed in the previous tests, the load increase was initially rapid and then slowed. This load step was ceased at Point 2 at a load of –463 KN and a displacement of –34 mm. Although the stiffness was obviously decreasing, it is evident that the maximum load had not quite been reached.

No cracking was observed in the soil around the structure at this point. Trenches similar to those formed in the previous two tests were opened up beside the foundation beams with gaps opening either side of the foundation beams.

Hairline cracking was observed in the slab of the structure, extending from the bottom to approximately the mid-depth of the slab near the foundation beam farthest from the reaction pile cap, as shown in Figure 4.15.

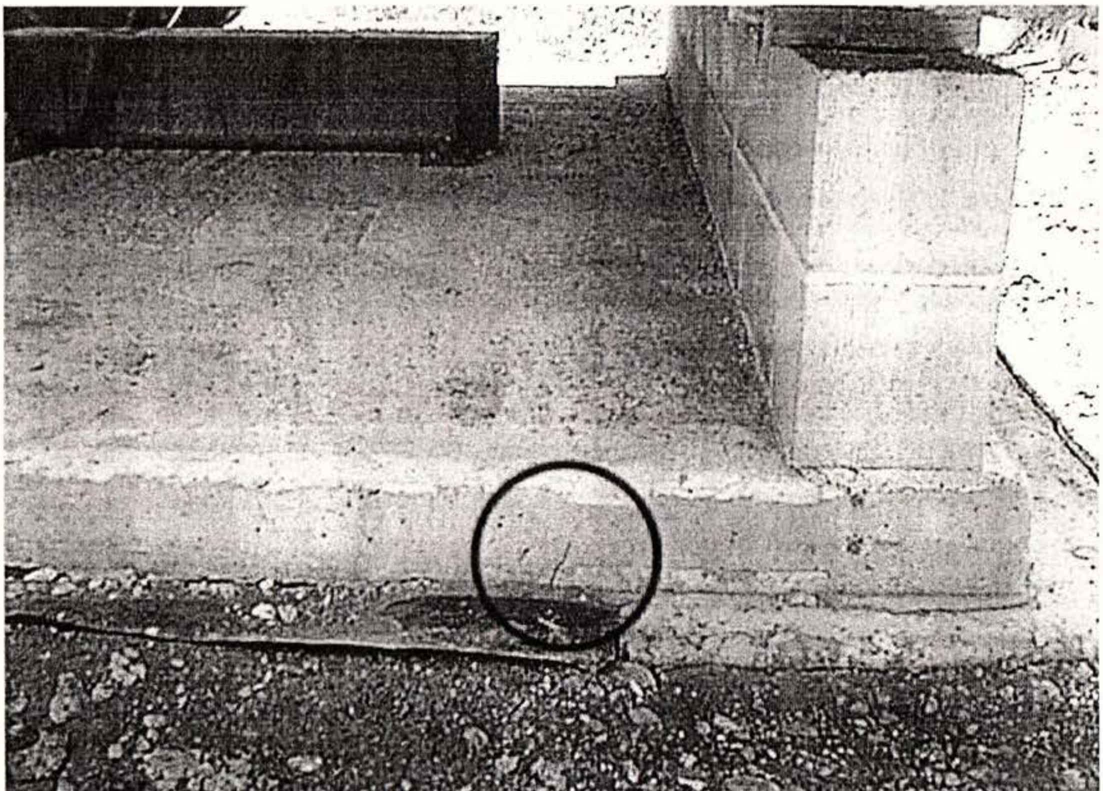

Figure 4.14. Hairline cracking in slab during load step 1.

4.3.2 Load step 2 (Points 2-5 on Figure 4.13)

Unloading was rapid once the direction of displacement was reversed, and zero load was achieved at a displacement of –15 mm at Point 3. The 19 mm of displacement required to completely unload the structure was almost identical to the 20 mm required in the equivalent load step in Test 2, despite the significantly higher load achieved for the same displacement in this test.

The rate of increase in load slowly decreased between Points 3 and 4 and proceeded at an average rate of 12 KN/mm. As the displacement moved past the zero (start) position, the rate of increase in load grew once again as the passive-resistance contribution became evident. The abrupt drop in load between Points 4 and 5 was due to a momentary stop in the testing to make observations.

As with load step 1, the load reached at the end of this load step was obviously not the maximum load. However, judging from the rate at which the load was stabilising to a peak value, this direction of loading appeared to be closer to the maximum load at this level of displacement. A load of 521 KN was achieved at Point 5, which was the limit of the capacity of the actuator, attained at 34 mm of displacement.

Cracking was again observed in the slab near the east foundation beam farthest from the reaction pile cap. However, owing to the different direction of loading, the cracking was this time across the top of the slab. Hairline cracks extended across the slab at 200 mm, 500 mm and 840 mm from the face of the masonry wall, as shown in Figure 4.15.

Figure 4.15 Arrows show cracking in the top of the slab during load step 2.

Cracking in the soil around the corners of the foundation beams occurred at maximum displacement and extended diagonally away from the edges in compression. The only other soil observations were the evidence of trenches at full displacement. No uplift or soil heave under the slab was observed, which can be attributed to both the increased dead load in the structure and the lesser displacement.

4.3.3 Load step 3 (Points 5-8 on Figure 4.13)

The unloading of the specimen was complete within a movement of 15 mm, slightly more rapidly than the unloading observed in load step 2. Between Points 6 and 7 the increase in negative load again slowed in rate and took place at an average rate of approximately -7 KN/mm. The load continued thus until just before –20 mm of displacement where there was an increase in the stiffness due to the contact with soil on the leading edge of the foundation beams.

The load step was terminated at Point 8, where the load level achieved appeared to be very close to the maximum lateral capacity in this direction (-504 KN at a displacement of –51 mm), again limited by the capacity of the actuator.

In terms of the structural observations, cracking became evident in the slab at both ends of the structure at the higher displacements. The cracking on the underside of the slab described in load step 1 widened significantly (Figure 4.16) as the entire specimen was pushed to a displacement 16 mm further than in load step 1. The maximum load in this load step was approximately 40 KN higher than previously achieved in this direction.

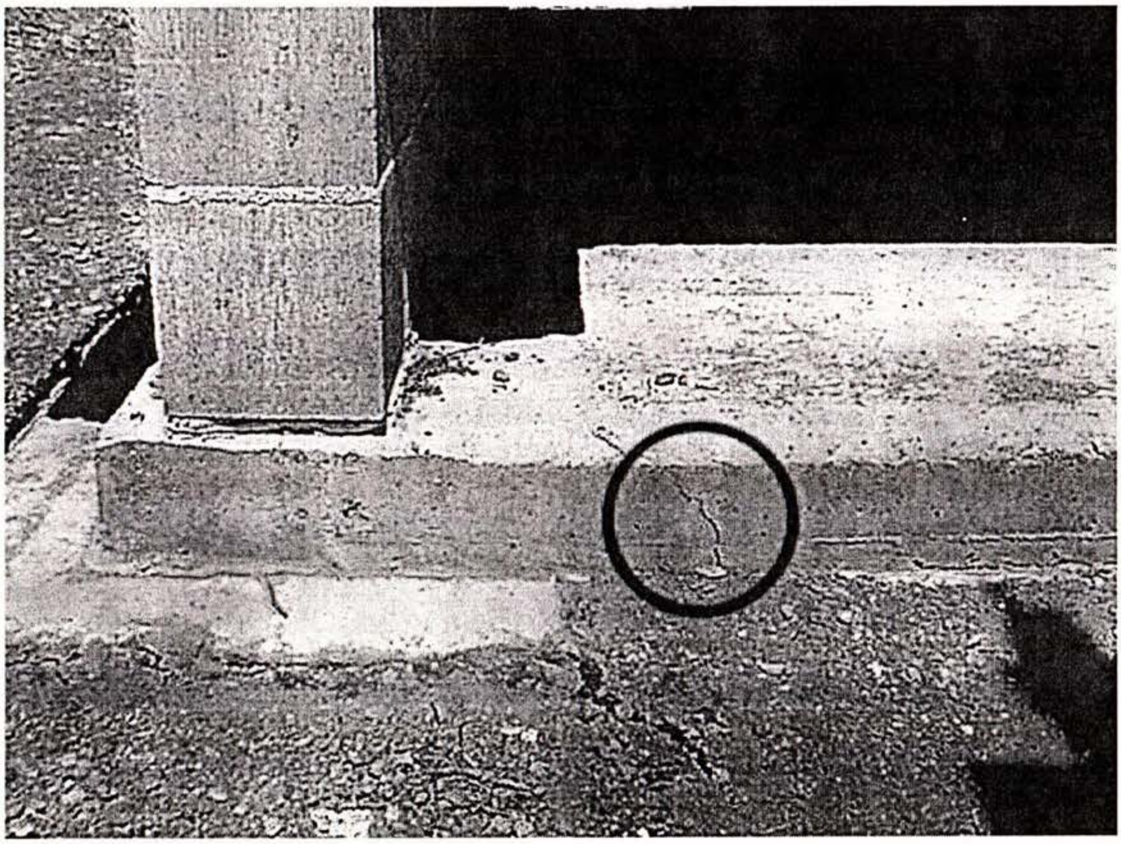

Figure 4.16. Cracking (circled) in the underside of the concrete slab near the foundation beam farthest from the reaction pile cap.

Hairline cracking was observed in the top of the slab near the foundation beam closest to the reaction pile cap. On the right-hand side of the test specimen there was cracking at both 400 mm and 780 mm off the masonry wall. On the left of the structure the cracking was observed at 550 mm off the masonry wall. This cracking was much less pronounced than that observed in load step 2 at the opposite end of the structure. The disparity in the size of the cracks appeared to be a result of the stiffening of the slab by the loading beam at the west foundation beam end. No visible rotation of the foundation beams or masonry walls was observed in either end of the structure.

Owing to the lower displacement of the test specimen compared with the previous two tests, no band of heave was observed parallel to the west foundation beam or adjacent to the intersection of the foundation beams with the slab, consistent with the earlier testing, as heave was not generally evident until at least 50 mm of displacement was reached. Cracking of the soil was evident at the compression corners of the foundation beams running at 45 degrees away from the direction of applied force, as shown in Figure 4.17.

Figure 4.17. Cracking in the soil, running diagonally away from the foundation beam edge closest to the reaction pile cap.

4.3.4 **Load step 4** (Points 8-11 on Figure 4.13)

The unloading of the structure as the direction of loading changed (Points 8-9) required a larger movement than that in load step 2 (Points 5-6). This follows the trend over all the tests that as the displacement is increased, the displacement required to fully unload the structure increases. Zero load was achieved at an absolute displacement of –27 mm.

Between Points 9 and 10, and through to a displacement of approximately 15 mm, the rate of increase in positive load degraded slightly as the maximum load of the frictional component of resistance was approached (Figure 7). The rise in rate of load increase due to the passive contribution occurred at a displacement corresponding to that experienced in load step 3.

The actual peak lateral load was not attained because the actuator reached its capacity at a load of 527 KN and displacement of 43 mm. Inspection of the load displacement plot indicates that the peak load would not have substantially exceeded 530 KN. As the actuator reached its capacity, the displacement slowed. Therefore the majority of movement at this load level was due to creep in the soil.

The slab showed widening of the cracking observed in the top of the slab in Load step 2 (Figure 10). No new cracks were observed, although the cracking at 500 mm on the right, and 600 mm on the left of the slab was most pronounced. On the west foundation beam end of the structure barely detectable hairline cracking was observed, extending from the bottom of the slab approximately 300 mm off the masonry wall. This was observed on both sides of the test specimen.

The only soil deformation observed in this direction was, as with the previous load step (Figure 9), cracking running diagonally from the compression corners of the foundation beams. The displacements in this test were simply not large enough to bring about any noticeable heave on the ground surface. Likewise, no uplift of the structure as a result of heave under the concrete slab was observed. This could, however, also be due to the increased dead load in this test.

4.3.5 **Load steps 5-11** (Points 13-30 on Figure 4.13)

Total unloading in load step 5 occurred within a change in displacement of 14 mm (Points 11-12). This unloading was more rapid than that in load step 4, which will have been partially due to the creep in the soil experienced at the end of load step 4 as the actuator capacity was reached. Between Points 12 and 13, however, the behaviour of the load versus displacement relationship was very similar to the corresponding behaviour between Points 9 and 10 in load step 4.

From Point 13 to Point 25 two hysteresis loops were completed which attained displacements of between -32 mm and 34 mm (Points 14 and 20). The shape of these hysteresis loops is very similar to those in Test 2, despite the larger forces achieved in this test. There was very little degradation in load carrying capacity between the two hysteresis loops.

An interesting aspect of these hysteresis loops was that the stiffness increases just before approaching the peak positive loads at Points 17 and 23, which can be attributed to the fact that the maximum displacement achieved in this direction in load step 4 was slightly less than that in the opposite direction and so the trench formed by the foundation beams will have applied passive resistance to the structure earlier in this direction of loading. The peak positive loads at Points 17 and 23 are correspondingly greater than those at Points 14 and 20 for the same reason.

The loads at the zero-displacement position (Points 13, 16, 19, 22, 25 and 28) are consistently smaller in magnitude in positive load than in negative load (average values of 114 KN as opposed to -152 KN), the opposite behaviour to that shown in the similar load steps in Test 2. This observation may be related to the more rapid unloading of the specimen when the direction of loading is changed towards the concrete pile cap.

Once total unloading had occurred in each load direction, the initial increase in load between the zero-load position and the zero-displacement position was consistently higher than that after the zero displacement position had been reached (that is, between Points 15 and 16 as opposed to after Point 16), indicating that the load versus displacement relationship was tending towards a limiting value of load while the passive resistance of the soil was not present. Unfortunately, owing to the limited displacement that was achieved in this test, a clear limiting load value was not arrived at before the passive contribution of the soil began to contribute to the load.

Structurally, the test specimen showed widening in the cracking that had developed in the first four load steps. With each load step the cracking progressively, but slowly, developed a little more. However, additional hairline cracking was observed across the centre of the slab at the end of load step 9 (Point 26). The cracking was only detectible in the top of the slab and extended from 1300 mm off the foundation beam masonry wall farthest from the reaction pile cap on the right-hand side, to 2000 mm off the masonry wall on the left side of the structure. No new soil deformation was observed.

Once load step 9 (Points 23-26) reached the zero-displacement position (Point 25), marking the completion of the two low-displacement hysteresis loops, the test specimen was pulled out to full displacement. The load versus displacement relationship closely followed the behaviour shown in load steps 5 and 7 before the stiffness increased when the displacements of Points 14 and 20 were exceeded. The load achieved at the maximum displacement of –51 mm was –485 KN, lower than that achieved in load step 3 owing to the previous compaction of the soil at this displacement.

The load displacement path followed in load step 10 was almost exactly the same as that observed in load step 4. The only real differences were the later increase in stiffness when nearing Point 29 and the slightly lower ultimate load achieved. The unloading was very similar to that in load step 5. The testing was terminated at Point 30.

4.3.6 Test 3 summary

The structural performance of the test structure proved to be far more satisfactory than Test 2, despite the much higher loads imposed upon the structure.

The main limitation of the test was that the capacity of the actuator was reached in both directions of loading prior to obtaining a steady state maximum load. Once the capacity was reached, further displacement was impossible. However, from the shape of the load versus displacement curve it was evident that the maximum lateral capacity of the structure was very nearly reached in both directions. The greatest problem posed by the limitation was that because the larger displacement cycles were not achieved, the trench in the soil was not developed in the same manner as in Test 2, so the maximum lateral capacity of the friction mechanism could not be fully isolated owing to the unwanted contribution of the passive resistance. The maximum load values in each direction are summarised in Table 4.6.

Table 4.6. Summary of maximum loads achieved in each direction of loading, Test 3.

Load Step No.	**3**	**4**
Load (KN)	-504	521

Limited cracking was observed in the slab. No uplift of the structure was measured, presumably because the passive soil wedge was not fully developed.

5 SLAB AND BEAM INTERACTION

This section discusses the results of the slab and beam experiments and summarises the main observations. A numerical model for predicting the ultimate lateral capacity of simple slab and beam foundations is proposed and compared with the measured results. A simple empirical relationship is derived for predicting initial stiffness of simple foundations under lateral loading.

5.1 General observations

The general failure mechanism for the structures under lateral loading was remarkably similar to the "Wedge Failure" cartoon of Figure 1.2. A clearly defined passive wedge developed under the slab in the direction of loading that "jacked" the structure up off the ground leaving a void under the slab. A single, significant difference from the cartoon is that, for the test structure, only one side was "jacked" off the ground because each foundation beam had slab attached to one side only, resulting in the motion indicated by the cartoon in Figure 5.1.

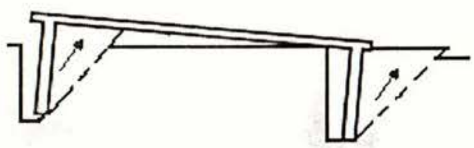

Figure 5.1. Observed failure mechanism.

A large gap opened up behind each foundation beam, as clearly seen in Figure 5.2, and as predicted in the cartoon of Figure 1.2. This gap proved to be significant because when the direction of loading was reversed the gap had to close before passive soil resistance could be mobilised in the opposite direction, causing substantial "pinching" of the load-displacement curves.

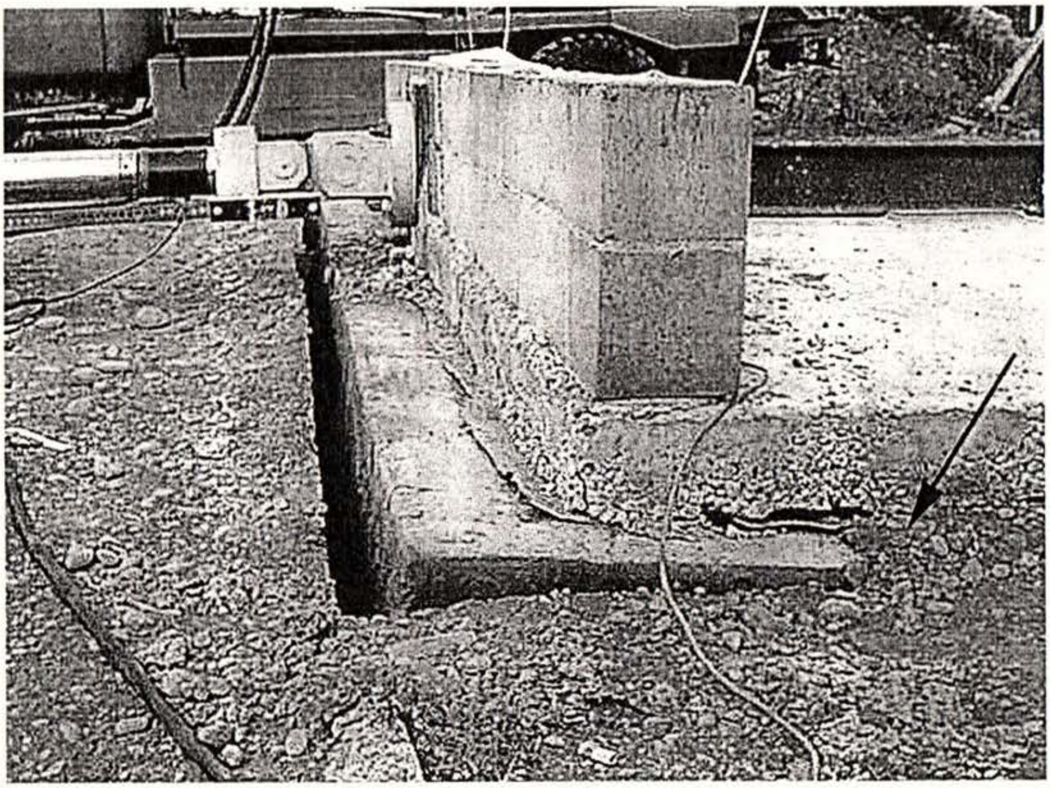

Figure 5.2. Rotation and uplift of foundation beam for Test 2. Arrow indicates location of the passive soil wedge.

5.2 Analysis of results

From the observed general failure mechanism, the forces acting on the structure may be summarised as shown in Figure 5.3. R_1 and R_3 represent the passive earth pressure acting against the faces of the foundation beams. R_2 represents the additional lateral earth pressure from the force R_5 acting on the passive wedge as it lifts one side of the structure. The line of thrust of R_5 is assumed to act through the centre of the wedge. R4 represents friction acting on the base of the foundation beam and F is the applied lateral load acting with eccentricity *e*.

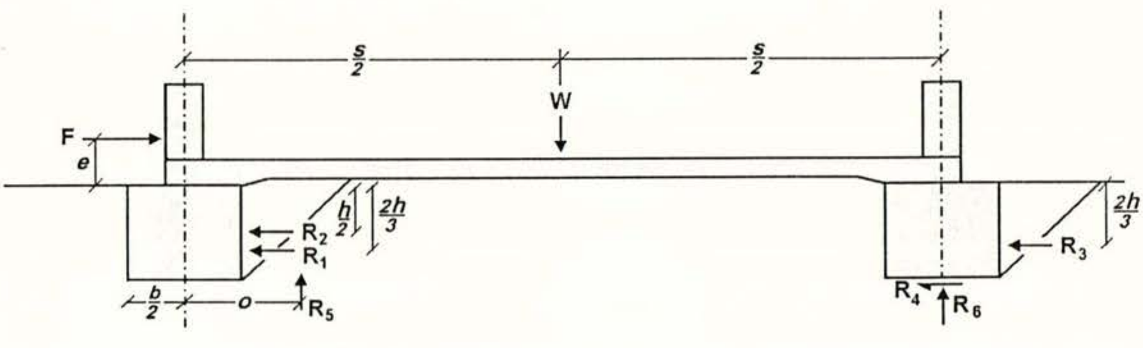

Figure 5.3. Forces acting on structure with lateral loading by force F.

Since the left hand beam is moving upwards with the passive soil wedge, there will be no friction acting on the vertical face of the beam and it may be treated as frictionless. Therefore, Rankine's simple theory may be used to compute R1:

$$R_1 = 0.5 K_p \gamma h^2 L \tag{5.1}$$

$$K_p = \frac{1+\sin\phi_b}{1-\sin\phi_b} \tag{5.2}$$

in which ϕ_b = the backfill material angle of internal friction, and L is the length of the foundation beam.

There will be friction between the right hand beam and the right hand passive wedge of soil. This friction tends to increase the passive resistance R_3 while simultaneously reducing R_6 and the resulting friction R_4. The net effect on the total lateral resistance is probably negligible and so the simplifying assumption of a frictionless wall was applied to the computation of R_3:

$$R_3 = R_1 \tag{5.3}$$

The remaining reaction forces are given by:

$$R_2 = R_5 K_p \tag{5.4}$$

$$R_4 = R_6 \tan\phi_g \tag{5.5}$$

$$W = R_5 + R_6 \tag{5.6}$$

in which ϕ_g is the interface friction angle between the base of the foundation beam and subgrade. The line of action of R_5 is given by:

$$o = \frac{h}{2}\tan(45^\circ + \frac{\phi_b}{2}) + \frac{b}{2} \tag{5.7}$$

An explicit expression for R_6 was obtained from consideration of rotational equilibrium of the structure, as follows:

$$R_6 = \frac{(R_1 + R_3)(1 + \frac{2h}{3e}) - W(\frac{o}{e} - \frac{s}{2e} - K_p(1 + \frac{h}{2e}))}{\frac{s}{e} - \tan\phi_g(1 + \frac{h}{e}) - \frac{o}{e} + K_p(1 + \frac{h}{2e})} \tag{5.8}$$

The lateral capacity then is given by:

$$F = R_1 + R_2 + R_3 + R_4 \tag{5.9}$$

Computations were made to predict the measured capacities for Tests 2 and 3 with the results summarised in Tables 5.1 and 5.2. Good agreement was obtained in both cases. The slight (6 – 10 percent) underestimate of capacity is probably because of a slight underestimate of the soil strength properties. The test soils were above the water table and were moist and might be expected to show some apparent cohesion. However, the soil strengths used in the computations are what a designer might reasonably estimate and the slight conservatism resulting is considered appropriate.

Table 5.1. Computed lateral capacity Test 2.

W	L	e	s	b	h	γ	ϕ_g	ϕ_b	F	Test 2*
(KN)	(m)	(m)	(m)	(m)	(m)	(KN/m^3)	(deg.)	(deg.)	(KN)	(KN)
118.1	4.25	0.125	4.0	0.6	0.45	17.2	40	35	263	292

* - average of both directions of loading

Table 5.2. Computed lateral capacity Test 3.

W	L	e	s	b	h	γ	ϕ_g	ϕ_b	F	Test 3*
(KN)	(m)	(m)	(m)	(m)	(m)	(KN/m^3)	(deg.)	(deg.)	(KN)	(KN)
233.4	4.25	0.125	4.0	0.6	0.45	17.2	40	35	482	515

* - average of both directions of loading

The computations are highly sensitive to changes in the ratio of load eccentricity (e) to width (s). Increasing load eccentricity causes transfer of structural weight from the left hand passive wedge to the right hand beam (in Figure 5.3). This weight transfer significantly reduces the lateral resistance of the structure because weight applied to the left hand passive wedge is very effective, increasing the lateral earth pressure on the left hand beam by factor K_p (values typically 3 – 4).

With reversal of loading direction, as the structure moved back through its central position, lateral load resistance was observed to decrease to low values as the vertical faces of the foundation beams lost contact with the backfill material. For Test 2, by the third cycle of loading, lateral resistance had dropped to approximately 40 KN. The structure presumably was sliding on the DPC/sand interface with an equivalent friction angle of 19 degrees. For Test 3 the minimum lateral resistance at zero displacement was 114 KN, equivalent to a friction angle of 26 degrees. These friction values are close to the measured values for a slab sliding on a single layer of DPC suggesting that, between displacement extremes, the structure is simply sliding back-and-forth supported by the slab resting "on grade".

The initial stiffness of the slab and beam foundation system, prior to development of the full passive soil wedges was high (21.3 KN/mm for Test 2 and 32 KN/mm for Test 3) and quite linear up to approximately 50 percent of the ultimate capacity. For design purposes, it is recommended that the initial stiffness for a shallow foundation system be taken as:

$$K_H = \frac{H_u}{15} \tag{5.10}$$

in which K_H = foundation initial stiffness (KN/mm) and H_u = foundation ultimate lateral resistance (KN). This equation is completely empirical and based on the results of Test 2, Test3, and Test 4. However, these tests used full-scale typical foundation details and backfill materials and should provide reliable guidance.

Continued loading beyond 50 percent of the ultimate lateral capacity causes a steady softening of load-displacement response as the full passive wedge develops, until eventually a completely flat, steady-state response is achieved at about 60 mm displacement.

6 PILE INTERACTION EXPERIMENT

This section describes the single load test performed on a combined slab, beam, and pile foundation, Test 4. The objective was to measure the overall load-displacement response of such a combined foundation system to allow development of a design methodology incorporating the load-displacement response of a shallow foundation system with that for lateral loading of a pile. The construction details are summarised together with the loading methodology and the load test measurements.

6.1 Construction procedure

A shallow foundation was constructed to the same pattern as Test 3, with details as shown in Figure 3.3. In addition, a single steel pipe pile with dimensions listed in Table 6.1 was placed in the centre of the slab.

Table 6.1. Dimensions of steel pipe pile.

Length Overall	4.55 m
Embedded Length	4.45 m
Overall Diameter	168 mm
Wall thickness	7 mm

The pile was placed prior to constructing the shallow foundation by excavating a pit 4.5 m deep with a hydraulic excavator, placing the pile, then backfilling carefully around the pile, tamping the soil with the excavator bucket. The installed pile is shown in Figure 6.1 after completing of the backfilling and before construction of the shallow foundation. The completed foundation with pile and shallow foundation, ready for testing, is shown in Figure 6.2.

Figure 6.1. Steel pipe pile in place prior to construction of shallow foundation.

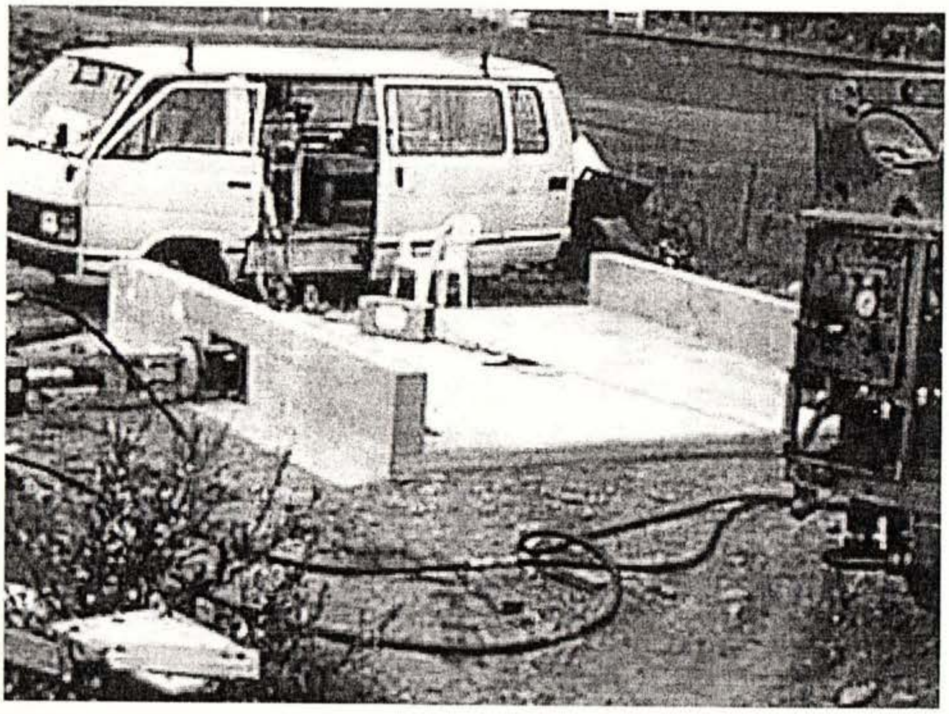

Figure 6.2. Completed foundation with slab on grade, foundation beams, and centrally located steel pipe pile.

6.2 Pile lateral load test

Prior to constructing the shallow foundation, the steel pipe pile was subjected to a lateral load test to establish the load-displacement characteristics for the pile-soil interaction. The test was conducted simply by using a hand-operated hydraulic actuator, an electronic load cell, and a linear variable displacement transformer

(LVDT). The pile was given two cycles of lateral displacement to 28 mm in one direction with the resulting load-displacement curve shown in Figure 6.3.

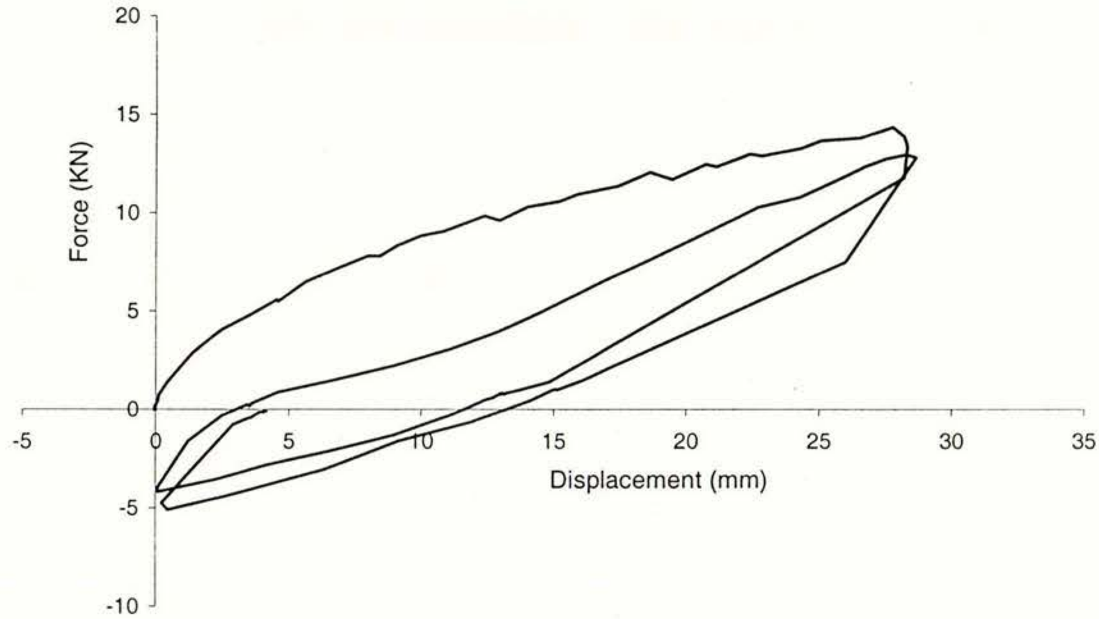

Figure 6.3. Load versus displacement for steel pipe pile in free-head condition.

The loading condition was "free-head", as shown in Figure 6.1, with an eccentricity of loading of 0.46 m. The average "stiffness" over the 28 mm displacement range was 0.5 KN/mm.

6.3 Testing procedure

The arrangement for load testing the foundation (Test 4) was generally similar to Tests 2 and 3 as described in Section 3, and is shown in Figure 6.4. The main difference from the previous tests was that no steel beam was placed on the slab.

The equipment used, instrumentation, and loading rates were all as described in Section 3 for Tests 2 and 3.

Some difficulties arose with the mechanical set up of the actuator that restricted movement in one direction (inwards, or pulling direction) to only 20 mm. However, movement in the opposite direction (outwards, or pushing direction) was correspondingly increased to 120 mm.

Also, a failure occurred with the data acquisition system during the initial part of the load test leading to some lost data from the first load cycle and a restart of the test for the second load cycle.

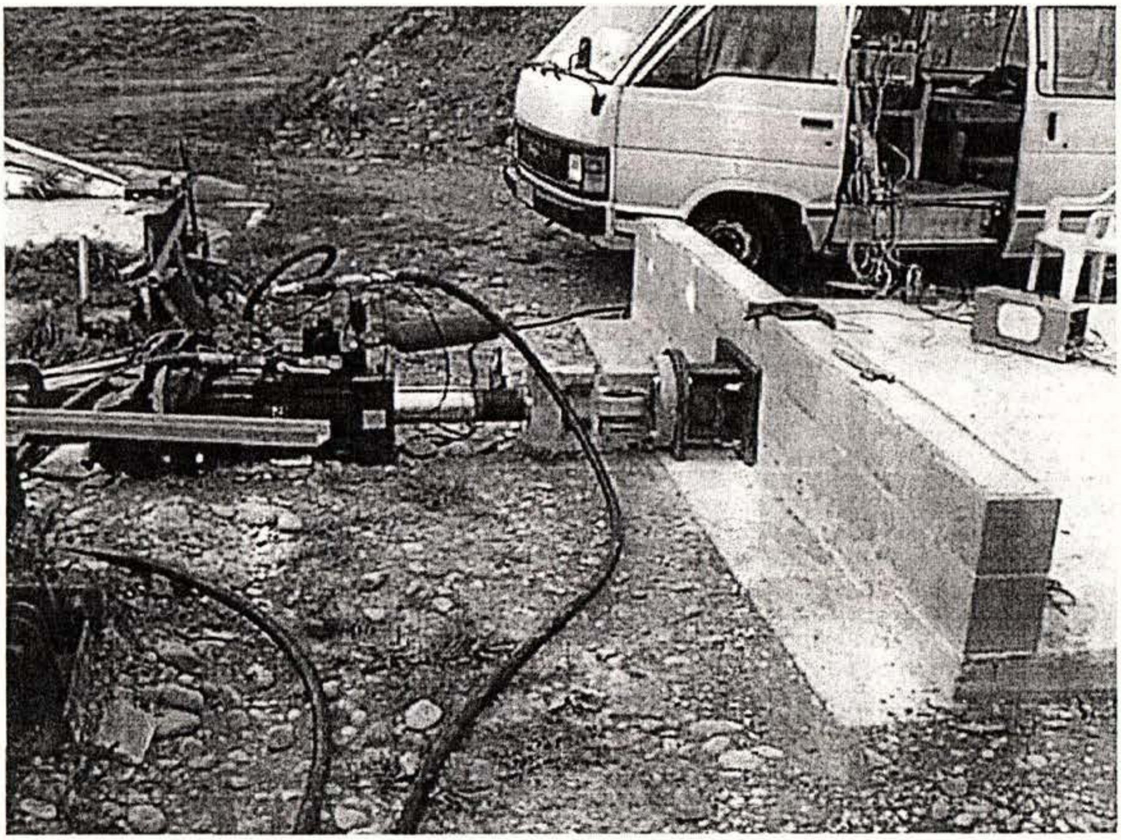

Figure 6.4. Load testing arrangement for Test 4.

6.4 Load test results

The results for the first load cycle and the remainder of load cycles for the test are shown separately in Figures 6.5 and 6.6, because the load test was restarted after difficulties during the first load cycle. Measured values of load and displacement are summarised for key points in Table 6.2.

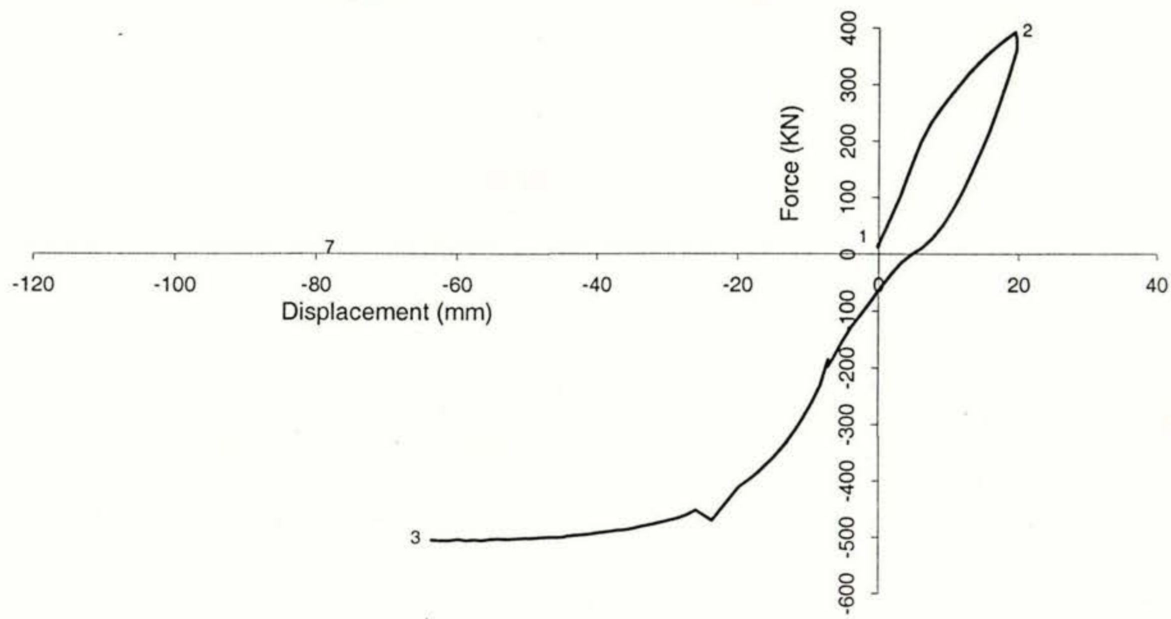

Figure 6.5. Load versus displacement for first load cycle (Marked points are referenced in Table 6.2).

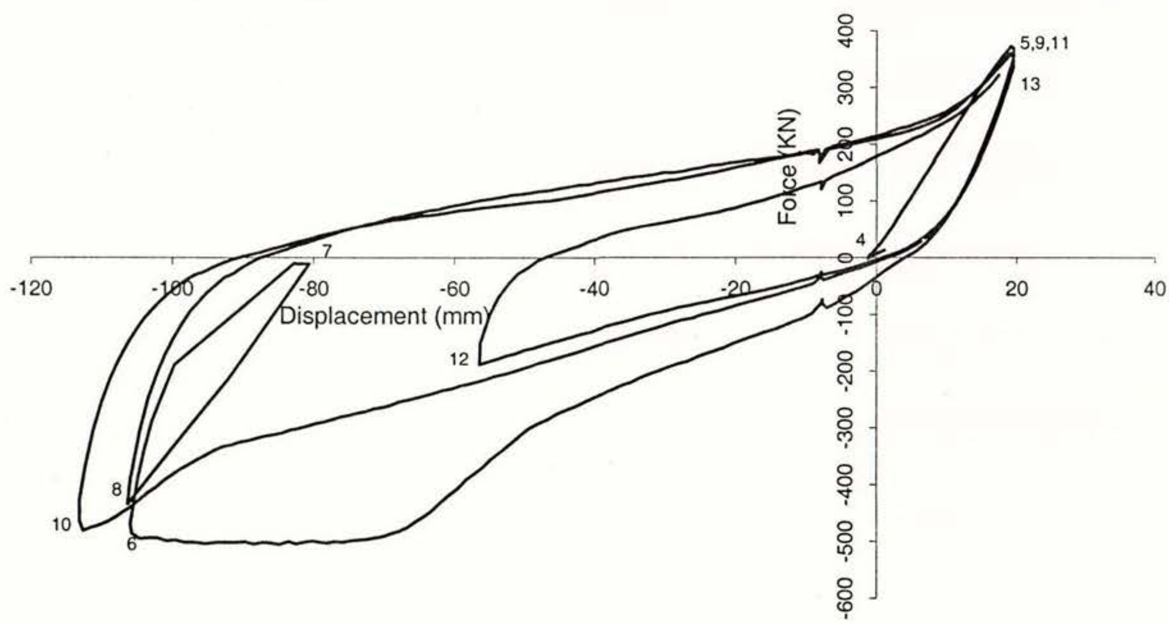

Figure 6.6. Load versus displacement for second load cycle (Marked points are referenced in Table 6.2).

Table 6.2. Summary of significant load steps for Test 4.

Point Number	Displacement (mm)	Load (KN)
1	0	20
2	19.4	392
3	-63.6	-505
4	-0.7	7
5	19.1	372
6	-105.8	-485
7	-80.7	-11
8	-106.4	-434
9	19.5	359
10	-112.7	-480
11	19.4	361
12	-56.5	-188
13	17.4	322

For the first load cycle, the actuator was initially retracted, "pulling" the structure towards the reaction block to the maximum available displacement in that direction (19.4 mm) and reaching a maximum load of 392 KN at Point 2. From Figure 6.5 it is clear that the load was still increasing at Point 2 and that the maximum capacity of the foundation system had not been reached. Then, the direction of loading was reversed and the structure was "pushed" away from the reaction block, initially causing the load to decrease in tension and then increase in compression. This "push" was terminated once a "steady state" condition had been achieved at Point 3 in Figure 6.5 at a displacement of -63.6 mm and a load in compression of -505 KN. Next, the direction of loading was reversed again, with the actuator "pulling" back towards the reaction block, however the data for this part of the load cycle was lost because of a malfunction and so the structure was re-positioned at the initial starting position (point 4 on Figure 6.6) and the second cycle of loading was restarted from there.

This first load cycle appears to have mobilised the full passive resistance of the soil during the "push" part of the cycle and the extent of the passive wedge can be seem in Figure 6.7, which shows cracking in the ground surface about 0.9 m in front of the foundation beam. A gap can also be seen between the foundation beam and the backfill material, which opened during the "pull" phase of the load cycle between Point 3 in Figure 6.5 and Point 4 in Figure 6.6.

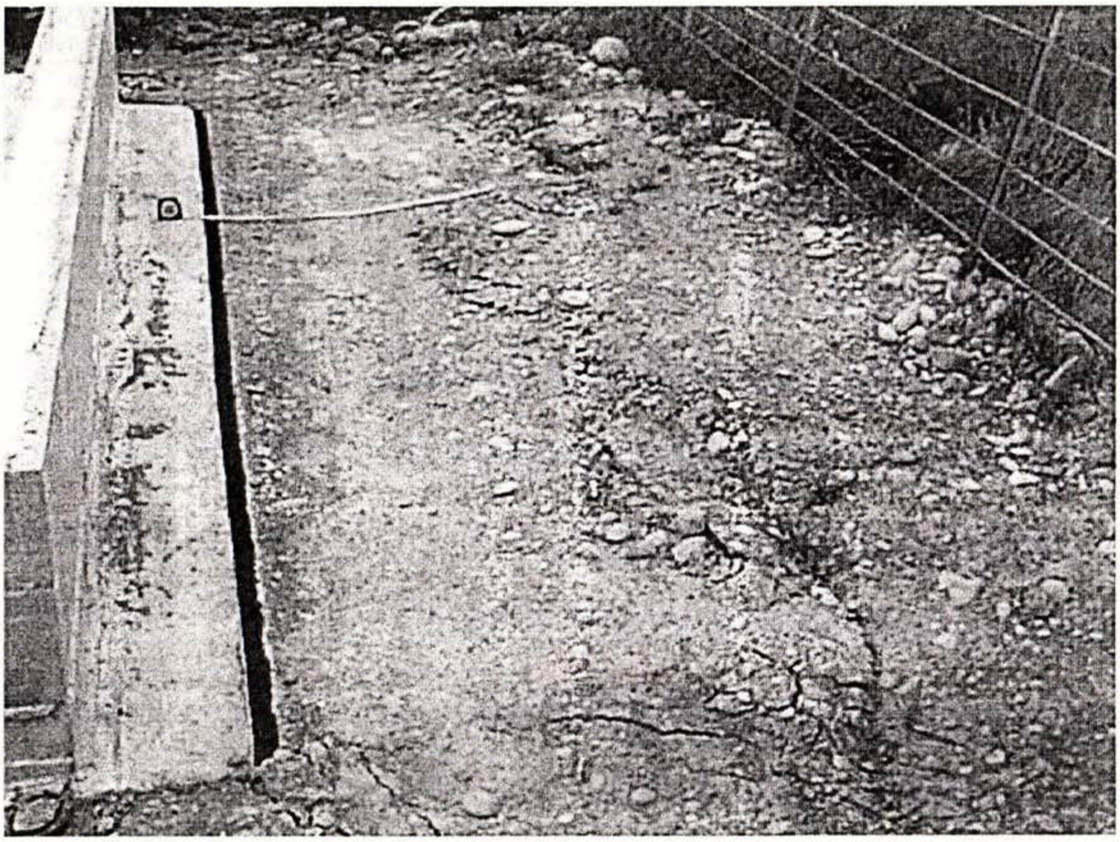

Figure 6.7. Extent of gapping and passive wedge after first load cycle, Point 4.

The second cycle of load was commenced from Point 4 in Figure 6.6 by "pulling" the structure to maximum retraction at Point 5 (19.1 mm). Again, the measured load of 372 KN did not appear to have reached a maximum value, but it was impossible to "pull" the structure any further in this direction. Then, the direction of loading was reversed and the structure was "pushed" to near maximum displacement away from the reaction block (-105.8 mm) with a steady state load of 485 KN being achieved at Point 6.

Again, the full passive resistance of the soil in "front" of the foundation and ahead of the "trailing" foundation beam appears to have been mobilised causing uplift of the "trailing" foundation beam and rotation of the entire structure, as shown in Figure 6.8.

"Heaving" of soil in the passive wedge between the "trailing" foundation beam and the adjacent slab is shown in Figure 6.9.

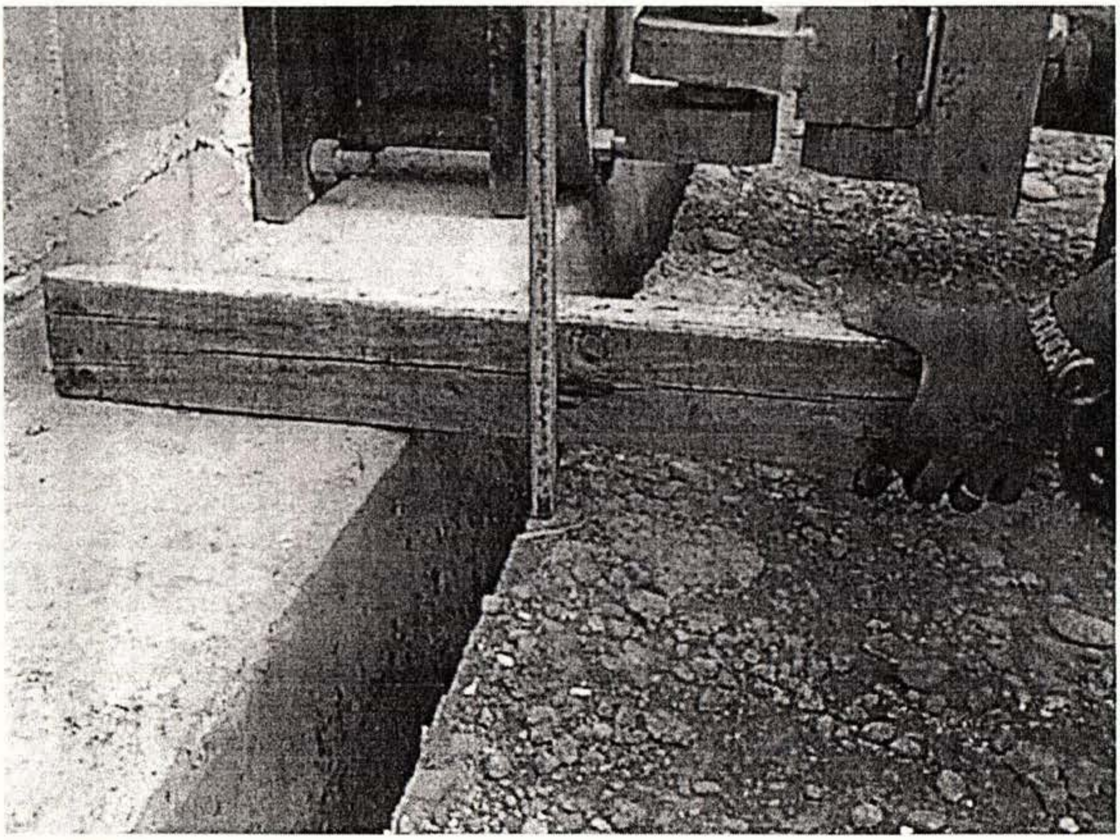

Figure 6.8. Foundation gapping and uplift after second load cycle, Point 6.

Next, the structure was completely unloaded to Point 7 in Figure 6.6, leaving a permanent displacement of -80.7 mm. The structure was next reloaded to Point 8 and then unloaded again and "pulled" back through the "zero" position to Point 9 being maximum retraction (19.5 mm) with a measured load of 359 KN.

The third load cycle was essentially a repeat of the second cycle described above, with the structure being "pushed" out to near maximum extension of the actuator (Point 10) then "pulled" back to maximum retraction (Point 11).

The fourth and final cycle of loading was made by "pushing" the structure to a lesser outwards displacement of -56.5 mm (Point 12) then "pulling" back to maximum retraction (Point13). The key measurements of load and displacement are listed in Table 6.2.

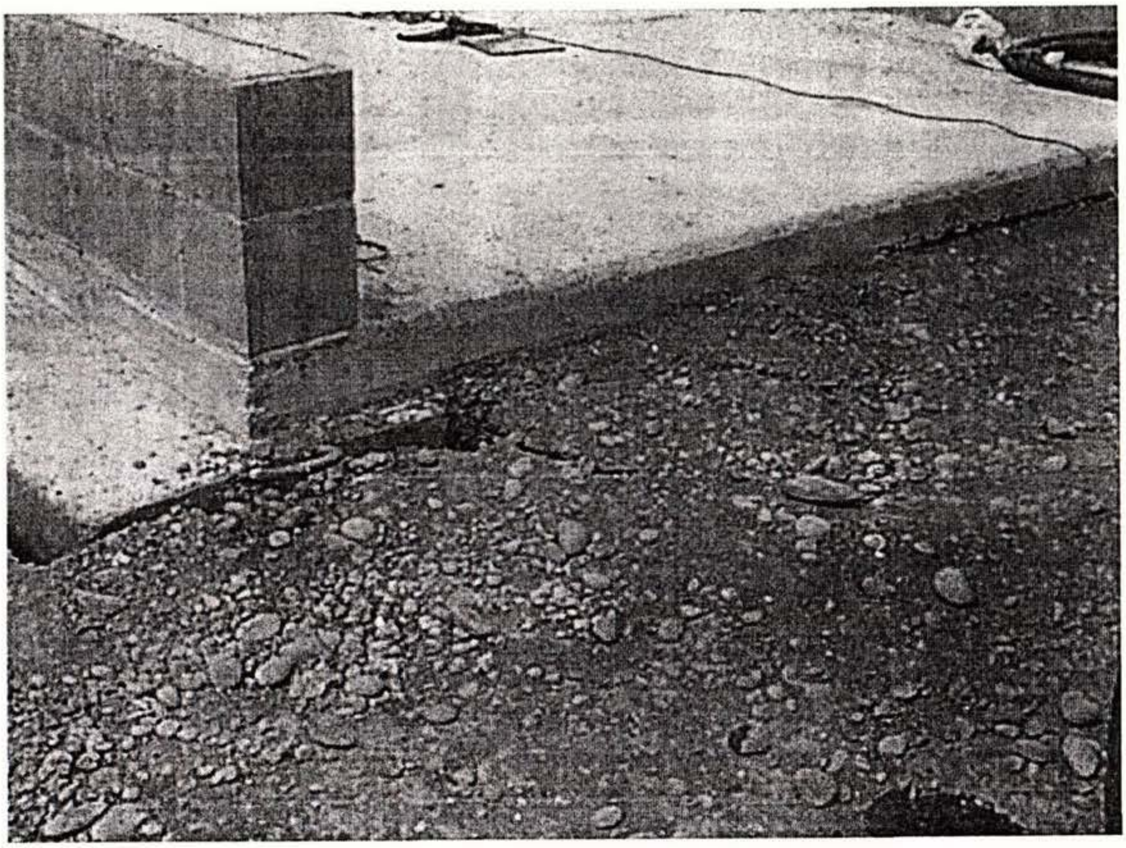

Figure 6.9. Passive wedge during push phase of load cycle 3, Point 10.

The final state of the foundation and adjacent soil is shown in Figure 6.10 after returning the foundation to the initial or "zero" displacement position. A gap is clearly defined either side of the foundation beam, larger on one side (the direction of "pushing") than on the other(the direction of "pulling") because of the asymmetry of loading. Cracking of the ground surface indicates the location of the passive soil wedge developed between the foundation beam and the adjacent slab.

Figure 6.10. Gapping and passive wedge after completion of testing.

7 PILE INTERACTION ANALYSIS

This section examines the results of the pile interaction load experiment (Test 4) and attempts to explain and predict the results using rational numerical models. First, the response of the single steel pipe pile is examined by back-analysing the measured free-head response. Then, the fixed-head response of the pipe pile after being cast into the foundation slab is predicted by using well established numerical procedures. The interaction between the pile and the shallow beam and slab foundation is then considered and compared with the observed behaviour of Test 4.

7.1 Free-head pile response

After installation of the pile and prior to pouring the foundation beams and slab, the steel pipe pile was subjected to a simple one-way load-displacement test to establish the in-situ soil modulus. The pile was in a free-head condition and the displacement under lateral load may be predicted using the following equation (Poulos, 1980):

$$\rho = \frac{H}{N_h L^2}\left(I'_{\rho H} + \frac{e}{L}.I'_{\rho M} \right) \tag{7.1}$$

in which $I'_{\rho H}, I'_{\rho M}$ =elastic influence factors for linearly varying soil modulus, E_s, and N_h = rate of increase of soil modulus E_s with depth.

From the above equation, and using the values for the steel pipe pile listed in Table 7.1, a value of N_h = 1100 KN/m^3 was back calculated for the backfill soil surrounding the pile. This value is at the lowest end of the range suggested by Terzaghi (1955) for loose moist sand (3.5 – 10.5 ton/ft^3 or 1100 – 3300 KN/m^3).

Table 7.1. Values used to back-calculate N_h for free-head pipe pile.

Property	Symbol	Value
Embedment length	L	4.09 m
Eccentricity of load	e	0.46 m
Pile moment of inertia	I_p	1.15×10^7 mm^4
Pile modulus of elasticity	E_p	200 GPa

7.2 Fixed-head pile response

Using the back-calculated value for N_h it was possible to predict the load-displacement response for the pile in the fixed-head condition after being cast into the concrete foundation slab, as follows:

First, the ultimate lateral capacity of the pile in the fixed-condition was estimated to be 70 KN using the method of Broms (1964), as described in Section 1, using the values for soil properties listed in Table 7.2 and pile properties listed in Table 7.1. Then, the load-displacement response was estimated using the following equation (Poulos, 1980):

$$\rho = \frac{H}{N_h L^2}\left(I'_{\rho F}\right)\frac{1}{F'_{\rho F}} \tag{7.2}$$

in which, $I'_{\rho F}$ =elastic influence factor and $F'_{\rho F}$ =yield displacement factor to account for soil non-linearity.

Property	Symbol	Value
Unit weight	γ	17.2 KN/m^3
Coefficient of passive earth pressure	K_p	5.3

The initial (or "elastic") stiffness was calculated to be 1.3 KN/mm and the complete prediction for load-displacement response is given in Figure 7.1.

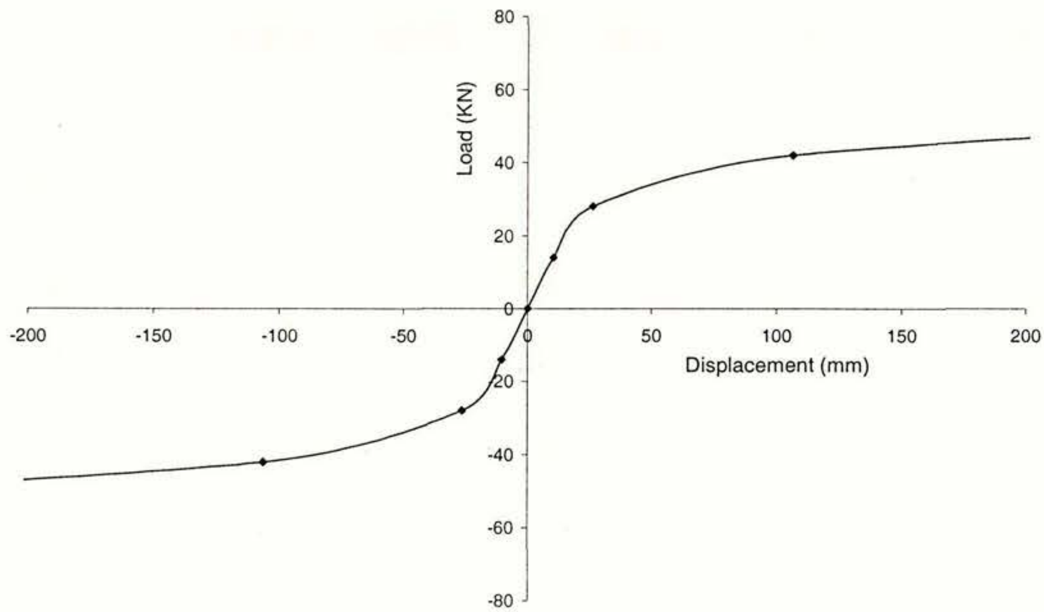

Figure 7.1. Load-displacement response estimated for fixed-head steel pipe pile.

7.3 Ultimate lateral capacity of beam-slab-pile foundation

The ultimate lateral capacity of the steel pipe pile was calculated to be 70 KN, by using the method of Broms (1964b). However, from Figure 7.1, the lateral resistance of the pile at the maximum displacement of the test foundation (112.7 mm) was calculated to be only 43 KN.

In addition to making this "direct" contribution to the lateral resistance of the foundation system of 43 KN, the steel pipe pile should have made an "indirect" contribution by resisting the uplift of the foundation by the passive wedge trapped underneath the slab. Therefore, the capacity of the beam-slab-pile foundation was calculated by using Equations 5.1 to 5.9 and adding the estimated uplift capacity of the steel pipe pile (26 KN) to the foundation weight, W.

The calculated value of 414 KN compares favourably with the measured maximum lateral capacity (505 KN first cycle to 480 KN third cycle), given the inherent uncertainty of the estimating procedures. The estimated value is comfortably conservative, with the variance possibly attributable to a number of factors such as slight apparent cohesion of the moist backfill and sub-grade materials. The soil strengths used in the calculation are what a designer might reasonably estimate and the slight conservatism resulting is considered appropriate.

7.4 Initial stiffness of beam-slab-pile foundation

The initial stiffness of the steel pipe pile in fixed-head condition was calculated to be 1.3 KN/mm. The initial stiffness for lateral loading of the beam and slab shallow foundations (Tests 2 and 3, measured over then first load cycle to 50 percent of maximum load) were both much higher (21.3 KN/mm and 32 KN/mm) and so the pile was not expected to make a significant direct contribution to foundation lateral stiffness. However, again, the pile is expected to make an "indirect" contribution to foundation stiffness by resisting foundation uplift and increasing soil passive resistance.

The initial stiffness was predicted by using Equation 5.10 to estimate the contribution from the slab and beam foundation elements and then adding the direct contribution from the pile to give a total prediction of 35.0 KN/mm compared with the measured value of 34.5 KN/mm for Test 4.

7.5 Ductility demands

Even though the steel pipe pile made only a minor contribution to the ultimate lateral capacity of the total foundation system, it is likely that the pipe pile had severe ductility demands placed upon it with yielding of the pile in bending initiating at a displacement (approximately 14 mm) well before the ultimate lateral capacity had been reached (approximately 60 mm). While the ductility of the steel pipe pile used for Test 4 was probably adequate, other pile types (e.g. reinforced concrete) may have been damaged unless special detailing had been applied.

8 SUMMARY AND CONCLUSIONS

This section summarises the results of the experiments and the main conclusions for this project. Where appropriate, recommendations for practice are included.

8.1 Sliding of slab on grade

The simplest shallow foundation is a concrete slab poured on grade, usually with either one or two layers of polymer damp course (DPC). The base sliding characteristics of such "slab-on-grade" construction were determined for large (2 m wide x 3 m long) slabs constructed using standard construction details and materials. One and two layers of DPC were used and some slabs were weighted with ballast. All of the test results are summarised in Table 2.1 with the main conclusions as follows:

1. Peak friction angles (measured during initial loading) ranged from 28 degrees for a single layer of DPC with 6.6 KPa contact pressure to 12 degrees for a double layer of DPC with 3.1 KPa contact pressure.

2. Mean friction angles were all 2 degrees less than for the peak friction angles.

3. Increasing the contact pressure (by adding ballast to the slabs) increased the friction angle in all cases.

4. Placing two layers of DPC significantly reduced the friction angle (although the amount of reduction was reduced for the ballasted slab).

The values for friction angle determined in these tests should be directly applicable to engineering practice because the details were chosen carefully to comply with standard New Zealand construction practice. However, the results seem to be sensitive to contact pressure and for cases where the contact pressure is greater than the maximum tested herein (6.6 KPa) it is likely that the friction angle will continue to increase, perhaps up to the full friction angle of the soil sub-grade.

8.2 Sliding of slab and beam foundations

Few foundations are ever made that consist only of "slab-on-grade" with no down turned foundation beams of some type. Most shallow foundations have foundation beams of some description together with floor slabs that are either suspended or built "on-grade". Even when slabs are built "on-grade" they usually are structurally connected to the foundation beams, or should be. Most foundations will have perimeter beams at least and these beams generate significant passive resistance to lateral movements.

In this study, three slab and beam type foundations were constructed and subjected to various cycles of lateral loading. The foundations were all of the same size (approximately 4 m square) with parallel foundation beams (600 mm wide x 500 mm deep) on two sides. Construction details were based on standard New Zealand design practice. Loads were applied at the level of the floor slab, perpendicular to the foundation beams. The results are all described in detail in Section 4, with the main conclusions as follows:

1. Lateral loading of the slab and beam foundations resulted in generation of clearly defined passive soil wedges ahead of the advancing foundation beams.

2. For the leading beam, the passive soil wedge pushed up towards the ground surface with corresponding surface cracking clearly seen.

3. For the trailing beam, the passive soil wedge was trapped beneath the floor slab causing the foundation to be uplifted resulting in a gap beneath the floor slab and a marked tilting of the structure.

4. Reversing the direction of loading caused passive soil wedges to be generated on the opposite faces of the beams with tilting in the opposite direction.

5. Reversing the direction of loading caused gaps to open between the training faces of the beams and the adjacent soil. These gaps caused a significant softening of load-displacement response whenever the direction of loading was reversed as the gaps had to be closed before there was significant contact between the beam faces and the soil and re-generation of passive soil resistance.

6. The ultimate lateral resistance of the foundations was greater than might be estimated from a simplistic analysis considering only self weight of the soil in the passive wedge adjacent to each foundation beam and sliding friction (153 KN compared with 292 KN measured for Test 2, and 250 KN compared with 515 KN measured for Test 3) . Significant additional resistance seems to be generated by the weight of part of the structure being applied as a surcharge to the top of the passive wedge adjacent to the trailing beam.

7. A set of equations (Equations 5.1 to 5.9) were derived to predict the ultimate lateral resistance for a simple beam and slab foundation system. Predictions using these equations were found to slightly under-estimate the measured results of Test 2 and Test 3. However, the soil strengths used in the computations were what a designer might reasonably estimate and the slight conservatism resulting is considered appropriate. It is recommended that these equations might be used by designers to predict the ultimate lateral resistance of simple shallow foundations with two parallel beams. Foundations with more than two parallel beams might be analysed using a similar approach to that explained in Section 5.

8. The computations are highly sensitive to changes in the ratio of load eccentricity (height of action of lateral load above ground line). Increasing load eccentricity causes transfer of structure weight from acting as a surcharge on the trailing passive wedge to acting as a surcharge underneath the leading beam where it generates simple friction only. Therefore, increasing eccentricity should significantly reduce the ultimate lateral resistance of the foundation system.

9. The initial stiffness of the slab and beam foundation system, prior to development of the full passive soil wedges was high (21.3 KN/mm for Test 2 and 32 KN/mm for Test 3) and quite linear up to approximately 50 percent of the ultimate capacity. For design purposes, it is recommended that the initial stiffness for a shallow foundation system be taken as:

$$K_H = \frac{H_u}{15} \tag{8.1}$$

in which K_H = foundation initial stiffness (KN/mm) and H_u = foundation ultimate lateral resistance (KN). This equation is completely empirical and based on the results of Test 2, Test3, and Test 4. However, these tests used full-scale typical foundation details and backfill materials and should provide reliable guidance.

10. Continued loading beyond 50 percent of the ultimate lateral capacity causes a steady softening of load-displacement response as the full passive wedge develops, until eventually a completely flat, steady-state response is achieved at about 60 mm displacement.

11. With reversal of loading direction, as the structure moved back through the central position, lateral load resistance was observed to decrease to low values as the vertical faces of the foundation beams lost contact with the backfill material. For Test 2 and 3, load resistance decreased to values close to the measured values for a slab sliding on a single layer of DPC, suggesting that, between displacement extremes, the structures were simply sliding back-and-forth supported by the slab resting "on grade".

8.3 Pile interaction with slab and beam foundation

Pile foundations may be used instead of shallow foundations where foundation loads exceed the bearing capacity of weak ground or where good ground is underlain by weak layers susceptible to settlement or liquefaction during earthquakes. Generally, the piled foundation system will also include foundation beams and, possibly, slab on grade construction.

With piled foundation systems it is important to know the interaction between the component piles and other foundation elements during lateral loading, because the piles may have limited capacity to withstand lateral loading without brittle failure (especially shear failure) and without loss of axial load capacity.

In this study, methods for estimating pile lateral load capacity and load-displacement response have been reviewed and summarised (Section1). Generally, the load-displacement response of laterally loaded piles is relatively soft unless the individual piles are quite massive. A single experiment (Test 4) was undertaken whereby a single steel pipe pile (168 mm diameter by 4.05 m long) was cast into a slab and beam foundation and then subjected to various cycles of loading. The results are described in detail in Section 6, with the main conclusions as follows:

1. The load-displacement response of the free-head pipe pile (tested prior to casting into the concrete slab) was able to be estimated using the methodology of Poulos (1980) described in Section 1.

2. The direct contribution to the total lateral resistance of the foundation system by the single pipe pile was relatively small for Test 4 (14 percent).

3. An additional, indirect contribution to the total lateral resistance of the foundation system is likely to have come from the uplift resistance of the pile adding to the effective "weight" of the foundation during the tilting and uplift associated with generation of the soil passive wedges.

4. By summing the ultimate lateral resistance of the steel pipe pile calculated (70 KN) using the method of Broms (1964b) and the calculated ultimate lateral resistance of the slab and beam foundation using Equations 5.1 to 5.9 (using estimated soil parameters and increasing the weight of the foundation, W, by the estimated uplift capacity of the pipe pile) a prediction for ultimate lateral capacity for Test 4 of 440 KN was made. However, elastic analysis showed that the actual direct contribution of the pile was probably only 43 KN at the maximum test displacement (112.7 mm), giving a total precited capacity of 413 KN. This value still compares favourably with the measured maximum lateral capacity of 505 KN – 480 KN given the inherent uncertainty of the estimating procedures. The estimated value is comfortably conservative, with the variance possibly attributable to a number of factors such as slight apparent cohesion of the moist backfill and sub-grade materials etc.

5. Even though the steel pipe pile made only a minor contribution to the ultimate lateral capacity of the total foundation system, it is likely that the pipe pile had severe ductility demands placed upon it with yielding of the pile in bending initiating at a displacement (approximately 14 mm) well before the ultimate lateral capacity had been reached (approximately 60 mm). While the ductility of the steel pipe pile used for Test 4 was probably adequate, other pile types

(e.g. reinforced concrete) may have been damaged unless special detailing had been applied.

6. This study has confirmed a general approach for design and analysis of combined beam-slab-pile foundations.

7. References

Brinch-Hansen, J. B. (1961) "The Ultimate Resistance of Rigid Piles against Transversal Forces," *Report 12,* Danish Geotechnical Institute, Copenhagen.

Broms, B.B. (1964a). "Lateral Resistance of Piles in Cohesive Soils," *J. of the Soil Mechanics and Foundations Division,* ASCE, Vol. 90, No. SM2, pp. 27-63.

Broms, B.B. (1964b). "Lateral Resistance of Piles in Cohesionless Soils," *J. of the Soil Mechanics and Foundations Division,* ASCE, Vol. 90, No. SM3, pp. 123-156.

Fang, H-Y., (1991) *Foundation Engineering Handbook, 2nd. Ed.*, Kluwer Academic Press, Boston, 923 p.

Gadre, A., Dobry, R. (1998) "Lateral cyclic loading centrifuge tests on square embedded footing." *Journal Geotechnical and Geoenvironmental Engineering.*, ASCE, Vol. 124, pp. 1128-1138.

Gazetas, G., and Tassoulas, J.L. (1987). "Horizontal stiffness of arbitrarily shaped embedded foundations." *J. Geotech. Engrg.*, ASCE, Vol. 113, pp. 440-457.

Hatzikonstantinou, E., Tassoulas, J., Gazetas, G., Kotsanopoulos, P., and Fotopoulou, M. (1989). "Rocking stiffness of arbitrarily shaped embedded foundations." *J. Geotech. Engrg.*, ASCE, Vol. 115, pp. 457-472.

McManus, K. J. (1997). "Axial Behaviour of Bored Pile Foundations," *Research Report NoEQC 95/184*, Earthquake Commission, Wellington, New Zealand.

McManus, K.J. and Alabaster, D. (2004) "Constant Force Shaking of a Group of Four Drilled Shafts," *J. Geotechnical and Geoenvironmental Engineering,* ASCE, Vol. 130, No. 2, pp.123-128.

Murff, J.D. and Miller, T.W. (1977) "Stability of offshore gravity structure foundations by the upper-bound method," *Proc. of the Offshore Technology Conference*, Vol. 3, pp. 147-154.

Poulos, H. G. and Davis E. H., (1980) *Pile Foundation Analysis and Design,* Wiley, New York, 397 p.

Richards, R., Elms, D.G., and Budhu, M. (1990). "Dynamic Fluidisation of soils." *Journal of Geotchnical Engineering*, ASCE, Vol. 116, pp. 740-759.

Richards, R., Elms, D., and Budhu. M. (1993). "Seismic bearing capacity and settlements of foundations", *Journal of Geotechnical Engineering*, ASCE, Vol. 119, pp. 662-674.

Sarma, S.K., and Iossifelis, I.S. (1990). "Seismic bearing capacity factors of shallow strip footings," *Geotechnique*, ICE, London, 40(2), 265-273.

Terzaghi, K. (1955)

Zeng, X., Steedman, R.S. (1998) "Bearing capacity failure of shallow foundations in earthquakes." *Geotechnique*, ICE, London, 48(2), 235-256.

Proc. NZ Soc for EQ Eng, Wairakei, 2001, Ref: 6P99/423

ENG 323

Lateral Resistance of Shallow Foundations

NZSEE 2001 Conference

K. J. McManus
Department of Civil Engineering, University of Canterbury.

N. R. R. Burdon
Holmes Consulting Group, Auckland.

ABSTRACT: Three shallow foundations each 4.25 m wide x 4.6 m long consisting of a 100 mm thick slab "on-grade" with two foundation beams 600 mm wide embedded 450 mm were constructed in coarse granular material. Each was tested by shoving back-and-forth by a powerful hydraulic actuator with several cycles of quasi-static lateral loading. These tests were supplemented with several, simpler interface sliding tests performed on 2 m wide x 3 m long concrete slabs constructed "on-grade" using one or two layers of polymer damp-proof membranes.

Lateral loading of the slab and beam foundations caused a wedge type of failure mechanism with significant passive soil pressures acting against the vertical faces of the foundation beams. The passive soil wedge developing against the trailing beam lifted one side of the structure vertically leaving hollow space beneath the floor slab. For the somewhat narrow structures tested, significant rotations of the structure occurred.

A simple method of analysis was developed and found to give good predictions for the experimental results while accounting for all of the main parameters. The analysis predicts that lateral load capacity is highly sensitive to the eccentricity (height above ground) of the applied lateral load.

1 INTRODUCTION

The resistance of shallow foundations to lateral loads is often relied upon to transmit the base shear forces from the ground to a building during an earthquake. Considering the importance of this link in the lateral load path it receives little attention in current design practice in New Zealand.

An assumption is commonly made, either explicitly or implicitly, that the combination of sliding friction along the base of the structure and passive earth pressure acting against embedded foundation elements will have ample capacity to resist the design base shear.

However, the actual mechanisms of lateral load resistance for shallow foundations are quite complex and poorly understood. Development of passive earth pressure requires significant plastic deformations within the soil mass and corresponding large movements of the structure. The required earth deformations may not be compatible with the structure's geometry. Also, sliding friction may be limited by the use of polymer based damp proof membranes.

Three possible failure mechanisms are commonly identified for shallow foundation systems (e.g. Clough and Duncan, 1991) as shown in Figure 1: "Wedge Failure", "Flow-Under Failure", and "Tip-to-Top Failure". The "Wedge Failure" is based on classical Rankine passive earth pressure theory, and shows that vertical movement of the structure may be necessary to develop full lateral earth pressure against the foundation beams. The "Wedge Failure" figure also shows the inherent incompatibility between the mechanisms of sliding friction and passive earth resistance with development of the failure wedges lifting the structure off its base.

The "Flow-Under Failure" would apply only to very soft soils such as soft clays. If the foundation beams are spaced closely then a "Tip-to-Tip" failure may occur with shearing of the soil beneath the foundation beams prior to development of a wedge failure mechanism.

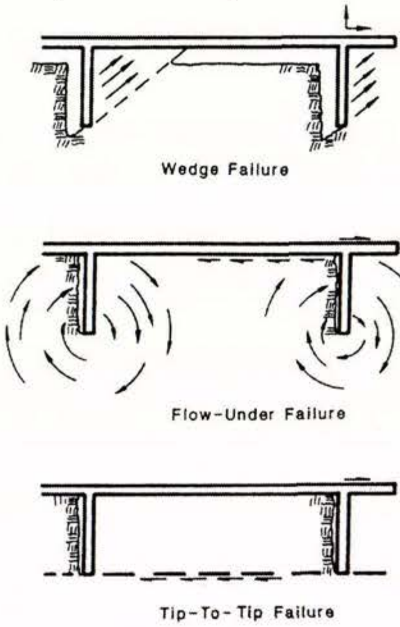

Figure 1. Failure mechanisms for shallow foundations with lateral loading. (Source: Clough and Duncan, 1991)

Murff and Miller (1977) developed equations for predicting the critical spacing of foundation beams necessary to generate a "Tip-to-Tip" failure mechanism. For the idealized foundation system shown in Figure 2, the lateral force developed for each foundation beam is given by:

$$F = 2k_a\sqrt{\frac{Qh}{k_a} + h} \tag{1}$$

in which k_a = weighted average shear strength of the soil, Q = vertical load, and h = depth of the foundation beams. The critical spacing of the foundation beams to generate a "Tip-to-Tip" failure then is given by:

$$\frac{q}{k_a} = 0.25\left(\frac{k_h}{k_a}\right)^2 \frac{S}{h} - \frac{h}{S} \tag{2}$$

in which q = vertical load per unit area, k_h = horizontal shear strength of the soil, S = beam spacing.

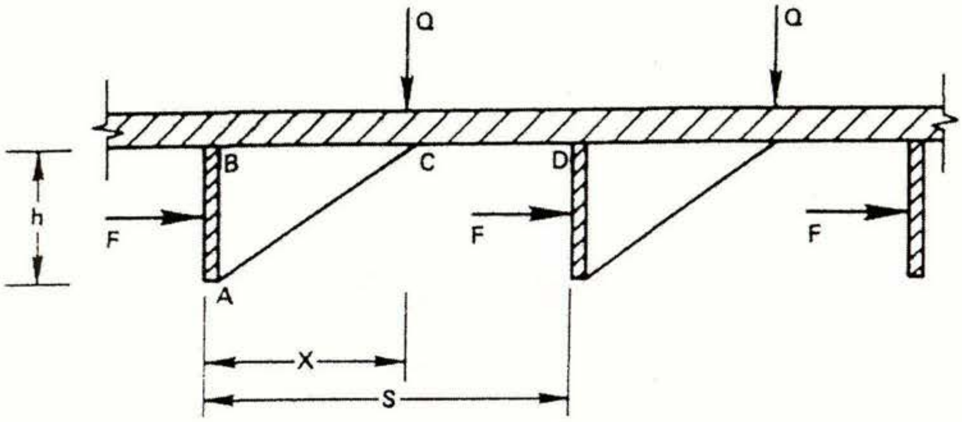

Figure 2. "Tip-to-Tip" failure mechanism. (Source: Murff and Miller, 1977).

The resulting relationship between vertical loading on the foundation and the critical foundation beam spacing is illustrated in Figure 3. The application of these results is limited in practice because the soil shear strengths k_a and k_h are only suitable for modeling the undrained soil condition, i.e. short term loading in silts and clays.

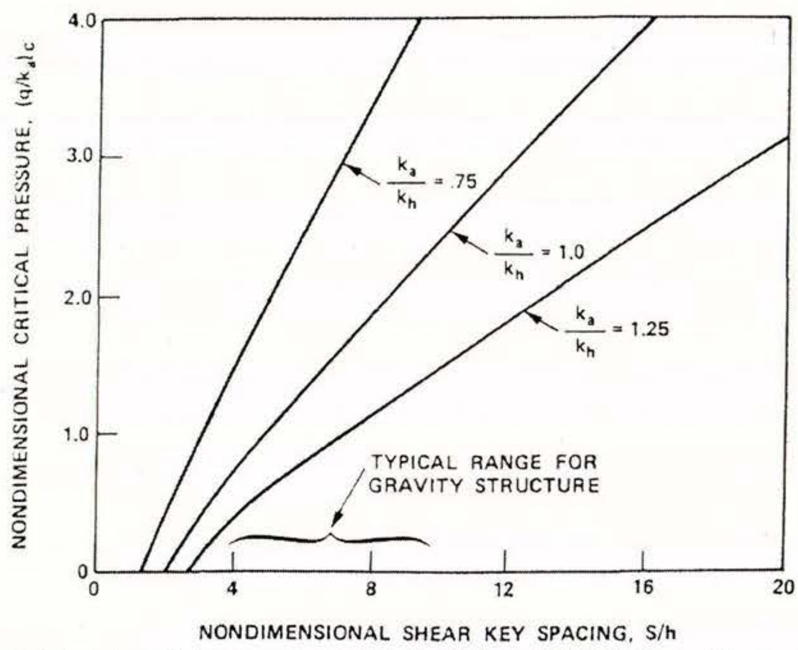

Figure 3. Critical foundation beam spacing for "Tip-to-Tip" failure. (Source: Murff and Miller, 1977).

Gadre and Dobry (1998) applied lateral loads to small-size square footings in a centrifuge at 30 g acceleration. The model dimensions of 38 mm x 38 mm x 28 mm deep scaled to prototype dimensions of 1.14 m x 1.14 m x 0.84 m deep. Significant degradation of lateral stiffness was observed at 25 mm displacement (prototype scale) with ultimate lateral resistance achieved at between 40 – 50 mm.

The objective in this present study was to gain better understanding of the mechanisms of lateral resistance of shallow foundations and to provide designers with both qualitative and quantitative guidance by field testing of full-scale but modest-size structures. Firstly, a series of simple sliding tests was performed to obtain data on the frictional characteristics of "slab-on-grade" foundations with polymer damp proof membranes (DPC). Then, more realistic structures combining both "slab-on-grade" and foundation beams were tested.

2 BASE SLIDING TESTS

The base sliding tests were intended to measure the sliding characteristics of typical "slab-on-grade" foundations. Concrete slabs 2 m wide x 3 m long x 135 mm thick were constructed without edge beams but otherwise using standard construction details and materials. One and two layers of DPC were used and some slabs were weighted with ballast. Each test slab was forced to slide back and forth parallel to its long axis while measurements of force and displacement were taken.

A diagram of the test setup is given in Figure 4. A wooden frame 3 m wide by 4 m long by 100 mm deep was constructed first. This was filled with pit-run granular material topped with a 25 mm thick sand blinding. The sand surface was leveled by screeding and then the DPC was rolled out and stapled to the wooden frame. The concrete slab then was constructed by pouring concrete into a steel form laying on top of the DPC. The concrete was cured for several days and then a hydraulic actuator was bolted to the slab and anchored to an adjacent large-size pile head. A 100 KN load cell was used to measure the force required to cause sliding while slab movement was monitored by a displacement transducer. Data was recorded electronically.

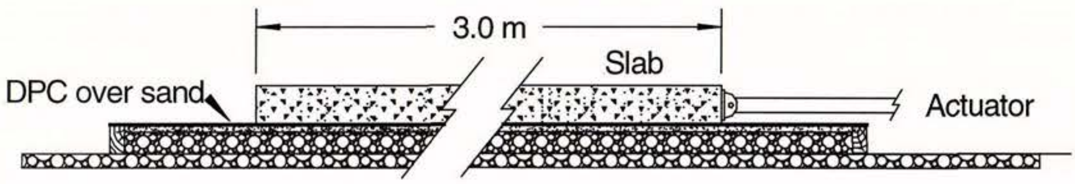

Figure 4. Section showing details of base sliding tests.

A simple test procedure was used as follows: each slab was pushed slowly, driven by a hand operated hydraulic pump, for 25 mm in one direction. Then the pump direction was reversed and the slab was dragged back to its starting position. Three or four cycles of load were applied in similar fashion until a steady load-displacement response was achieved. The results are summarised in Table 1.

Table 1. Base sliding friction for "slab-on-grade" foundations.

Foundation Type	Contact Pressure (KPa)	Peak Friction Angle (degrees)	Mean Friction Angle (degrees)
Single Layer DPC	3.0	23	21
	6.6	28	26
Two Layers DPC	3.1	12	10
	6.2	24	22

For some tests, the slab was ballasted by laying a previously tested slab on top supported on timbers laid at quarter points, effectively doubling the interface contact pressure. All tests were conducted on freshly made slabs.

For a single layer of DPC, there was a slight increase in friction with increased surcharge, probably caused by indentation of the sand grains into the soft material of the membrane. Some scuffing of the DPC was evident after testing.

Placing two layers of DPC resulted in halving of the interface friction angle for the single slab without ballasting. However, ballasting of the slab to 6.2 KPa caused the interface friction to increase significantly and to be nearly the same as for a single layer of DPC. This result is surprising and no explanation is immediately obvious. A small amount of "bulldozing" of sand occurred in front of each slab as it was pushed back and forth, more for the ballasted slabs than the unballasted slabs. However, the effect of such "bulldozing" should be the same whether one or two layers of DPC were used. Further testing of interface friction using increased weights of ballast are recommended to investigate this phenomenon.

3 COMBINATION SLAB AND BEAM EXPERIMENTS

Few foundations are ever made that consist only of "slab-on-grade" with no downturned foundation beams of some type. Most shallow foundations have foundation beams of some description together with floor slabs that are either suspended or built "on-grade". Even when slabs are built "on-grade" they usually are structurally connected to the foundation beams, or should be. Isolated pad foundations supporting individual columns may also be part of a foundation design and sometimes these will not be inter-connected using beams. However, most foundations will have perimeter beams at least and it is beams that offer most potential for generating passive resistance to lateral movements. The effect of attached piles will be the subject of a further study.

A main objective of this study was to investigate the interaction between the passive resistance to lateral movement generated against vertical embedded surfaces such as beams and attached horizontal surfaces such as floor slabs. Therefore, a simplified structure consisting of two parallel foundation beams connected by a floor slab constructed "on-grade" was designed to incorporate the essential features of interest. Details of the structural design are given in Figure 5.

The structures were built as large as practicable given the limitations of available hydraulic actuators and field reaction points, the intention being to simulate behaviour at full-scale. Loads were applied by using a 500 KN MTS servo-hydraulic actuator under computer control. Measurements of load and horizontal displacement were collected electronically by using a Hewlett Packard HP34970 data acquisition system linked to a computer. Details of the loading system and test setup are shown in Figure 6.

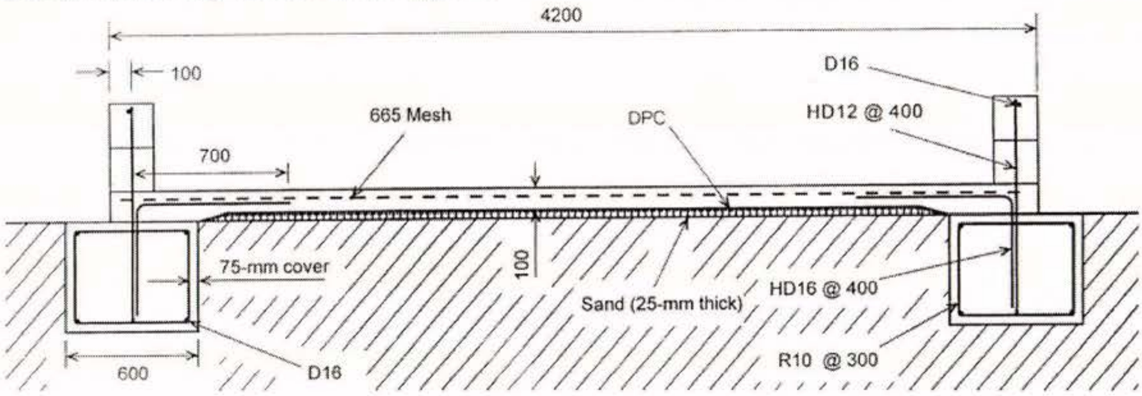

Figure 5. Section showing construction details of Test 3.

Three similar structures were built. The first acted somewhat as a shakedown test. Significant rotations of the structure occurred unexpectedly during loading and these caused the hydraulic loading system to apply undesirable moments which may have upset the results. For the second test, the loading system was re-designed to better accommodate rotation of the structure. The third test was ballasted by laying the first structure on top, effectively simulating a two storey structure.

The test procedure was essentially quasi-static. Each test proceeded as a series of shoves at a constant rate of displacement of 37.5 mm/min. At the end of each shove the test was stopped briefly so that observations of soil cracking, soil movements, structural rotation, and structural distress could be made. Then the direction of movement was reversed and the slab shoved to the opposite extreme of movement. For the first cycle of loading, the

shove was terminated once a steady state load had been reached. For subsequent cycles the structure was shoved to the full range of the actuator (+/- 76 mm).

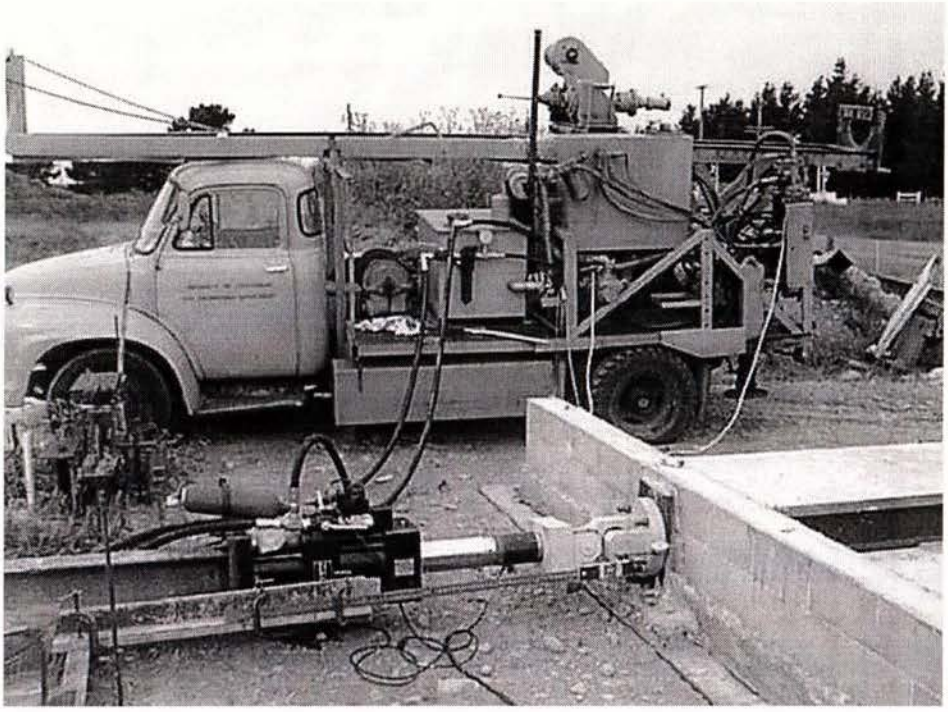

Figure 6. Load actuator setup for Test 2.

Load-displacement curves for Test 2 are shown in Figure 7 and for Test 3 in Figure 8. For Test 3, the ballasted "two-storey" structure, the 500 KN capacity of the actuator was barely adequate. The full lateral capacity of the structure appears to have been just mobilised in one direction and not quite in the other.

Figure 7. Load versus displacement for Test 2.

For Test 2, the HD16 bars tying the slab to the foundation beams were omitted and the slab failed in flexure. Also, the foundation beams were able to rotate somewhat independently of the slab, as seen in Figure 9. Rotation of the foundation beams should not have affected the mobilisation of soil passive pressure.

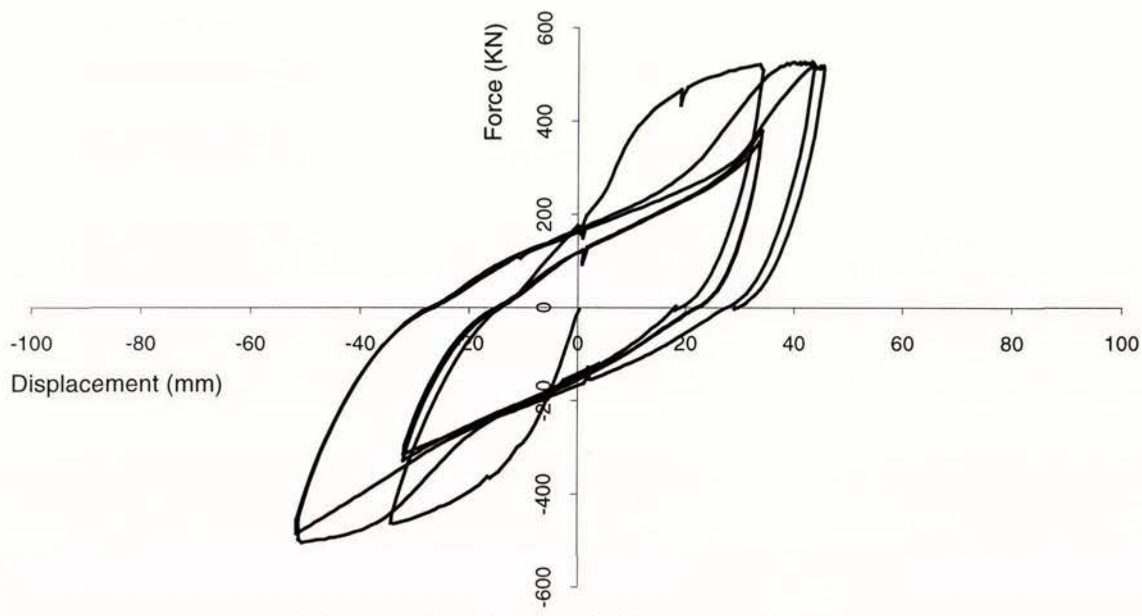

Figure 8. Load versus displacement for Test 3.

4 GENERAL OBSERVATIONS

The general failure mechanism for the structures under lateral loading was remarkably similar to the "Wedge Failure" cartoon of Figure 1. A clearly defined passive wedge developed under the slab in the direction of loading which "jacked" the structure up off the ground leaving a void under the slab. A single, significant difference from the cartoon is that, for the test structure, only one side was "jacked" off the ground because each foundation beam had slab attached to one side only, resulting in the motion indicated by the cartoon in Figure 10.

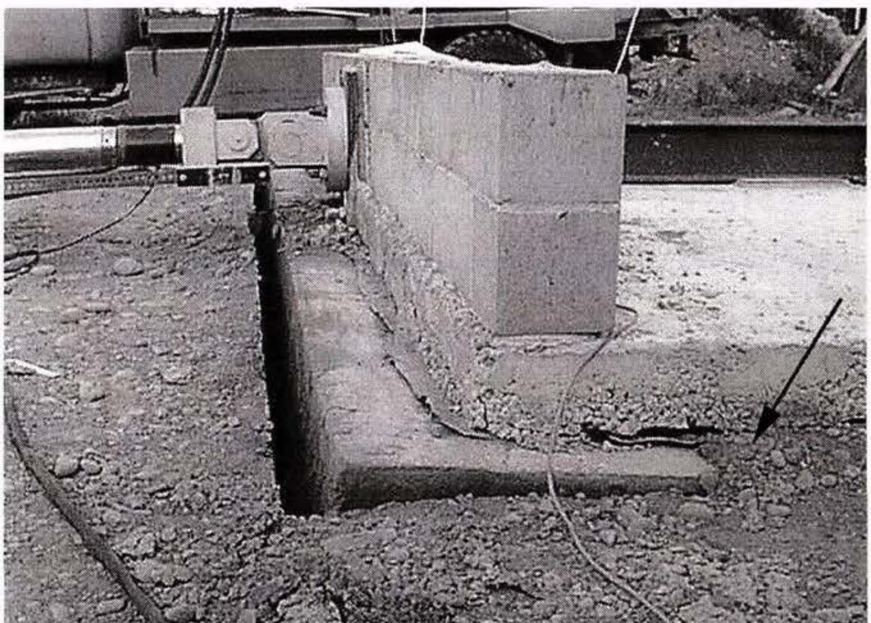

Figure 9. Rotation and uplift of foundation beam for Test 2. Arrow indicates location of the passive soil wedge.

A large gap opened up behind each foundation beam, as clearly seen in Figure 9, and as predicted in the cartoon of Figure 1. This gap proved to be significant because when the direction of loading was reversed the gap had to close before passive soil resistance could be mobilised in the opposite direction, causing substantial "pinching" of the load-displacement curves.

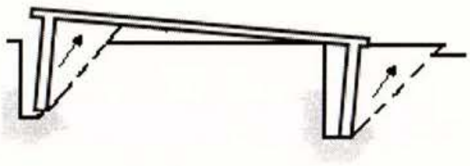

Figure 10. Observed failure mechanism.

5 ANALYSIS OF RESULTS

From the observed general failure mechanism, the forces acting on the structure may be summarised as shown in Figure 11. R_1 and R_3 represent the passive earth pressure acting against the faces of the foundation beams. R_2 represents the additional lateral earth pressure from the force R_5 acting on the passive wedge as it lifts one side of the structure. The line of thrust of R_5 is assumed to act through the centre of the wedge. R_4 represents friction acting on the base of the foundation beam and F is the applied lateral load acting with eccentricity e.

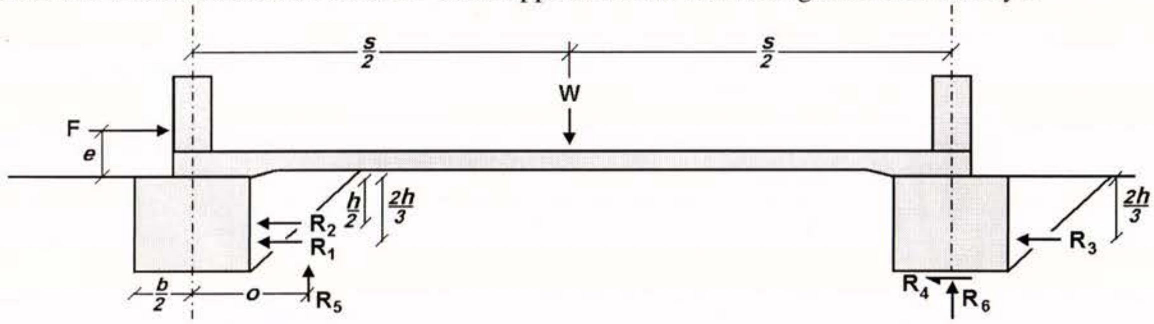

Figure 11. Forces acting on structure with lateral loading by force F.

Since the left hand beam is moving upwards with the passive soil wedge, there will be no friction acting on the vertical face of the beam and it may be treated as frictionless. Therefore, Rankine's simple theory may be used to compute R_1:

$$R_1 = 0.5 K_p \gamma h^2 L \tag{3}$$

$$K_p = \frac{1+\sin\phi_b}{1-\sin\phi_b} \tag{4}$$

in which ϕ_b = the backfill material angle of internal friction, and L is the length of the foundation beam.

There will be friction between the right hand beam and the right hand passive wedge of soil. This friction tends to increase the passive resistance R_3 while simultaneously reducing R_6 and the resulting friction R_4. The net effect on the total lateral resistance is probably negligible and so the simplifying assumption of a frictionless wall was applied to the computation of R_3:

$$R_3 = R_1 \tag{5}$$

The remaining reaction forces are given by:

$$R_2 = R_5 K_p \tag{6}$$

$$R_4 = R_6 \tan \phi_g \tag{7}$$

$$W = R_5 + R_6 \tag{8}$$

in which ϕ_g is the interface friction angle between the base of the foundation beam and subgrade. The line of action of R_5 is given by:

$$o = \frac{h}{2}\tan(45^\circ + \frac{\phi_b}{2}) + \frac{b}{2} \tag{9}$$

An explicit expression for R_6 was obtained from consideration of rotational equilibrium of the structure, as follows:

$$R_6 = \frac{(R_1 + R_3)(1 + \frac{2h}{3e}) - W(\frac{o}{e} - \frac{s}{2e} - K_p(1 + \frac{h}{2e}))}{\frac{s}{e} - \tan\phi_g(1 + \frac{h}{e}) - \frac{o}{e} + K_p(1 + \frac{h}{2e})} \tag{10}$$

The lateral capacity then is given by:

$$F = R_1 + R_2 + R_3 + R_4 \tag{11}$$

Computations were made to predict the measured capacities for Tests 2 and 3 with the results summarised in Tables 2 and 3. Good agreement was obtained in both cases. The slight (6 – 10 percent) underestimate of capacity is probably because of a slight underestimate of the soil strength properties. The test soils were above the water table and were moist and might be expected to show some apparent cohesion. However, the soil strengths used in the computations are what a designer might reasonably estimate and the slight conservatism resulting is considered appropriate.

Table 2. Computed lateral capacity Test 2.

W	L	e	s	b	h	γ	ϕ_g	ϕ_b	F	Test 2*
(KN)	(m)	(m)	(m)	(m)	(m)	(KN/m^3)	(deg.)	(deg.)	(KN)	(KN)
118.1	4.25	0.125	4.0	0.6	0.45	17.2	40	35	263	292

* - average of both directions of loading

Table 3. Computed lateral capacity Test 3.

W	L	e	s	b	h	γ	ϕ_g	ϕ_b	F	Test 3*
(KN)	(m)	(m)	(m)	(m)	(m)	(KN/m^3)	(deg.)	(deg.)	(KN)	(KN)
233.4	4.25	0.125	4.0	0.6	0.45	17.2	40	35	482	515

* - average of both directions of loading

The computations are highly sensitive to changes in the ratio of load eccentricity (e) to width (s). Increasing load eccentricity causes transfer of structural weight from the left hand passive wedge to the right hand beam (in Figure 11). This weight transfer significantly reduces the lateral resistance of the structure because weight applied to the left hand passive wedge is very effective, increasing the lateral earth pressure on the left hand beam by factor Kp (values typically 3 – 4).

With reversal of loading direction, as the structure moved back through its central position, lateral load resistance was observed to decrease to low values as the vertical faces of the foundation beams lost contact with the backfill material. For Test 2, by the third cycle of loading, lateral resistance had dropped to approximately 40 KN. The structure presumably was sliding on the DPC/sand interface with an equivalent friction angle of 19 degrees. For Test 3 the minimum lateral resistance at zero displacement was 114 KN, equivalent to a friction angle of 26 degrees. These friction values are close to the measured values for a slab sliding on a single layer of DPC suggesting that, between displacement extremes, the structure is simply sliding back-and-forth supported by the slab resting "on grade".

6 CONCLUSIONS

Three shallow foundations each 4.25 m wide x 4.6 m long consisting of a 100 mm thick slab "on-grade" with two foundation beams 600 mm wide embedded 450 mm were constructed in coarse granular material. Each was tested by shoving back-and-forth by a powerful hydraulic actuator with several cycles of quasi-static lateral loading. These tests were supplemented with several, simpler interface sliding tests were performed on 2 m wide x 3 m long concrete slabs constructed "on-grade" using one or two layers of polymer damp-proof membranes.

Lateral loading of the slab and beam foundations caused a wedge type of failure mechanism with significant passive soil pressures acting against the vertical faces of the foundation beams. The passive soil wedge developing against the trailing beam lifted one side of the structure vertically leaving hollow space beneath the floor slab. For the somewhat narrow structures tested, significant rotations of the structure occurred.

A simple method of analysis was developed and found to give good predictions for the experimental results while accounting for all of the main parameters. The analysis predicts that lateral load capacity is highly sensitive to the eccentricity (height above ground) of the applied lateral load.

Full development of the lateral load resistance required 30 – 50 mm displacement. After being shoved to a displacement extreme in one direction, the structure was free to slide back in the opposite direction, with relatively low load resistance from base sliding friction only.

7 RECOMMENDATIONS FOR PRACTICE

Designers need to account for the significant vertical movements and redistribution of vertical loads caused by development of passive soil wedges adjacent to foundation beams with lateral loading. Also, knowledge of the overturning moment accompanying each pulse of lateral load is necessary to be able to predict the lateral load capacity of the foundation.

The method for computing lateral resistance of shallow foundations given by Equation 3 to 11 gave good predictions for the experimental results and could be extended to more complex foundations.

8 ACKNOWLEDGEMENTS

This study was funded by the EQC Research Foundation under project 99/423. John van Dyk constructed the experiments and assisted with the testing. The authors are grateful for his enthusiasm and "can do" spirit.

REFERENCES:

Clough, G.W., Duncan, J.M. (1991) "Earth Pressures". In: Foundation Engineering Handbook 2nd Edition. Ed: Fang, H., Chapman & Hall, New York

Gadre, A., Dobry, R. (1998) "Lateral cyclic loading centrifuge tests on square embedded footing." Journal Geotechnical and Geoenvironmental Engineering. 124. 1128-1138

Murff, J.D. and Miller, T.W. (1977b), Stability of offshore gravity structure foundations by the upper-bound method, Proceedings of the Offshore Technology Conference, 3, pp. 147-154

9 PAPER DETAILS

(Note this information is to be used by the administrator only and will not appear in this form in the finished paper.)

Paper Number			
Paper Title	Lateral loading of shallow foundations		
Authors	K.J.McManus	N.R.R.Burdon	
Author Affilation	Department of Civil Engineering, University of Canterbury	Holmes Consulting Group, Auckland	
Topic Area	geotechnical engineering		
Key words (5)	lateral load, shallow foundation, interface friction, passive pressure, wedge failure		

Please cut abstract from front of paper and paste after this line

ABSTRACT: Three shallow foundations each 4.25 m wide x 4.6 m long consisting of a 100 mm thick slab "on-grade" with two foundation beams 600 mm wide embedded 450 mm were constructed in coarse granular material. Each was tested by shoving back-and-forth by a powerful hydraulic actuator with several cycles of quasi-static lateral loading. These tests were supplemented with several, simpler interface sliding tests were performed on 2 m wide x 3 m long concrete slabs constructed "on-grade" using one or two layers of polymer damp-proof membranes.

Lateral loading of the slab and beam foundations caused a wedge type of failure mechanism with significant passive soil pressures acting against the vertical faces of the foundation beams. The passive soil wedge developing against the trailing beam lifted one side of the structure vertically leaving hollow space beneath the floor slab. For the somewhat narrow structures tested, significant rotations of the structure occurred.

A simple method of analysis was developed and found to give good predictions for the experimental results while accounting for all of the main parameters. The analysis predicts that lateral load capacity is highly sensitive to the eccentricity (height above ground) of the applied lateral load.

Proc. NZ Geotech Symp., Tauranga, NZ. 2003. Ref: 6P99/423

ENG 323

Earthquake resistant foundation design

K J McManus
BE (Hons), ME, PhD, Regd Engr
Dept. Civil Engineering, University of Canterbury

Abstract: Recent experimental research at the University of Canterbury concerned with the load-displacement behaviour of both shallow and deep foundations is outlined. Issues addressed include base sliding friction and passive resistance mechanisms of shallow foundations, capacity of deep foundations with cyclic axial and lateral loading, and interactions between shallow and deep foundations. Practical considerations are discussed including two design examples.

Several full-scale shallow foundations were tested by shoving back-and-forth by using a powerful hydraulic actuator with several cycles of quasi-static lateral loading. These tests were supplemented with several, simpler interface sliding tests performed on concrete slabs constructed "on-grade" using one or two layers of polymer damp-proof membranes. A simple method of analysis was developed and found to give good predictions for the experimental results while accounting for all of the main parameters.

Many load tests have been made on large model piles with cyclic axial loading, combined cyclic axial and lateral loading, and monotonic and cyclic axial loading in a shaking soil deposit. Several full-scale load tests on driven and bored concrete piles were made to confirm applicability of the model test results to prototype foundation designs.

Application of the test results to practical design situations is discussed and illustrated by two design examples. The need for close interaction between the geotechnical designer and the structural designer in order to obtain optimum design solutions is stressed.

INTRODUCTION

Foundations are key elements in determining the overall performance of structural systems subjected to earthquake shaking, yet their behaviour is largely taken for granted by structural designers. Especially overlooked is the fact that during earthquakes the foundations actually apply the loads to the structure rather than the usual situation where the foundations receive gravity and environmental loads from the structure. Structural designers often make elaborate calculations assuming high levels of shear being applied to the base of a structure without a clear understanding of the load path necessary to transfer the shear force from the moving ground into the superstructure.

Some foundations are simply not capable of transferring large shear forces and act somewhat as a fusible link, limiting the base shear applied to the structure, structural accelerations, and resulting damage. Such foundations, however, frequently are severely damaged and unable to carry the gravity loads after the earthquake. During the 1999 Turkey earthquake for example, a very large number of buildings suffered brittle failure in shear, causing a huge loss of life. A smaller number of buildings were protected from significant damage when their foundations tipped, limiting the shear forces in the structure and structural damage, as shown in Figure 1. While these buildings were protected from shear failure, collapse, and resulting loss of life, they were no longer serviceable because of permanent rotations of their foundations.

Figure 1. Overturned building in Adapazzari.

Clearly, a better understanding of the behaviour of foundation systems during earthquakes is required, particularly the load-displacement response of the various foundation elements when taken to their ultimate limit state, including the effects of cyclic actions.

This paper summarises recent research carried out at the University of Canterbury where the load-displacement behaviour of all elements of foundation systems including base friction, passive soil resistance against shallow elements, and cyclic behaviour of deep foundations have been investigated. This summary is necessarily brief in details and the reader is referred to sources of additional information in some places. It is a snapshot of work in progress, with many aspects of foundation performance requiring further study. In particular, the interaction of foundation systems with liquefying soil strata is not directly addressed here. However, an attempt is made to introduce an integrated, systems view of foundation design by using simple examples.

SHALLOW FOUNDATIONS

Base Sliding

The simplest shallow foundation is a concrete slab poured on grade, usually with either one or two layers of polymer damp course (DPC). The sliding characteristics of such systems have been investigated experimentally.

Concrete slabs 2 m wide x 3 m long x 135 mm thick were constructed without edge beams but otherwise using standard construction details and materials. One and two layers of DPC were used and some slabs were weighted with ballast. Each test slab was forced to slide back and forth parallel to its long axis while measurements of force and displacement were taken.

A diagram of the test set-up is given in Figure 2. A wooden frame 3 m wide by 4 m long by 100 mm deep was constructed first. This was filled with pit-run granular material topped with a 25 mm thick sand blinding. The sand surface was levelled by screeding and then the DPC was rolled out and stapled to the wooden frame. The concrete slab then was constructed by pouring concrete into a steel form lying on top of the DPC. The concrete was cured for several days and then a hydraulic actuator was bolted to the slab and anchored to an adjacent pile head. A 100 KN load cell was used to measure the force required to cause sliding while a displacement transducer monitored slab movement. Data was recorded electronically.

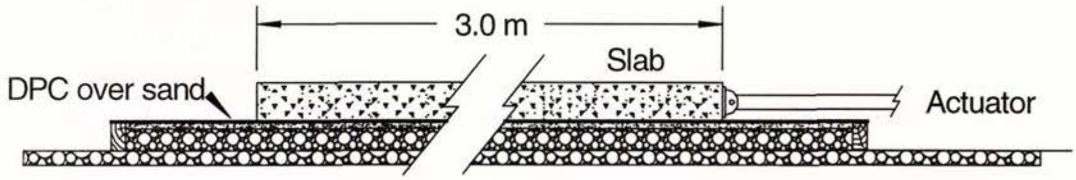

Figure 2. Section showing details of base sliding tests.

A simple test procedure was used as follows: each slab was pushed slowly, driven by a hand operated hydraulic pump, for 25 mm in one direction. Then the pump direction was reversed and the slab was dragged back to its starting position. Three or four cycles of load were applied in similar fashion until a steady load-displacement response was achieved. The results are summarised in Table 1.

Foundation Type	Contact Pressure (KPa)	Peak Friction Angle (degrees)	Mean Friction Angle (degrees)
Single Layer DPC	3.0	23	21
	6.6	28	26
Two Layers DPC	3.1	12	10
	6.2	24	22

Table 1. Base Sliding Friction for "Slab-on-Grade" Foundations.

For some tests, the slab was ballasted by laying a previously tested slab on top supported on timbers laid at quarter points, effectively doubling the interface contact pressure. All tests were conducted on freshly made slabs.

For a single layer of DPC, there was a slight increase in friction with increased surcharge, probably caused by indentation of the sand grains into the soft material of the membrane. Some scuffing of the DPC was evident after testing. Placing two layers of DPC resulted in halving of the interface friction angle for the single slab without ballasting. However, ballasting of the slab to 6.2 KPa caused the interface friction to increase significantly and to be nearly the same as for a single layer of DPC. This result is surprising and no explanation is immediately obvious. A small amount of "bulldozing" of sand occurred in front of each slab as it was pushed back and forth, more for the ballasted slabs than the un-ballasted slabs. However, the effect of such "bulldozing" should be the same whether one or two layers of DPC were used. Further testing of interface friction using increased weights of ballast are recommended to investigate this phenomenon.

Combination Slab and Beam Experiments

Few foundations are ever made that consist only of "slab-on-grade" with no down-turned foundation beams of some type. Most shallow foundations have foundation beams of some description together with floor slabs that are either suspended or built "on-grade". Even when slabs are built "on-grade" they usually are structurally connected to the foundation beams, or should be. Isolated pad foundations supporting individual columns may also be part of a foundation design and sometimes these will not be inter-connected using beams. However, most foundations will have perimeter beams at least and it is beams that offer most potential for generating passive resistance to lateral movements.

A main objective of this study was to investigate the interaction between the passive resistance to lateral movement generated against vertical embedded surfaces such as beams and attached horizontal surfaces such as floor slabs. Therefore, a simplified structure consisting of two parallel foundation beams connected by a floor slab constructed "on-grade" was designed to incorporate the essential features of interest. Details of the structural design are given in Figure 3.

The structures were built as large as practicable given the limitations of available hydraulic actuators and field reaction points, the intention being to simulate behaviour at full-scale. Loads were applied by using a 500 KN MTS servo-hydraulic actuator under computer control.

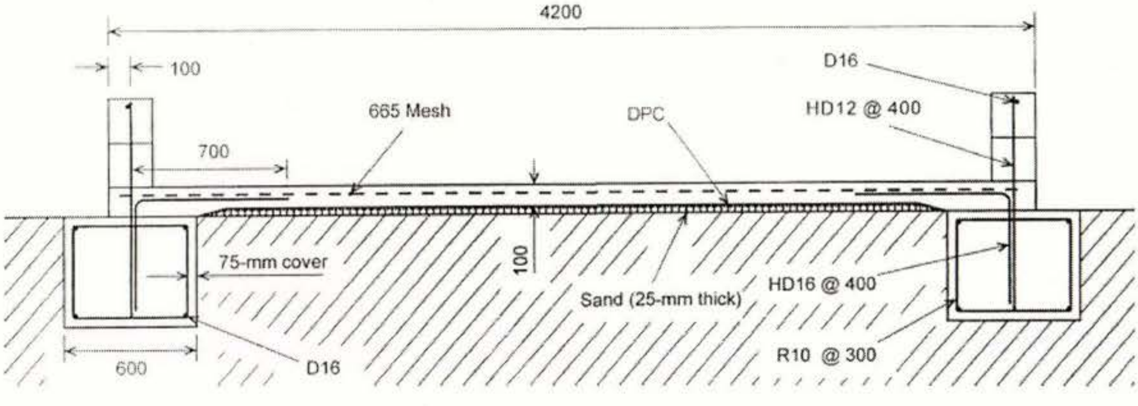

Figure 3. Section showing construction details of combination slab and beam tests.

Three similar structures were built. The first acted somewhat as a shakedown test. Significant rotations of the structure occurred unexpectedly during loading and these caused the hydraulic loading system to apply undesirable moments that may have upset the results. For the second test, the loading system was re-designed to better accommodate rotation of the structure. The third test was ballasted by laying the first structure on top, effectively simulating a two-storey structure.

The test procedure was essentially quasi-static. Each test proceeded as a series of shoves at a constant rate of displacement of 37.5 mm/min. At the end of each shove the test was stopped briefly so that observations of soil cracking, soil movements, structural rotation, and structural distress could be made. Then the direction of movement was reversed and the slab shoved to the opposite extreme of movement. For the first cycle of loading, the shove was terminated once a steady state load had been reached. For subsequent cycles the structure was shoved to the full range of the actuator (+/- 76 mm). Figure 4 shows a typical test in progress.

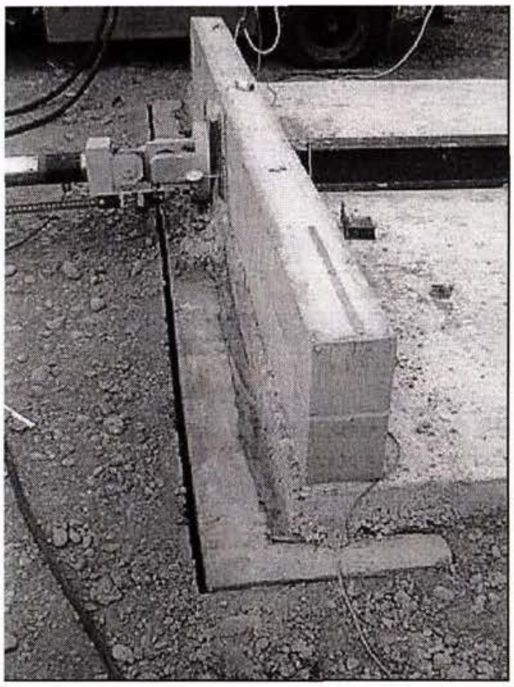

Figure 4. Test set-up for Test 3. (Burdon, 2000)

Load-displacement curves for Test 2 are shown in Figure 5. The curves for Test 3, the ballasted "two-storey" structure, were similar in shape although much higher peak loads were reached.

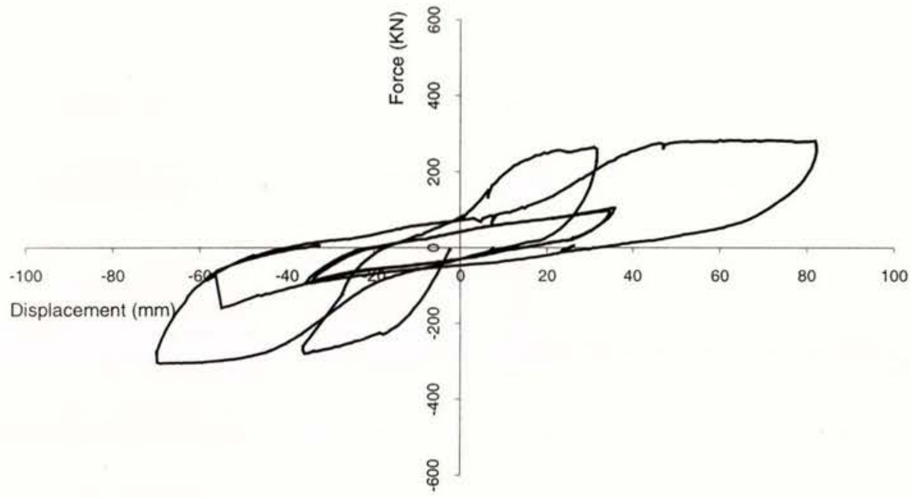

Figure 5. Load versus displacement for Test 2.

A cartoon in Figure 6 indicates the general failure mechanism for the structures under lateral loading. A clearly defined passive wedge developed under the slab in the direction of loading that "jacked" the structure up off the ground leaving a void under the slab. Only one side was "jacked" off the ground because each foundation beam had slab attached to one side only. A large gap opened up behind each foundation beam as the foundation moved away from the soil. This gap proved to be significant because when the direction of loading was reversed the gap had to close before passive soil resistance could be mobilised in the opposite direction, causing substantial "pinching" of the load-displacement curves as seen in Figure 5.

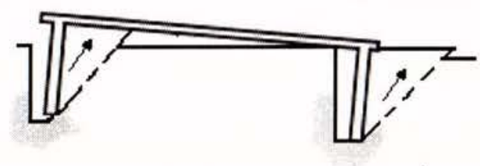

Figure 6. Observed failure mechanism.

From the observed general failure mechanism, the forces acting on the structure may be summarised as shown in Figure 7. R1 and R3 represent the passive earth pressure acting against the faces of the foundation beams. R2 represents the additional lateral earth pressure from the force R5 acting on the passive wedge as it lifts one side of the structure. The line of thrust of R5 is assumed to act through the centre of the wedge. R4 represents friction acting on the base of the foundation beam and F is the applied lateral load acting with eccentricity e. The value of R6 is determined from equilibrium of forces.

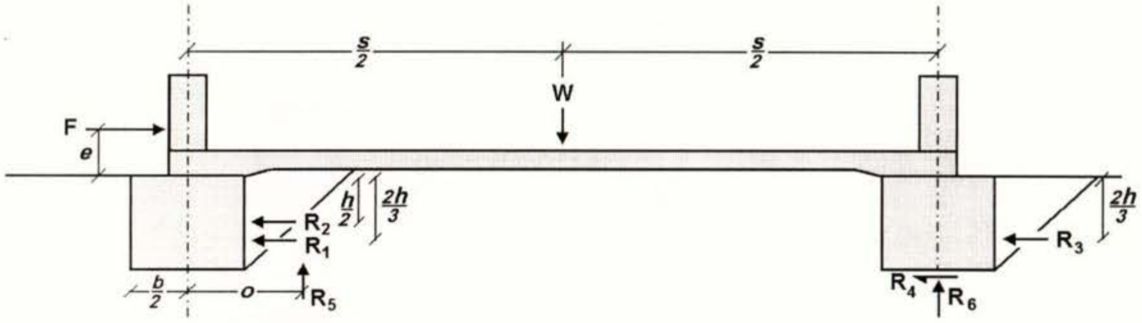

Figure 7. Forces acting on structure with lateral loading by force F.

Since the left hand beam is moving upwards with the passive soil wedge, there will be no friction acting on the vertical face of the beam and it may be treated as frictionless. Therefore, Rankine's simple theory may be used to compute R_1:

$$R_1 = 0.5K_p \gamma h^2 L \tag{1}$$

$$K_p = \frac{1+\sin\phi_b}{1-\sin\phi_b} \tag{2}$$

in which ϕ_b = the backfill material angle of internal friction, and L is the length of the foundation beam. There will be friction between the right hand beam and the right hand passive wedge of soil. This friction tends to increase the passive resistance R_3 while simultaneously reducing R_6 and the resulting friction R_4. The net effect on the total lateral resistance is probably negligible and so the simplifying assumption of a frictionless wall was applied to the computation of R_3:

$$R_3 = R_1 \tag{3}$$

The remaining reaction forces are given by:

$$R_2 = R_5 K_p \tag{4}$$

$$R_4 = R_6 \tan\phi_g \tag{5}$$

$$W = R_5 + R_6 \tag{6}$$

in which ϕ_g is the interface friction angle between the base of the foundation beam and subgrade. The line of action of R_5 is given by:

$$o = \frac{h}{2}\tan(45^\circ + \frac{\phi_b}{2}) + \frac{b}{2} \tag{7}$$

An explicit expression for R_6 was obtained from consideration of rotational equilibrium of the structure, as follows:

$$R_6 = \frac{(R_1+R_3)(1+\frac{2h}{3e}) - W(\frac{o}{e} - \frac{s}{2e} - K_p(1+\frac{h}{2e}))}{\frac{s}{e} - \tan\phi_g(1+\frac{h}{e}) - \frac{o}{e} + K_p(1+\frac{h}{2e})} \tag{8}$$

The lateral capacity then is given by:

$$F = R_1 + R_2 + R_3 + R_4 \tag{9}$$

Computations were made to predict the measured capacities for Tests 2 and 3 with the results summarised in Tables 2 and 3. Good agreement was obtained in both cases. The slight (6 – 10 percent) underestimate of capacity is probably because of a slight underestimate of the soil strength properties. The test soils were above the water table and were moist and might be expected to show some apparent cohesion. However, the soil strengths used in the computations are what a designer might reasonably estimate and the slight conservatism resulting is considered appropriate.

	W (KN)	L (m)	e (m)	s (m)	b (m)	h (m)	γ (KN/m^3)	ϕ_g (deg.)	ϕ_b (deg.)	F (KN)	F^* (KN)
Test 2	118.1	4.25	0.125	4.0	0.6	0.45	17.2	40	35	263	292
Test 3	233.4	4.25	0.125	4.0	0.6	0.45	17.2	40	35	482	515

Table 2. Comparison of Calculated and Measured Lateral Resistance

* - measured peak loads, average of both directions of loading.

The computations are highly sensitive to changes in the ratio of load eccentricity (e) to width (s). Increasing load eccentricity causes transfer of structural weight from the left hand passive wedge to the right hand beam (in Figure 7). This weight transfer significantly reduces the lateral resistance of the structure because weight applied to the left hand passive wedge is very effective, increasing the lateral earth pressure on the left hand beam by factor Kp (values typically 3 – 4).

With reversal of loading direction, as the structure moved back through its central position, lateral load resistance was observed to decrease to low values as the vertical faces of the foundation beams lost contact with the backfill material. For Test 2, by the third cycle of loading, lateral resistance had dropped to approximately 40 KN. The structure presumably was sliding on the DPC/sand interface with an equivalent friction angle of 19 degrees. For Test 3 the minimum lateral resistance at zero displacement was 114 KN, equivalent to a friction angle of 26 degrees. These friction values are close to the measured values for a slab sliding on a single layer of DPC suggesting that, between displacement extremes, the structure is simply sliding back-and-forth supported by the slab resting "on grade".

These load tests were quasi-static and did not include dynamic effects. Passive soil resistance will be reduced by the inertia of the mass of soil within the passive wedge, although the reduction will be small.

DEEP FOUNDATIONS

As well as contributing directly to the transfer of lateral base shear forces to the structure, deep foundations, when present, may also be required to carry gravity loads and to resist overturning moments induced by the lateral base shear. Such earthquake induced overturning moments generate cyclic axial loads in deep foundations, as shown in Figure 8.

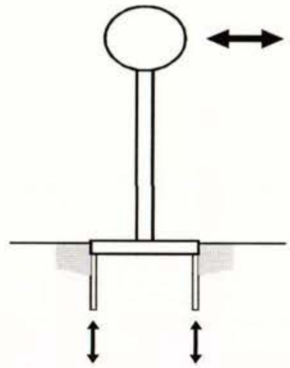

Figure 8. Earthquake induced axial loads on bored piles.

The effect of cyclic axial loading on the load-displacement behaviour of deep foundations is poorly understood, but of considerable concern. Previous research (e.g. Charlie et. al., 1985, Turner and Kulhawy, 1990, McManus and Kulhawy, 1994) has shown that end bearing capacity of deep foundations is not significantly affected by cyclic loading but that side resistance may be reduced, in some cases to as low as 8 percent of static capacity. Unfortunately, most available studies have involved large numbers of load cycles appropriate to wind and wave loading of transmission line structures and oil platforms and may not be truly relevant to earthquake loading. Therefore, a study was undertaken to quantify the effect of cyclic axial loading for the reduced numbers of load cycles applied during earthquakes.

Initial testing was of model bored piles in a static (non-shaking) deposit of sand. Firstly, axial loads only were applied and then combined axial and lateral loads were investigated. Next similar models were tested in a laminated box mounted on a shaking table, with simultaneous axial loading of the piles and ground shaking. Finally, some full-size piles were tested in the field at three sites around Christchurch.

Model Study of Axial Loading in Static Tank

Model studies are the most practical way to explore a wide range of parameters economically. Unfortunately, normal scaling laws do not apply to soils because soil properties are highly dependent on overburden pressure. This limitation may be overcome by modelling geotechnical systems in centrifuges, which are able to simulate high gravitational acceleration and thus high overburden stresses. An alternative approach, adopted here, is to make the model as large as possible and consider it to be a small prototype. Also, by using deposits of dry soil, without buoyant effects, a scale factor equivalent to 2 g in a centrifuge may be assumed, and by using loose soil the undesirable effects of excessive soil dilatancy at low confining pressure are avoided.

The first study was performed on model bored piles in static sand deposits. Soil deposits of 1 m diameter by 2 m deep were prepared inside steel tanks by air pluviation of silica sand. The model bored piles, nominally 95 mm diameter by 1450 mm long were constructed by pouring concrete into an embedded steel casing and then removing the casing. Each shaft was reinforced using a single 16 mm diameter deformed steel bar threaded at the top to allow fixing of a load actuator. Additional details of these tests are given by McManus and Chambers (1995).

Loads were applied to the model bored piles by a computer controlled servo-hydraulic actuator. Each "earthquake" consisted of 20 sine wave cycles at a frequency of 1 Hz. Each pile was tested with a different combination of cyclic load amplitude and constant mean (dead) load, either in compression or uplift. Each pile was tested only once.

Failure in uplift was defined either as being complete pullout of the model bored pile (to the limit of the hydraulic actuator) prior to completion of the simulated earthquake, or as an accelerating cycle-by-cycle upwards movement of the shaft with pullout clearly imminent. A definition for failure in compression is always more problematic, even for static load tests. For this study, a limiting displacement of 10 percent of the shaft diameter (9.5 mm) was chosen to define failure in compression

The load-displacement response for Test 21 is shown in Figure 9 and is typical of all the model bored piles which exhibited stable behaviour during simulated earthquake loading. During cyclic loading, the shaft walked slowly down into the soil, but at a decreasing rate per cycle. Immediately after the last cycle of loading, the shaft was deliberately failed in uplift. The uplift capacity was found to be unchanged at 101 percent of static capacity without cyclic loading.

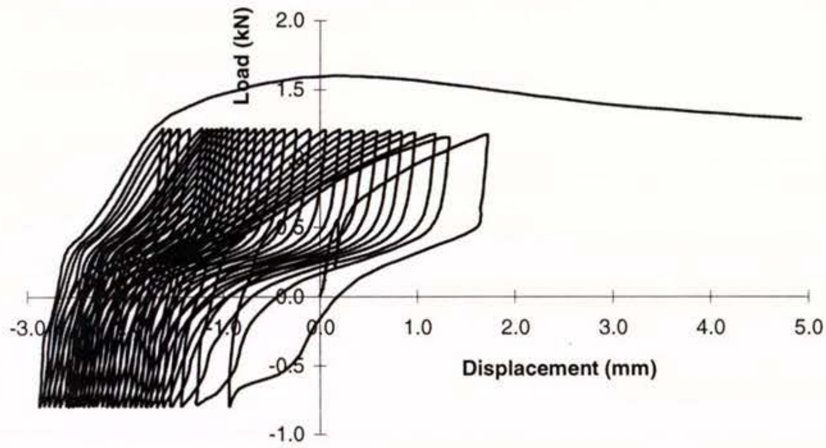

Figure 9. Load versus displacement for simulated earthquake loading, Test 21.

Load Test 22 failed in uplift during the cyclic loading and the load-displacement response is shown in Figure 10. For the first 8 cycles of simulated earthquake loading the response appeared stable, with the shaft slowly walking down into the soil. Then, the shaft started walking upwards at an accelerating rate with the test terminating when the actuator travel was exceeded.

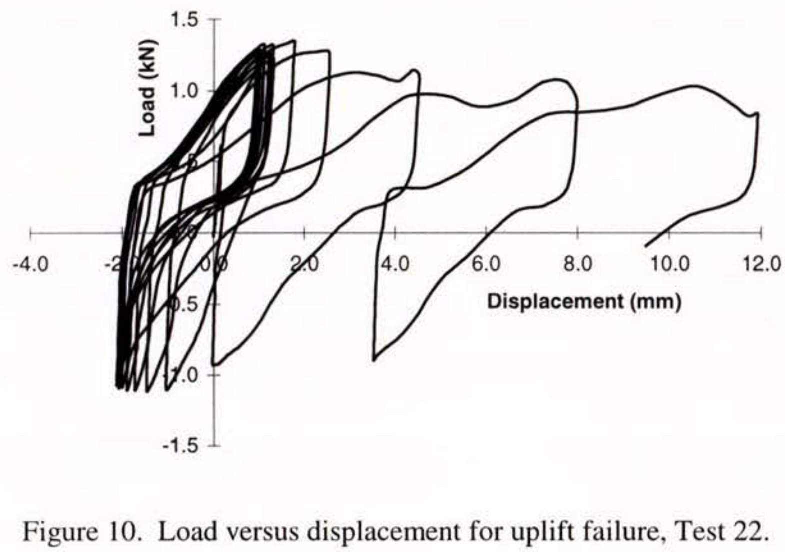

Figure 10. Load versus displacement for uplift failure, Test 22.

A typical compression failure is shown in Figure 11 for model bored pile Load Test 39. The shaft simply walked down into the soil and exceeded the displacement failure criteria in compression (10 percent of tip diameter).

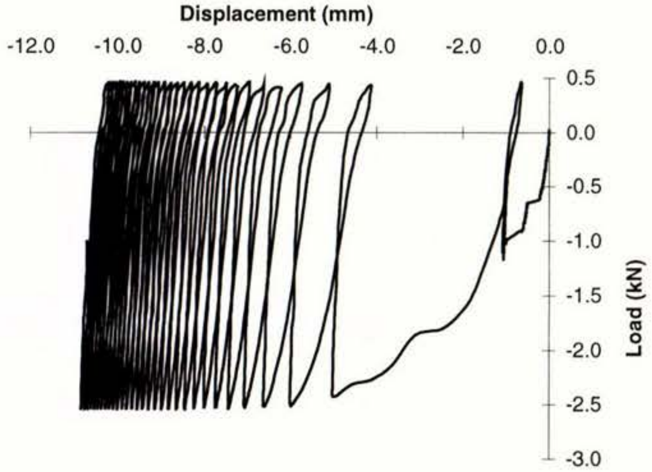

Figure 11. Load versus displacement for compressive failure, Test 39.

A cyclic stability diagram (CSD) for the model bored piles tested in this study is shown in Figure 12. Each individual cyclic load test has been plotted on the diagram by using a small square. The CSD is a useful way of representing all of the possible combinations of cyclic and static axial loads for a pile and the load combinations causing instability. A more detailed explanation of the CSD is given by Poulos (1988).

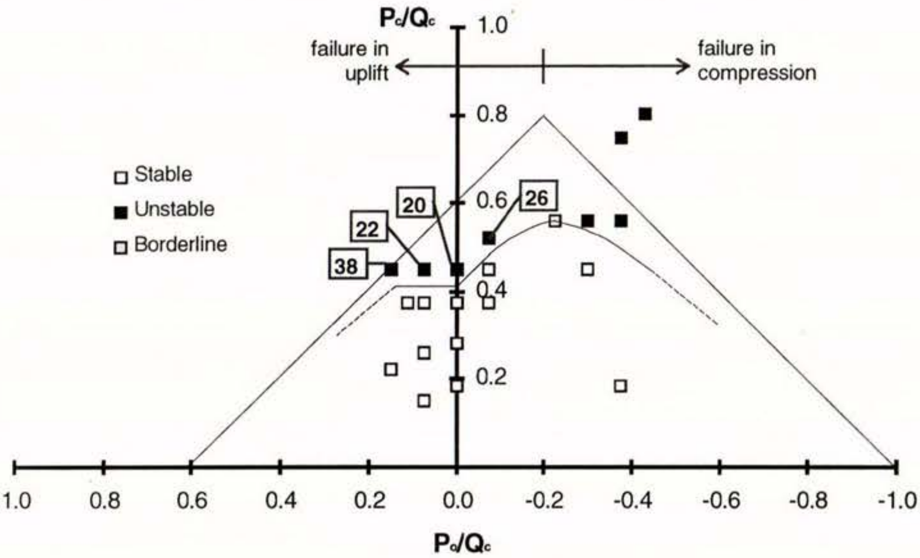

Figure 12. Cyclic stability diagram for model bored piles with simulated earthquake loading.

The shape of the stable/unstable boundary within the cyclic stability diagram for the model bored piles has a pronounced dip where the boundary crosses the Po = 0 axis. In other words, the worst case for cyclic loading occurred when zero mean load was applied to the shafts. For this case, a cyclic load of 75 percent of static uplift capacity caused failure.

A further conclusion of this study was that the key parameter for cyclic axial loading of piles is the magnitude of load reversal, i.e. the extent to which the direction of loading changes from compression to uplift for each cycle of loading. If no load reversal occurs, then there is little degradation of capacity although some permanent displacements might accumulate. If load reversal does occur, then significant degradation of pile capacity is possible, the amount of degradation being dependent on the amount of load reversal. Additional conclusions are contained in the original paper (McManus & Chambers, 1995).

Combined Axial-Lateral Loading

Most pile foundations will be subjected to some combination of both axial and lateral loading during an earthquake. Generally, repeated or cyclic lateral loading seems to have limited effect on the lateral capacity of pile foundations, although some reduction in stiffness may occur because of gapping.

A model study has been initiated at the University of Canterbury to investigate the effect of simultaneous cyclic lateral and axial loading on both the axial and lateral capacities of piles. The test set-up is complex, requiring computer controlled servo-actuators operating in two axes of motion, as shown in Figure 13. This study is incomplete but early indications suggest that while the lateral loading has little affect on axial capacity, the axial loading reduces the lateral capacity. Further work is required before design recommendations can be made.

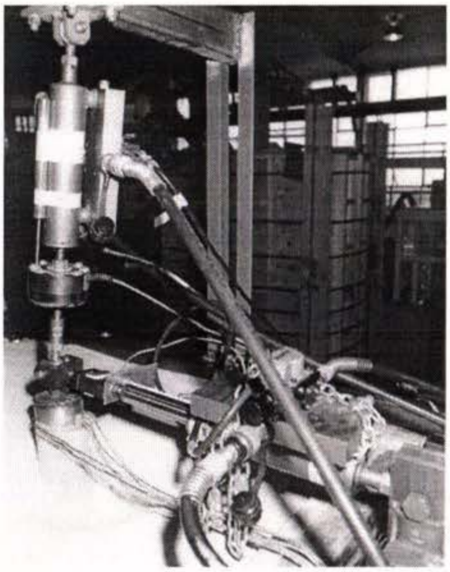

Figure 13. Combined axial-lateral model load test.

Model Study on Shaking Table

In order to truly simulate earthquake conditions it is necessary to test either model or full-size piles in ground that is shaking. Ground shaking during an earthquake induces shear strains in the soil that interact with the pile and are likely to affect pile load-displacement response. Since it is difficult to know when and where an earthquake is going to occur, the most practical approach to investigating the affect of ground shaking on pile performance is to simulate the earthquake on a shaking table in the laboratory.

For this study, a large 2 m deep x 2 m long x 1 m wide laminar box was filled with sand and shaken on the Department of Civil Engineering's 20 tonne capacity, single axis shaking table. The tank size was chosen so that similar model piles could be tested as used for the earlier tests in the static tank. The box was laminated so that the soil was free to deform in simple shear simulating free field behaviour. The laminar box and filling hopper is shown in Figure 14.

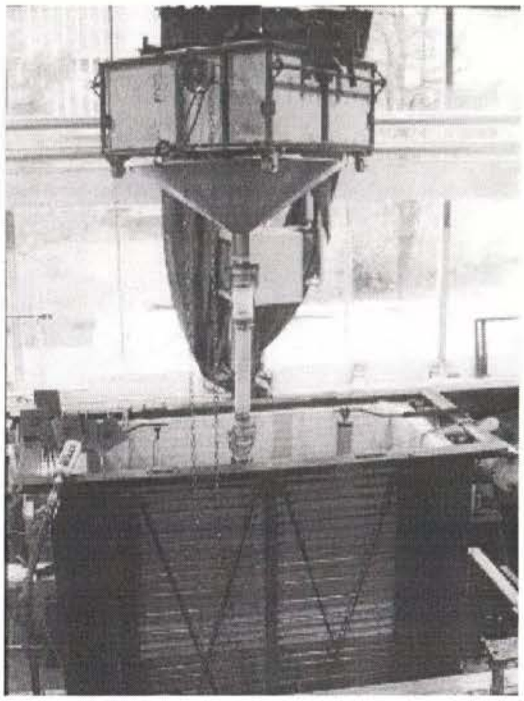

Figure 14. Preparation of soil deposit in laminar box.

Because of the extensive effort required to prepare and test each model pile in the laminar box, only a limited range of parameters were investigated, with the objective being to determine the relative performance of piles in static and shaking soil deposits. Specifically, all tests were axial load only with zero mean load (worst case from the static tests). Simulated "earthquakes" consisted of 20 cycles at 1 Hz and simultaneous pile axial loads were either in phase with the shaking or out of phase. Some shaking tests were performed without simultaneous cyclic pile loads but with mean uplift loads applied. Full details of the test programme including development of the laminar box are given by Chambers (1999).

The results from the laminar box study are summarised in Figure 15. At low levels of pile cyclic load the piles were stable and settled approximately 30 mm because of the densification and settlement of the soil deposit with shaking. For tests with applied cyclic loads of more than 40 percent of uplift capacity the piles became unstable with large uplift displacements. For tests with cyclic loads applied out of phase with the ground shaking this threshold to instability occurred at approximately 50 percent of uplift capacity. The average peak shear strain in the soil deposit during shaking was between 1.3 to 1.6 percent.

This threshold to instability of between 40 to 50 percent of uplift capacity of the model piles with zero mean load compares with a threshold of 75 percent found for the similar model piles tested in static soil deposits. Apparently, the shaking soil deposit significantly reduced the resistance of the model piles to cyclic axial loading.

Model tests also were performed with static uplift loads applied to the pile during soil shaking and no cyclic axial load component, with the results summarised in Figure 16. For low level shaking (average peak shear strain, APSS = 0.11 percent) the piles remained stable. For higher levels of shaking (APSS = 0.59 and 0.96 percent) the piles became unstable and started to pull out of the soil at applied axial loads of between 50 to 60 percent of uplift capacity.

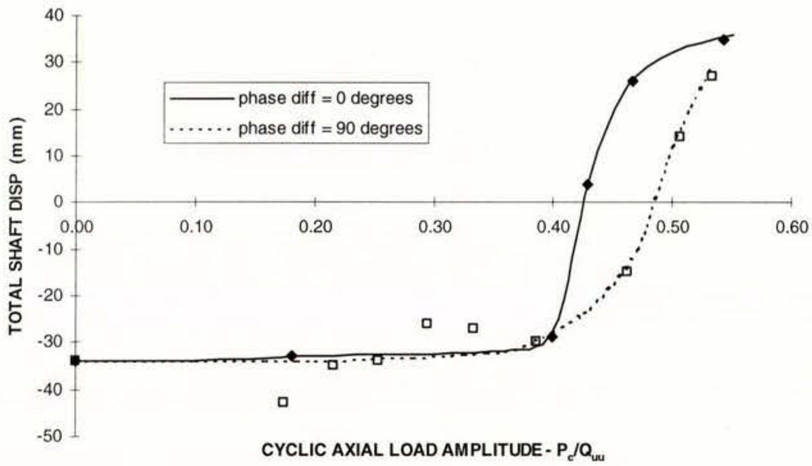

Figure 15. Pile displacement versus cyclic axial load amplitude normalised by uplift capacity for the shaking tests. (Chambers, 1999)

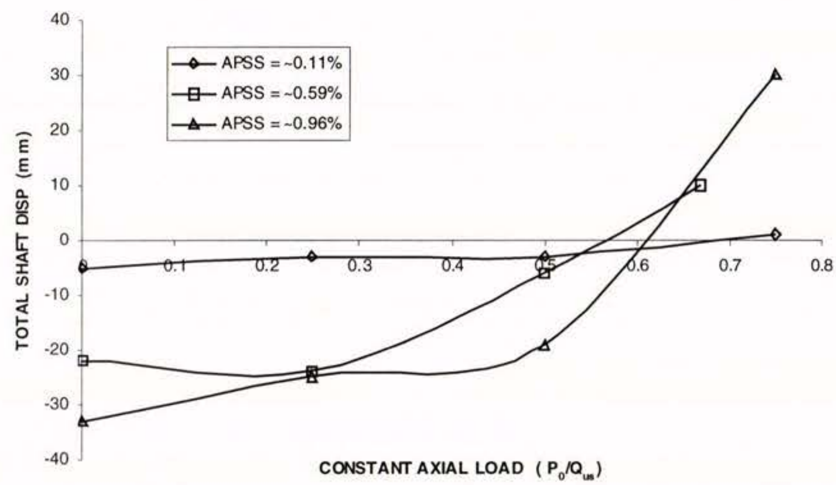

Figure 16. Pile displacement versus constant uplift load normalised by uplift capacity for the shaking tests (APSS means average peak shear strain for the soil shaking). (Chambers, 1999)

Full Scale Cyclic Load Tests

The objective of the full-scale pile load tests was to provide general verification of the findings of the model studies. The cost of full-scale field testing precludes a thorough examination of the full range of parameters investigated in the model studies. Also, it is clearly impractical to arrange earthquake magnitude ground shaking to occur simultaneously. However, by checking some of the model predictions at full-scale it allows the model results to be applied with greater confidence.

Three field tests have been performed to date: 750 mm diameter x 6 m deep bored piles in loose sandy gravel at Templeton (McManus, 1997), 275 mm x 275 mm x 8 m long reinforced concrete driven piles at Park Terrace in central Christchurch (McManus, 1999), and 275 mm x 275 mm x 8 m long reinforced concrete driven piles at Salisbury Street in central Christchurch (Lyons, 2000).

Park Terrace Site

Three 275 mm square reinforced concrete piles were driven 7.75 m into typical Christchurch overbank deposits of soft silts, silty fine sands, and peats, bearing in dense fine to medium sands. Driving of the piles was monitored by using a pile driving analyser and a CAPWAP analysis was performed on one pile giving a prediction for pile ultimate capacity of 930 KN in compression and 495 KN in uplift. The centre pile was subjected to several sequences of cyclic axial loading by a computer controlled, 500 KN MTS servo-hydraulic actuator mounted in a loading frame spanning between the two outer piles, as shown in Figure 17. Amplitudes of up to +/- 350 KN at frequencies of either 1 Hz or 0.5 Hz were applied as simulated "earthquakes" of up to 30 cycles duration. Each "earthquake" was increased in magnitude and the pile was then rested for about one hour.

Figure 17. Full-scale cyclic load test frame and actuator.

At applied cyclic loads of up to +/- 300 KN the pile load-displacement response was essentially stable with only minor upward displacement creep, as shown typically in Figure 18. However, when the applied cyclic load was increased to +/- 350 KN severe degradation of pile stiffness occurred, exceeding the capacity of the hydraulic loading system, as shown in Figure 19. It proved impossible to increase the cyclic axial load using the available system and 350 KN was taken as the load level causing onset of pile instability. Monotonic uplift capacity of the pile after completion of the cyclic loading was measured as 300 KN.

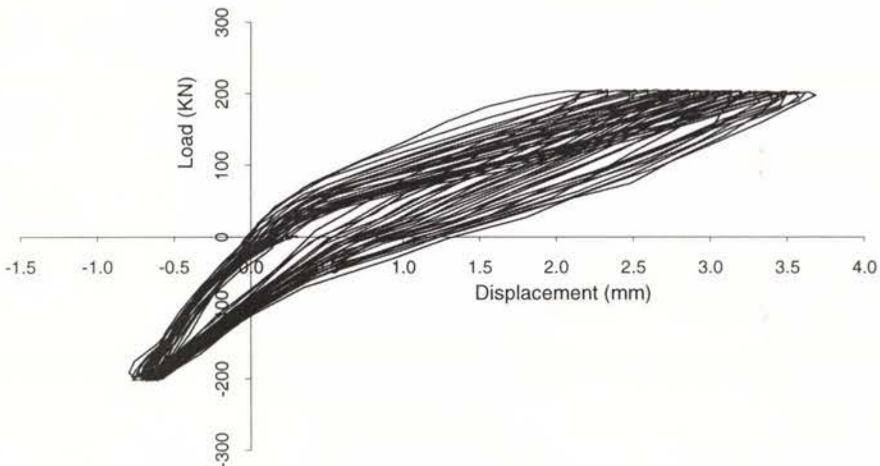

Figure 18. Park Terrace full-scale load test, +/- 200 KN, 1.0 Hz, 30 cycles.

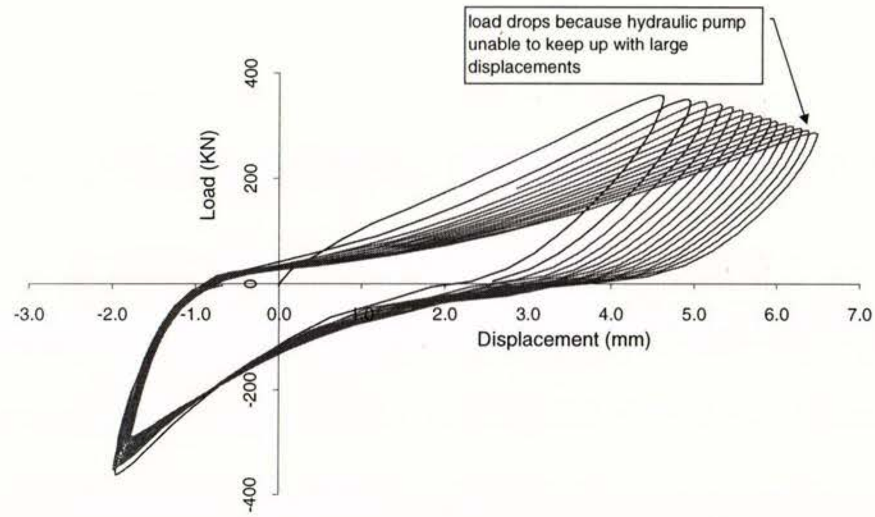

Figure 19. Park Terrace full-scale load test, +/- 350 KN, 0.5 Hz, 15 cycles.

The two outer piles were then subsequently tested in uplift to determine a reference uplift capacity for the piles without cyclic loading (or at least with half the level of cyclic loading of the test pile and after several weeks "rest".) These uplift tests were crudely performed using a 70 tonne crane and indicated 530 KN capacity at 20 mm displacement with a peak value of 596 KN at 32 mm.

In summary, the level of cyclic axial load causing onset of instability of the pile was found to be approximately 66 percent of uplift capacity (assuming capacity to be 530 KN), which is close to the value of 75 percent for the model pile test it most closely resembles.

Salisbury Street Site

Full-scale cyclic load tests were performed on similar piles at the Salisbury Street site using the same equipment and procedures. The 275 mm square x 8 m long reinforced concrete piles were driven into silts, silty fine sands, and peats, bearing in dense fine to medium sands. The site soils were more competent than at the Park Terrace site and the pile driving analyser predicted higher capacities for the test pile of 2,630 KN in compression and 1,049 KN in uplift.

Again, cyclic load amplitudes of up to +/- 350 KN at frequencies of 1 Hz were applied as simulated "earthquakes" of 30 cycles duration. Each "earthquake" was increased in magnitude and the pile was then rested for about one hour. The load-displacement response of the pile remained stable for all of the load tests. It was not possible to increase the level of cyclic loading above 350 KN , which represents only 33 percent of the presumed uplift capacity of the pile.

The level of cyclic load required to cause instability of the Salisbury Street pile was not determined but the stable behaviour of the pile at applied loads of up to 33 percent of uplift capacity was confirmed.

Templeton Site

Nine bored pile foundations, each nominally 0.75 m diameter by 5.5 m deep, were constructed in a deposit of loose gravel above the water table at a disused gravel quarry at Templeton, near Christchurch. Four of the piles were loaded monotonically to failure in uplift while the remaining five piles were subjected to 30 cycles of 1 Hz sine wave loading at various amplitudes using similar equipment to the Park Terrace and Salisbury Street load tests. The uplift capacity and axial stiffness of the cyclically loaded piles was compared with that of the monotonically loaded piles.

At low levels of cyclic loading (50 percent or less of uplift capacity) the pile response was largely elastic with no significant degradation in strength or stiffness. At higher levels, there was a large reduction in load-displacement stiffness (by a factor of up to 16). The transition from stable to unstable behaviour occurred at a ratio of cyclic load amplitude to axial uplift capacity of about 0.6, slightly less than the value of 0.66 for the driven concrete piles at the Park Terrace site, and 0.75 for the model piles in the static sand deposits.

Design Example 1 - Multi-Storey Building on Shallow Foundations.

The first design example considers the lateral resistance of shallow foundations for multi-storey buildings of various heights, with dimensions shown in Figure 20. The building is founded on shallow beams with integral "slab on grade" construction, similar to the test foundation of Figure 11. The building was assumed to be founded on "intermediate" soils, to be of "limited ductility", to have a natural period of 0.5 seconds, and to be located in Christchurch, giving a seismic acceleration coefficient of 0.3 according to NZS4203 (1992). The lateral capacity of the foundation system for several different building heights was calculated by using the procedure outlined in Equations 1 to 9, with the results summarised in Table 3.

The vertical bearing capacity of the foundation during the earthquake must also be given careful consideration. Overturning moments may significantly increase vertical loads applied to the foundation elements, and the simultaneous application of lateral loads significantly reduces the bearing capacity. Ground shaking may further reduce bearing capacity because of the inertia of the soil failure wedge and overburden.

For Design Example 1 the bearing capacity of the foundation beams was checked two ways: using conventional, quasi-static analysis including load inclination factors (e.g. McCarthy, 2002), and by using seismic bearing capacity factors (e.g. Ghahramani and Berrill, 1995). The bearing capacity is highly dependent on the ratio of applied horizontal to vertical loads. For Example 1 the seismic acceleration coefficient was 0.3, and so the ratio of horizontal to vertical loads for the quasi-static analysis was set to 0.3, assuming that most of the lateral load would be resisted initially by friction under each foundation beam. The seismic bearing factor method assumes implicitly that lateral loads are directly in proportion to the vertical loads factored by the acceleration. The resulting factors of safety for both methods are given in Table 3.

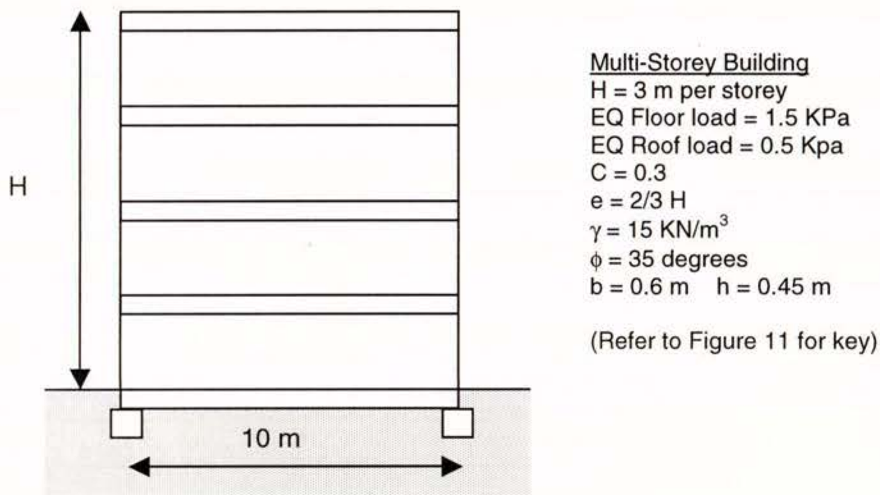

Figure 20. Design Example 1.

No. Storeys	W	R_6 (max reaction)	F (ultimate lateral resistance)	R_4/F (proportion as beam friction)	FS (lateral load)	FS (bearing) (quasi-static)	FS (bearing) (seismic factors)
	(KN/m)	(KN/m)	(KN/m)	.	.		
1	20	17.5	32.8	0.37	5.5	9.8	7.0
2	35	34.2	38.2	0.63	3.6	5.1	3.6
3	50	50	46.2	0.76	3.1	3.2	2.3
4	65	65	56.7	0.80	2.9	2.3	1.6
5	80	80	67.2	0.83	2.8	1.7	1.2
6	95	95	77.7	0.85	2.7	1.3	1.0

Table 3. Ultimate Lateral resistance for Design Example 1.

For the one and two storey buildings the failure mode under lateral loading is as per the cartoon of Figure 6. The high factors of safety (5.5 and 3.6) imply that for the design earthquake acceleration (0.3 g) displacements will remain small and there should be no significant rotation of the building. A large proportion of the lateral resistance of the foundation for the one storey building is provided by passive resistance of the soil trapped between one foundation beam and the slab, with a lesser proportion being provided by friction beneath the opposing beam (R4/F = 0.37) and by passive soil resistance against the leading beam. For the three storey and higher buildings the failure mode is tipping, with rotation about one foundation beam, with most of the lateral resistance being provided by friction under the beam (R4/F = 0.76 - 0.85). The factors of safety for these taller buildings are reduced (3.1 - 2.7) but are still healthy.

The shallow foundations of Example 1 seems adequate for up to four storeys, assuming that soil liquefaction is not an issue for the site and that settlements are satisfactory. For five or more storeys it would seem prudent to use deep foundations because of the increasing risk of a bearing failure (FS 1.7 or less).

Design Example 2 - Multi-Storey Building on Pile Foundations.

The second example considers the same simple multi-storey building of Figure 20, but supported on driven concrete piles beneath the foundation beams. For convenience, the piles will be similar to those tested at the Park Terrace site since the capacity and cyclic behaviour are reasonably well understood. A building height of 10 storeys was chosen for consideration because such a building will tip under the design earthquake acceleration of 0.3 g, requiring the restraint of pile foundations.

First, a conventional pile design was made by considering structure gravity loads for the load case 1.2G + 1.6Q, as shown in Figure 21. The pile capacities were taken from the results of the CAPWAP analysis with a geotechnical strength reduction factor $\Phi_g = 0.85$ applied, as recommended by AS 2159 (1995). A pile spacing of 7 m under each foundation beam was determined.

Next, the earthquake load case $G + Q_u + E_u$ is considered. Since any earthquake will generate cyclic axial loads in the piles (as in Figure 8), the first step is to generate a cyclic stability diagram for the piles in order to fully understand the interaction between the cyclic and non-cyclic components of loading on the capacity of each pile. A cyclic stability diagram for the Park Terrace piles is shown in Figure 22.

Inside of the triangle represents the range of load combinations (cyclic and non-cyclic) that would be possible if there were no cyclic or dynamic effects on pile capacity. The coordinates of the triangle were determined from the un-factored compression and uplift capacities from the CAPWAP analysis (Q_c = 930 KN, Q_t = 495 KN). The dashed line represents the failure envelope for the pile including the cyclic and dynamic effects of earthquake loading on pile capacity and was constructed as follows: Point A was determined from the model testing in the laminar box, which showed that uplift capacity of a pile in shaking ground without simultaneous cyclic loading was reduced by a factor of 0.5 to 0.6. Point B, the cyclic capacity at zero mean load, was set at Q_t reduced by a factor of 0.4, also taken from the model testing in the laminar box and somewhat confirmed by the full-scale cyclic load testing at the Park Terrace site.

Points C, D, and E were taken from the model test results shown in the cyclic stability diagram of Figure 12. From point B to C the envelope rises at a slope of 1:1 because the increase in mean compression load allows a corresponding increase in cyclic load magnitude without increasing the amount of cyclic load reversal. Point C is under the triangle apex (balanced failure), C to D is flat (transition), and D to E is tentatively set at a factor of 0.7 of cyclic capacity, although there is little experimental data within this range.

<u>10 Storey Building</u>

$KN := 1000\,N$

$Floor_{dead} := 5\cdot\frac{KN}{m}$ $\quad$ $Floor_{live} := 10\cdot\frac{KN}{m}$ $\quad$ $Roof_{dead} := 5\cdot\frac{KN}{m}$ (all per m length of building)

$G := 10\cdot Floor_{dead} + Roof_{dead}$ $\quad$ $Q := 10\cdot Floor_{live}$

$\alpha F_{gravity} := 1.2\cdot G + 1.6\cdot Q$ $\quad$ $\alpha F_{gravity} = 226\frac{KN}{m}$

Pile Capacity: $Q_c := 930\cdot KN$ $\quad$ $Q_t := 495\cdot KN$ $\quad$ $\Phi_g := 0.85$ (from CAPWAP)

Pile Spacing: $S := \frac{\Phi_g \cdot Q_c}{0.5\alpha F_{gravity}}$ $\quad$ $S = 6.996m$ (say 7 m)

Figure 21 Conventional gravity pile design.

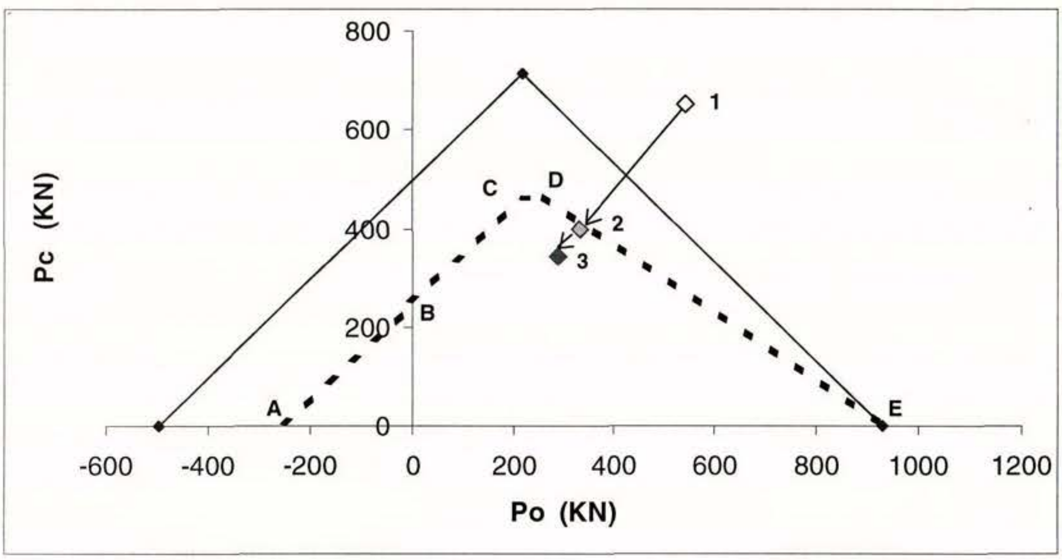

Figure 22. Cyclic stability diagram for piles of design example 2.

Each pile foundation will have a unique cyclic stability diagram, depending on the particular soil conditions, the type of pile construction, the pile depth to diameter ratio, and pile relative stiffness. The cyclic stability diagrams for the piles considered in this study have been assumed to be generally similar in shape because all of the piles, both model and prototype, are relatively short and stiff and are in predominantly loose, granular soils. Guidance for developing cyclic stability diagrams for other conditions are available (e.g. Poulos, 1988).

Design calculations for the earthquake load case are shown in Figure 23. The assumption is made that the piles resist all of the vertical loads and the overturning moment with no contribution from the foundation beams. The initial design from gravity loads of piles spaced at 7 m is clearly inadequate, with the piles likely to fail in compression. The load combination for this case is plotted as Point 1 in the cyclic stability diagram, Figure 22, and falls well outside the triangle of possible load combinations. For the next trial design, the pile spacing was reduced to 4.3 m, resulting in the load combination shown as Point 2 in Figure 22. Point 2 falls on the failure envelope of the cyclic stability diagram and the piles may fail in compression during the design earthquake. For the final trial design, the pile spacing was further reduced by a factor 0.85 to 3.7 m, resulting in the load combination shown as Point 3 in Figure 23. The factor 0.85 was selected as being equivalent to the geotechnical strength reduction factor, Φ_g ,= 0.85, specified in AS 2159 (1995).

10 Storey Building

$KN := 1000\,N$

$Floor_{dead} := 5 \cdot \frac{KN}{m}$ $\quad Floor_{live} := 10 \cdot \frac{KN}{m}$ $\quad Roof_{dead} := 5 \cdot \frac{KN}{m}$ (all per m length of building)

$G := 10 \cdot Floor_{dead} + Roof_{dead}$ $\quad Q := 10 \cdot Floor_{live}$

Seismic hazard coefficient: $C := 0.3$

Base shear: $V := C \cdot (G + Q)$ $\quad V = 46.5 \frac{KN}{m}$

Overturning moment: $H := 30 \cdot m$ $\quad M_o := V \cdot \frac{2 \cdot H}{3}$ $\quad M_o = 930 \frac{KN \cdot m}{m}$

Pile spacing: $S := 7 \cdot m$ (initial trial)

Pile cyclic load: $Lever := 10 \cdot m$ $\quad P_c := \frac{M_o \cdot S}{Lever}$ $\quad P_c = 651 KN$ (+/-)

Pile mean load: $P_o := \frac{(G + Q) \cdot S}{2}$ $\quad P_o = 543 KN$

Figure 23. Pile design including overturning effects for Design Example 2.

The lateral load resistance of the foundation system also needs to be addressed. By assuming that the vertical loads and overturning moments are resisted entirely by the piles, the main mechanism of lateral resistance of the shallow foundation elements (friction under the leading foundation beam) has been removed from consideration. Also, the passive resistance of the soil ahead of the leading foundation beam is small relative to the weight of the 10 storey building. However, the soil between the leading and trailing foundation beams is forced to slide with the building because a passive wedge is prevented from forming ahead of the trailing beam by the slab, which is held down by the piles. These mechanisms yield an ultimate lateral capacity for the shallow foundation elements of 32 KN/m for a factor of safety of 0.7.

Clearly, the lateral resistance of the piles, estimated to be 29 KN/m at the 3.7 m spacing, will be mobilised giving a combined ultimate lateral resistance of 60 KN/m for a factor of safety of 1.3. With such a low FS hinging of the piles is likely and the structural capacity of the piles will need to be checked for combined actions by the structural engineer. Exceeding the lateral capacity of the foundation system during an earthquake should not be a major concern, provided the axial load capacity is maintained.

In summary, the consideration of earthquake actions together with cyclic and dynamic effects on pile capacity have doubled the number of piles required for the 10 storey example building. Also, the number of piles required is significantly more than for considering earthquake actions alone without cyclic or dynamic effects on pile capacity. Pile design for axial loads needs to be made with reference to a cyclic stability diagram. The final design for the example structure is considered to be nearly at optimum since the final load combination for the piles falls right under the "peak" of the cyclic stability diagram of Figure 22. If either more or less dead load was carried by each pile then the cyclic load capacity would be reduced.

Key to the design process for Example 2 is a detailed knowledge of the structure and its various load scenarios. An optimum design solution is only possible with close interaction between the geotechnical designer and the structural designer. Regrettably, such interaction is rare in New Zealand today.

Liquefaction Comments for Design Example

The above example assumes that soil liquefaction does not occur in the soil surrounding the piles. In the event of liquefaction, pile axial capacity will be reduced by a loss of side resistance through the liquefied layer and above. A partial loss of side resistance for the pile has already been assumed in the cyclic design process and in preparing the cyclic stability diagram. Also, once soil liquefaction has been triggered, the ground surface and structure will receive some degree of base isolation, reducing the overturning moments that are the source of the cyclic axial loads, and, hopefully, preventing pile failure. The main issue for the piles then becomes one of surviving the associated ground displacements and pile bending loads, which requires adequate ductility, principally.

SUMMARY

Recent experimental research at the University of Canterbury concerned with the load-displacement behaviour of both shallow and deep foundations has been outlined. Issues being addressed include base sliding friction and passive resistance mechanisms of shallow foundations, capacity of deep foundations with cyclic axial and lateral loading, and interactions between shallow and deep foundations. Practical considerations have been discussed including two design examples.

ACKNOWLEDGEMENTS

Cyrille Eude, Pierre Guillou, Luc Barahona, and Laurent Barra, final year students from Ecole Nationale d'Ingenieurs de Saint-Etienne, France, performed many of the model pile tests. John van Dyk constructed most of the shallow foundation field tests, George Clarke and John Maley constructed most of the laboratory model testing apparatus, and Siale Faitotonu assisted with the full-size field pile tests.

The Earthquake Commission provided much of the funding through research grants EQC95/184 and EQC99/423. Daniel Smith Industries generously provided the test piles at the Park Terrace site and also assisted with the testing.

REFERENCES

Australian Standard AS 2159 (1995). *Piling, Design and Installation,* Standards Australia, Homebush, NSW, 52 p.

Burdon, N.R.R. (2000). *Earthquake Resistance of Shallow Foundations*, Masters Thesis, University of Canterbury.

Chambers, A. (1999). *The Seismic Response of Drilled Shaft Foundations*, PhD Thesis, Unversity of Canterbury, 152 p.

Charlie, W. A., Turner, J. P., and Kulhawy, F. H. (1985). "Review of repeated axial load tests on deep foundations," *Drilled Piers and Caissons II*, Ed. C. N. Baker, Jr. ASCE, New York, pp. 129-150.

Ghahramani, A. and Berrill, J. B. (1995). "Seismic Bearing Capacity Factors by Zero Extension Line Method," *Proc. Pacific Conference on Earthquake Engineering*, Nov. 1995, pp. 147-156.

Lyons, C. D. (2000). *Degradation of Pile Capacity from Cyclic Axial Loading,* Masters Thesis, University of Canterbury, 165 p.

McCarthy, D. F. (2002). *Essentials of Soil Mechanics and Foundations, 6th Ed.,* Prentice Hall, New Jersey, 788 p.

McManus, K.J. and Kulhawy, F.H., (1994). "Cyclic Axial Loading of Drilled Shaft Foundations in Cohesive Soil," *Journal of Geotechnical Engineering*, ASCE, Vol. 120, No. 9, Sep. 1994, pp. 1481-1497.

McManus, K.J. and Chambers, A.,(1995) "Stability Of Drilled Shafts Under Earthquake Induced Axial Loads," in *Performance of Deep Foundations Under Seismic Loading*, Ed. J. P. Turner, ASCE Geotechnical Special Publication No. 51, p. 1-16.

McManus, K. J. (1997). *Axial Behaviour of Bored Pile Foundations*, Research Report EQC 95/184, Earthquake Commission, Wellington, 47 p.

McManus, K.J. (1999). "Axial Response of a Driven Pile to Cyclic Loading", *Proc. Tech Conf. N.Z. Soc. for Earthquake Engg*, Rotorua, NZ, March 1999.

McManus, K.J. and Burdon, N.R.R. (2001) "Lateral Resistance of Shallow Foundations", *Proc. Tech Conf. N.Z. Soc. for Earthquake Engg*, Wairakei, NZ, March 2001, Paper No. 6.03, 11 p.

New Zealand Standard NZS 4203 (1992). *Code of Practice for General Structural Design and Design Loadings for Buildings,* Standards New Zealand, Wellington, 134 p.

Poulos, H. G., (1988). "Cyclic stability diagram for axially loaded piles," *Journal of Geotechnical Engineering*, ASCE, Vol.114, No.8, Aug. 1988, pp. 877-895.

Turner, J. P. and Kulhawy, F. H. (1990). "Drained uplift capacity of drilled shafts under repeated axial loading," *Journal of Geotechnical Engineering*, ASCE, Vol.116, No.3, pp. 470-491.